Solving Large-Scale AC Optimal Power Flow Problems Including Energy Storage, Renewable Generation, and Forecast Uncertainty

by

Jennifer Felder Marley

A dissertation submitted in partial fulfillment
of the requirements for the degree of
Doctor of Philosophy
(Electrical Engineering: Systems)
in The University of Michigan
2017

Doctoral Committee:

Professor Ian Hiskens, Chair
Assistant Professor Ruiwei Jiang
Assistant Professor Johanna Mathieu
Professor Bruce F. Wollenberg

Jennifer Felder Marley
jkfelder@umich.edu
ORCID iD 0000-0001-5234-0224

To my parents, for teaching me the value of education and always believing in me.

ACKNOWLEDGEMENTS

The past five years have been an incredible experience and would not have been possible without the support of many people. I would first like to thank my advisor, Ian Hiskens, for his patience, guidance, and encouragement throughout my graduate education. It has been a privilege to learn about power systems from him. I particularly appreciate the freedom to explore new ideas and encouragement of collaboration that he provided. I am also very grateful for the many opportunities to travel and see the world (especially Australia!) that he offered.

This work would not have been possible without the help of my collaborators, Dan Molzahn and Maria Vrakopoulou. I have learned so much from working with them and am grateful for all the advice they have shared with me. Their creativity and insight have been invaluable. Thank you for your enthusiasm in exploring these ideas.

Thank you also to professors Johanna Mathieu, Ruiwei Jiang, and Bruce Wollenberg for agreeing to serve on my committee. I have enjoyed discussing my work with them and appreciate them taking the time to provide valuable feedback to improve this research.

Thank you to Professor Daniel Kirschen, Hrvoje Pandzic, and the rest of the ARPA-E team from the University of Washington with whom I had the opportunity to work during the first few years of my graduate program. The many fruitful discussions that I shared with them were instrumental in developing this research.

I would like to thank the MPEL group at Michigan, especially Mads Almassalkhi, Ian Beil, Jon Martin, Max Markov, Jonas Kersulis, Mike Fisher, Salman Nazir, Steph Ross, and Greg Ledva. Thank you for always being available for practice presentations, coffee breaks, and interesting conversations. I've really enjoyed getting to know you all and appreciate all of your help getting through homework, qualifying exams, research challenges, and paper deadlines.

Professor Aranya Chakrabortty gave me my first research experience. His enthusiasm for his research motivated me to continue my education in power systems. Thank you for your encouragement and advice throughout my time at NC State. Going back to my high school education, I

would also like to thank Dr. John Sprague. His classes always challenged me and really piqued my interest in mathematics. He played a pivotal role in my decision to pursue a career in engineering.

I cannot express enough my gratitude to my family for their love and support, particularly over the past five years. Thank you to my parents for never letting me give up and always encouraging me. They have been such wonderful role models of perseverance and hard work. I can't thank them enough for all the sacrifices they have made to get me to this point. Thank you to my brother and sister, Jake and Beth, and my siblings-in-law, Mandy and Matt, for always having time for me, providing endless entertainment, and helping me through the stressful periods of the last few years. Thank you also for giving me the best nephews, Odin, Wyatt, and Will, who always help me maintain perspective and not take life too seriously, never fail to make me laugh, and constantly remind me to "*finally* finish school". I am also very thankful for my husband's family and their support throughout this process. Finally, I am immensely grateful to my husband, Daniel, for helping me survive grad school. Having a commiserator (sometimes a competitor) has made this process much more enjoyable. Thank you for always pushing me to set higher goals and working to help me achieve them. I could never have done this without you!

TABLE OF CONTENTS

LIST OF FIGURES

Figure

LIST OF TABLES

Table

ABSTRACT

Renewable generation and energy storage are playing an ever increasing role in power systems. Hence, there is a growing need for integrating these resources into the optimal power flow (OPF) problem. While storage devices are important for mitigating renewable variability, they introduce temporal coupling in the OPF constraints, resulting in a multiperiod OPF formulation. This work explores a solution method for multiperiod AC OPF problems that combines a successive quadratic programming approach (AC-QP) with a second-order cone programming (SOCP) relaxation of the OPF problem. The solution of the SOCP relaxation is used to initialize the AC-QP OPF algorithm. Additionally, the lower bound on the objective value obtained from the SOCP relaxation provides a measure of solution quality. Compared to other initialization schemes, the SOCP-based approach offers improved convergence rate, execution time and solution quality.

A reformulation of the the AC-QP OPF method that includes wind generation uncertainty is then presented. The resulting stochastic optimization problem is solved using a scenario based algorithm that is based on randomized methods that provide probabilistic guarantees of the solution. This approach produces an AC-feasible solution while satisfying reasonable reliability criteria. The proposed algorithm improves on techniques in prior work, as it does not rely upon model approximations and maintains scalability with respect to the number of scenarios considered in the OPF problem. The optimality of the proposed method is assessed using the lower bound from the solution of an SOCP relaxation and is shown to be sufficiently close to the globally optimal solution. Moreover, the reliability of the OPF solution is validated via Monte Carlo simulation and is demonstrated to fall within acceptable violation levels. Timing results are provided to emphasize the scalability of the method with respect to the number of scenarios considered and demonstrate its utility for real-time applications.

Several extensions of this stochastic OPF are then developed for both operational and planning purposes. The first is to include the cost of generator reserve capacity in the objective of the stochastic OPF problem. The need for the increased accuracy provided by the AC OPF is highlighted by a case study that compares the reliability levels achieved by the AC-QP algorithm to those from the solution of a stochastic DC OPF. Next, the problem is extended to a planning

context, determining the maximum wind penetration that can be added in a network while maintaining acceptable reliability criteria. The scalability of this planning method with respect not only to large numbers of wind scenarios but also to moderate network size is demonstrated. Finally, a formulation that minimizes both the cost of generation and the cost of reserve capacity while maximizing the wind generation added in the network is investigated. The proposed framework is then used to explore the inherent tradeoff between these competing objectives. A sensitivity study is then conducted to explore how the cost placed on generator reserve capacity can significantly impact the maximum wind penetration that can be reliably added in a network.

CHAPTER I

Introduction

1.1 The Optimal Power Flow Problem

The goal of an optimal power flow (OPF) is to determine the optimal operating point for an electric power system relative to a specified objective, such as minimizing generation cost, losses, or renewable spillage. In optimizing the specified objective, the solution must satisfy engineering and physical constraints. These consist of the nonlinear AC power flow equations, line-flow limits, and operational limits on decision variables (including voltage magnitude limits and generator active and reactive power output limits) [1]. Let all decision variables be collected in a vector, x. Given the particular objective function of interest, denoted $C(x)$, the general AC OPF can be compactly represented in the following form:

$$\min_x C(x) \tag{1.1a}$$

subject to:

$$g(x) \leq 0 \tag{1.1b}$$

$$h(x) = 0, \tag{1.1c}$$

where $g(x)$ is used to represent all inequality constraints, including decision variable operational limits and nonconvex line-flow constraints. Likewise, $h(x)$ denotes the nonconvex power balance equality constraints. The exact formulation used in this work is discussed in detail in Chapter II.

Many solution methods have been applied to AC OPF problems. These include gradient methods, Newton's method, successive quadratic programming methods (AC-QP), and interior point methods [1–4]. Additionally, the DC OPF formulation is often used to approximate the AC OPF problem as a quadratic program (QP) [5–7]. Due to its convexity and scalability to large networks, the DC OPF approximation offers a variety of computational benefits. Under normal operating

conditions, it usually provides a reasonable approximation of the AC OPF problem [8]. However, it does not necessarily result in an AC feasible solution, and there are cases where the DC power flow has non-negligible errors compared to the AC power flow [9, 10].

The AC-QP OPF algorithm forms the basis of the work in this dissertation. This algorithm uses a successive linearization procedure adapted from [1]. Given an AC power flow solution, x_0, the nonconvex AC OPF problem is approximated as a QP by linearizing all constraints around the power flow solution. Decision variables in this QP are changes from the power flow solution, represented by Δx, and can be represented as follows:

$$\min_{\Delta x} C(x_0 + \Delta x) \tag{1.2a}$$

subject to:

$$g(x_0) + \frac{\partial g(x)}{\partial x}\Big|_{x_0} \Delta x \leq 0 \tag{1.2b}$$

$$h(x_0) + \frac{\partial h(x)}{\partial x}\Big|_{x_0} \Delta x = 0. \tag{1.2c}$$

The feasibility of the QP solution is checked with an AC power flow, and a new linearization is formed in the next QP if all constraints are not satisfied. These iterations continue until the QP and power flow iterations agree within a reasonably small tolerance. The AC-QP algorithm has the advantage of providing an AC-feasible solution, as each iteration solves an AC power flow. Additionally, solvers for quadratic programs and AC power flow methods scale well, making the AC-QP algorithm applicable to large networks. However, these advantages come with some trade-offs: this method is dependent on an initial converged AC power flow and the optimality of the final solution is sensitive to this initialization. Depending on the proximity of the initialization to the globally optimal solution, the AC-QP algorithm runs the risk of failing to converge or converging to only a locally optimal solution. Thus, developing better initialization procedures is important for improving the performance of the AC-QP algorithm. The initialization challenges of the AC-QP algorithm are particularly pronounced following a large change in loading and/or network topology which results in a significant change in the operating point (e.g., contingency events), as well as for planning scenarios which offer limited prior knowledge of the solution.

There have been many recent developments in applying semidefinite programming (SDP) and second-order cone programming (SOCP) methods to formulate convex relaxations of the OPF problem. Several examples of these relaxations can be found in [11–23]. Convex relaxations lower bound the objective value, can certify problem infeasibility, and, in many cases, provide the global

solution (i.e., the relaxations are often *exact*). However, there are many practical problems for which existing relaxations fail to be exact, so the solutions they produce are not physically realizable [24–26]. While solvers for the SDP relaxations are available for moderately sized networks, application to large networks is generally more complicated than other solution methods [14, 18]. Thus, further research is needed to employ these methods in real-time applications for large networks. In contrast, the SOCP relaxation in [13] can be quickly solved for large networks to obtain a lower bound on the globally optimal objective value. The SOCP solution provides generation and voltage schedules, which are used to solve the first AC power flow to initialize the AC-QP algorithm. This approach enables consideration of problems for which the SOCP relaxation is not exact. Providing a procedure for combining these two methods in this manner is the first contribution of this research.

1.1.1 Security-Constrained Optimal Power Flows

As previously described, a common objective of OPF problems is to minimize the cost of conventional generation. While such formulations ensure the economic operation of power systems, the resulting solution may be insecure. The $(N-1)$ reliability criteria are used to define a secure operating point. These require that any single contingency, meaning an outage of any single component in a network, should not induce any further constraint violations. This operating strategy is designed to avoid a cascading failure of the network. To enforce these criteria in an optimal way, standard OPF formulations can be modified to ensure that the resulting solution is not only feasible under normal operation, but also that there are no constraint violations in any post-contingency states. Given a set of contingencies to be considered in the OPF problem, denoted $\mathcal{C}$, the security-constrained OPF (SCOPF) takes the following form:

$$\min_{x} C(x) \tag{1.3a}$$

subject to:

$$g(x) \leq 0 \tag{1.3b}$$

$$h(x) = 0 \tag{1.3c}$$

$\forall m \in \mathcal{C}$:

$$g^m(x) \leq 0 \tag{1.3d}$$

$$h^m(x) = 0, \tag{1.3e}$$

where g^m and h^m represent the network constraints under contingency m, and are referred to as the security (or contingency) constraints. For example, if contingency m considers a particular line being out of service, then the network model in constraints g^m would not contain that line.

There is an inherent tradeoff between optimality and reliability present in such problems. While the security constraints ensure that the resulting solution will be feasible for any contingency considered, doing so frequently requires adjusting generation schedules and voltage setpoints to a less economic operating point. As formulated, they also introduce additional computational complexity, as the number of security constraints could be quite large when considering the full set of $(N-1)$ constraints for realistically large networks. As described in [1], this additional computational burden is often reduced by using a contingency screening process. Such approaches individually introduce contingencies in an iterative manner until the resulting OPF solution is feasible for all contingencies under consideration.

While the OPF formulations described in the chapters that follow do not explicitly include security constraints, it should be noted that each is directly applicable to such an extension. In the AC-QP algorithm, each contingency considered requires including an additional set of (modified) linearized OPF constraints in the QP, as well as solving an additional power flow at each iteration.

1.2 Incorporating Energy Storage Devices

Renewable generation offers economic and environmental benefits, but also challenges system reliability due to its inherent variability. Storage devices provide a means of (at least partially) mitigating this variability. Thus, OPF methods must be adapted to incorporate both renewable generation and storage [27]. However, the state-of-charge dynamics of storage devices [28] introduce temporal coupling, requiring a multiperiod OPF formulation. Multiperiod versions of both an AC-QP algorithm and an SOCP relaxation which include renewable generation and storage devices that have non-ideal charging and discharging efficiencies are provided in the chapters that follow.

Many multiperiod OPF formulations that include renewable generation and storage, as in [29] and [30], use a horizon of 24 hours. The size and complexity of the multiperiod OPF problem when using such a long horizon may substantially increase the computation time, thus limiting the real-time applications of the OPF tool developed. However, the length of the horizon affects the benefits that are derived from solving the multiperiod OPF, as decisions seek to minimize cost over the entire horizon, not simply the cost at the current time period. Implementing a longer horizon may thus increase the quality of solution in terms of minimum cost of generation, but also makes

the solution more susceptible to forecast error. This tradeoff becomes particularly important in real-time applications for realistically large networks. Various horizons have been explored in this work, ranging from 1 hour to 8 hours, with a time-step length of half an hour. An 8-hour horizon therefore requires optimizing over 16 time steps. Results that explore various choices of horizons are included, offering insights into the sensitivity of the solution to this choice.

1.3 A Stochastic Optimal Power Flow Formulation

The second class of contributions made in this work involves adapting the AC-QP method to solve a stochastic AC OPF problem. This problem aims to find a solution that satisfies the non-convex constraints of the OPF problem in a probabilistic sense, while providing certain confidence on the constraint violation level due to the uncertain realizations of renewable generation. In other words, given a base case wind forecast, P_w, the AC OPF solution must first be feasible for this forecast. However, given that forecast errors can be significant, the reliability of the solution for any plausible realization of wind generation, $\tilde{P}_w$, must also be considered. Note that the presence of $\tilde{P}_w$ introduces uncertainty into the nonconvex OPF constraints. Applying a chance-constrained formulation, the stochastic AC OPF considered in this work takes the general form

$$\min_x C(x) \tag{1.4a}$$

subject to:

$$g(x, P_w) \leq 0 \tag{1.4b}$$

$$h(x, P_w) = 0 \tag{1.4c}$$

$$h(x, \tilde{P}_w) = 0 \qquad \forall \tilde{P}_w \in \Omega \tag{1.4d}$$

$$\mathbb{P}\big[\tilde{P}_w \in \Omega | g(x, \tilde{P}_w) \leq 0\big] \geq 1 - \epsilon, \tag{1.4e}$$

where Ω is the support for the probability distribution of uncertain wind generation, and ϵ is the desired reliability level (i.e. a choice of $\epsilon = 0.1$ would imply that the OPF constraints will be satisfied with probability of at least 90%).

There are many approaches that try to incorporate the stochasticity of the problem assuming the DC power flow model [31–35]. However, the lack of AC feasibility may result in violation of the desired reliability levels. Numerous works consider the uncertainty by including in the optimization problem a certain set of scenarios that is heuristically chosen [31–33], usually using a scenario reduction technique. However, the latter does not provide any solution performance guarantees. Moreover, different directions look into analytical reformulations that mainly assume a closed form

for the uncertainty distribution (e.g Gaussian) [35, 36] and hence can provide solutions with probabilistic performance. However, as the uncertainty realizations (e.g wind power forecast errors) may not necessarily closely follow such analytical distributions, there is an inherent inaccuracy in such descriptions. Moreover, the complexity of those methods may increase dramatically when the nonconvex OPF nature is considered. Furthermore, many formulations are based on robust optimization [37], where it is difficult to quantify the solution performance since (similar to the heuristic scenario techniques) the selected uncertainty set might end up being overly conservative or too risky.

This work proposes an OPF methodology which finds solutions that come with guarantees, does not require a specific distribution of the uncertainty, and maintains reasonable complexity and solution time for real-time operation. Randomized optimization techniques like [38–40] satisfy those objectives. Those techniques are basically scenario based methods; however, their solution is a-priori guaranteed to satisfy the system constraints with certain probability and at a certain confidence level. These techniques were first applied in the stochastic DC OPF problem in [34] and later, using the SDP relaxation of the power flow constraints, in the stochastic AC OPF in [41]. The AC-QP OPF method is employed to achieve better scalability properties compared to convex relaxations. As the underlying problem solved by this method is nonconvex, the methods in [38,39] cannot be used, since they require the convexity of the underlying problem. Additionally, [40] cannot be practically applied, as it requires finding the optimal solution of a robust counterpart of the initial problem. This cannot be easily achieved in the AC-QP OPF algorithm. The proposed formulation therefore relies on a recent algorithm presented in [42] that does not require convexity of the problem, but requires identifying the so called support set of the scenarios used in the optimization. The definition of this support set is discussed in detail in Chapter VII.

The stochastic AC-QP algorithm is also applicable to planning problems involving renewable generation. As such, two planning problems are also considered in this work. The objective of the first is to determine the maximum wind penetration that can be added in a network, while maintaining reliability standards. As in the operational setting, the reliability guarantees to accompany the solution come from the application of the scenario approach in [42]. Introducing large amounts of renewable generation in a network can potentially displace a significant amount of conventional generation, reducing total operating costs. However, significant generator reserve capacity is needed to ensure that the system is able to respond to potential forecast errors. A second planning problem is thus proposed, the objective of which is to minimize the total cost of conventional generation

and of generator reserve capacity, while maximizing the wind penetration. Because a stochastic OPF formulation is utilized, the optimal wind investment schedule determined in both cases is also accompanied with theoretical reliability guarantees. While such planning problems have been investigated in the DC OPF context [43], this work extends such formulations to the AC OPF setting, increasing the accuracy of the resulting solution.

1.4 Summary of Contributions

The following list summarizes the major contributions of the research discussed in the chapters that follow.

- The AC-QP OPF has been extended to a multiperiod formulation that includes renewable generation and storage.
- An improved initialization technique is proposed for the AC-QP algorithm using the solution of an SOCP relaxation.
- A stochastic AC-QP OPF algorithm has been developed to address wind uncertainty. A scenario approach is applied to solve the underlying chance-constrained optimization and to provide a-posteriori theoretical reliability guarantees to accompany the OPF solution.
- Several operational and planning decisions involving renewable generation have been investigated in a stochastic setting.

1.5 Organization

The remainder of this dissertation is organized as follows. Chapter II describes the multiperiod OPF problem formulation with storage and wind. It is deterministic, in the sense that it assumes a perfect wind generation forecast is available. Chapter III presents the details of the AC-QP solution method, while Chapter IV proposes a method for enforcing storage complementarity. Chapter V provides an improved initialization procedure for the AC-QP algorithm using a second order cone program relaxation of the AC OPF problem. Chapter VI explores the sensitivity of this method to the choice of optimization horizon under various assumptions of forecast uncertainty. A modified version of the AC-QP method for solving the stochastic AC OPF problem including wind forecast uncertainty is given in Chapter VII. This stochastic OPF is extended to optimally allocate generator

reserve capacity in Chapter VIII. It is then applied in a planning context to determine the maximum wind penetration that can be added in a network in Chapter IX. The cost of conventional generation and of generator reserve capacity is included in this planning formulation in Chapter X. Conclusions and proposed directions of future research are then offered in Chapter XI.

CHAPTER II

Multi-period AC OPF Problem

The OPF problem seeks to minimize the cost of conventional generation while satisfying power balance constraints and operational limits on control variables. The formulation presented includes both storage devices and wind generation. Consider an n-bus power system with buses in the set $\mathcal{N} = \{1, \ldots, n\}$. Define the set of buses with traditional generators as $\mathcal{G}$. Each generator $i \in \mathcal{G}$ has an associated convex quadratic cost curve of its active power generation, $P_{g,i}$, denoted $C_i(P_{g,i}) = c_{2,i}P_{g,i}^2 + c_{1,i}P_{g,i} + c_{0,i}$. In this expression, $c_{2,i}$, $c_{1,i}$, and $c_{0,i}$ are the quadratic, linear, and constant cost coefficients, respectively. Let $\mathcal{S}$ denote the set of storage buses and $\mathcal{W}$ denote the set of buses with wind generation. The slack bus is denoted by *slack*.

A line from node i to node j is modeled by the equivalent circuit given in Figure 2.1. Each line is modeled as an ideal transformer with a specified turns ratio $\tau_{ij}e^{\mathbf{j}\theta_{shift,ij}} : 1$ in series with a Π-circuit with series impedance $R_{ij} + \mathbf{j}X_{ij}$ and shunt admittance $\mathbf{j}b_{sh,ij}$, where $\mathbf{j}$ is the imaginary unit. The corresponding series admittance is given by $g_{ij} + jb_{ij} = 1/(R_{ij} + jX_{ij})$. The active and reactive flows into the line's terminal i are denoted P_{ij} and Q_{ij} respectively. The squared current flow is given by $L_{ij} = I_{ij}^2$, where I_{ij} represents the current flow into terminal i. Similarly, I_π gives the current flow in the π circuit. The complex voltages across the i and j terminals are represented by $\tilde{V}_i$ and $\tilde{V}_j$ respectively. The set of lines within the network is denoted by $\mathcal{L}$. Branches within this set are represented as $(i, j) \in \mathcal{L}$; the ordering of this pair indicates that the ideal transformer is at end i of the line. The maximum apparent power flow on line (i, j) is S_{ij}^{max}.

The time horizon is denoted by $\mathcal{T} = \{0, \ldots, T-1\}$, and the time steps are indexed by t. The length of each time step is T_s. Upper and lower limits on active and reactive power injection at generator bus $i \in \mathcal{G}$ are denoted by $P_{g,i}^{max}$, $P_{g,i}^{min}$ and $Q_{g,i}^{max}$, $Q_{g,i}^{min}$, respectively. This formulation models storage at bus $i \in \mathcal{S}$ as a sink or source of active power with charging and discharging

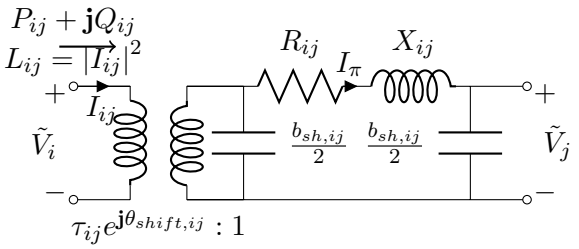

Figure 2.1: Line model.

efficiencies $\eta_{c,i}$ and $\eta_{d,i}$, respectively, and corresponding maximum rates $R_{c,i}^{max}$ and $R_{d,i}^{max}$. The initial and final state of charge are e_i^{init} and e_i^{term}, respectively, and the maximum state of charge is E_i. Wind generation at bus $i \in \mathcal{W}$ and time $t \in \mathcal{T}$ is modeled as a source of active power injection with a maximum capacity $W_i^{max}(t)$, zero marginal cost and full curtailment allowed.

The decision variables are the (complex) voltages at each bus and each time, $\tilde{V}_i(t) = V_i(t)\angle\theta_i(t)$, $i \in \mathcal{N}$, $t \in \mathcal{T}$, and the battery state of charge $e_i(t)$ for each storage device $i \in \mathcal{S}$ and time $t \in \mathcal{T}$. If positive, the charging rate at time $t \in \mathcal{T}$ is $r_{c,i}(t) = (e_i(t+1) - e_i(t))/(T_s\eta_{c,i})$. Otherwise, the discharge rate at time $t \in \mathcal{T}$ is $r_{d,i}(t) = \eta_{d,i}(e_i(t) - e_i(t+1))/T_s$. As modeled by the power flow equations, the voltages are dependent upon power injections into the network given by $P_{g,i}(t)$, $Q_{g,i}(t)$, $i \in \mathcal{G}$; $P_{w,i}(t)$, $i \in \mathcal{W}$; $r_{d,i}(t) - r_{c,i}(t)$, $i \in \mathcal{S}$; and the active and reactive power loads $P_{d,i}(t)$, $Q_{d,i}(t)$, $i \in \mathcal{N}$ at all times $t \in \mathcal{T}$. The shunt admittance at bus $i \in \mathcal{N}$ is given by $g_{sh,i} + \mathbf{j}b_{sh,i}$. The upper and lower limits on the voltage magnitude at bus $i \in \mathcal{N}$ are V_i^{max} and V_i^{min}, respectively.

With these definitions, the multiperiod OPF problem can be expressed as:

$$\min_{\substack{\tilde{V}(t),e(t),r_c(t),r_d(t),\\ P_g(t),Q_g(t),P_w(t)}} \quad \sum_{t\in\mathcal{T}}\sum_{i\in\mathcal{G}} C_i(P_{g,i}(t)) \qquad \text{subject to } (\forall t \in \mathcal{T}) \tag{2.1a}$$

$$P_{g,i}^{min} \le P_{g,i}(t) \le P_{g,i}^{max} \qquad \forall i \in \mathcal{G} \tag{2.1b}$$

$$Q_{g,i}^{min} \le Q_{g,i}(t) \le Q_{g,i}^{max} \qquad \forall i \in \mathcal{G} \tag{2.1c}$$

$$0 \le P_{w,i}(t) \le W_i^{max}(t) \qquad \forall i \in \mathcal{W} \tag{2.1d}$$

$$0 \le r_{c,i}(t) \le R_{c,i}^{max} \qquad \forall i \in \mathcal{S} \tag{2.1e}$$

$$0 \le r_{d,i}(t) \le R_{d,i}^{max} \qquad \forall i \in \mathcal{S} \tag{2.1f}$$

$$0 \le e_i(t) \le E_i \qquad \forall i \in \mathcal{S} \tag{2.1g}$$

$$e_i(0) = e_i^{init} \qquad \forall i \in \mathcal{S} \tag{2.1h}$$

$$e_i(T) = e_i^{term} \qquad \forall i \in \mathcal{S} \tag{2.1i}$$

$$T_s\left(\eta_{c,i}r_{c,i}(t) - \frac{r_{d,i}(t)}{\eta_{d,i}}\right) = e_i(t+1) - e_i(t) \qquad \forall i \in \mathcal{S} \tag{2.1j}$$

$$r_{c,i}(t)\, r_{d,i}(t) = 0 \qquad \forall i \in \mathcal{S} \qquad (2.1k)$$

$$V_i^{min} \le V_i(t) \le V_i^{max} \qquad \forall i \in \mathcal{N} \qquad (2.1l)$$

$$\theta_{slack}(t) = 0 \qquad (2.1m)$$

$$P_{ij}(t) = \frac{V_i(t)^2 g_{ij}}{\tau_{ij}^2} - \frac{V_i(t)V_j(t)}{\tau_{ij}} \cdot [g_{ij}\cos(\theta_{ij}(t)) + b_{ij}\sin(\theta_{ij}(t))] \qquad \forall (i,j) \in \mathcal{L} \qquad (2.1n)$$

$$P_{ji}(t) = V_j(t)^2 g_{ij} - \frac{V_i(t)V_j(t)}{\tau_{ij}} \cdot [g_{ij}\cos(\theta_{ji}(t)) + b_{ij}\sin(\theta_{ji}(t))] \qquad \forall (i,j) \in \mathcal{L} \qquad (2.1o)$$

$$Q_{ij}(t) = \frac{-V_i(t)^2}{\tau_{ij}^2}\left(b_{ij} + \frac{b_{sh,ij}}{2}\right) + \frac{V_i(t)V_j(t)}{\tau_{ij}} \cdot [b_{ij}\cos(\theta_{ij}(t)) - g_{ij}\sin(\theta_{ij}(t))] \qquad \forall (i,j) \in \mathcal{L} \qquad (2.1p)$$

$$Q_{ji}(t) = -V_j(t)^2\left(b_{ij} + \frac{b_{sh,ij}}{2}\right) + \frac{V_i(t)V_j(t)}{\tau_{ij}} \cdot [b_{ij}\cos(\theta_{ji}(t)) - g_{ij}\sin(\theta_{ji}(t))] \qquad \forall (i,j) \in \mathcal{L} \qquad (2.1q)$$

$$P_{ij}(t)^2 + Q_{ij}(t)^2 \le \left(S_{ij}^{max}\right)^2 \qquad \forall (i,j) \in \mathcal{L} \qquad (2.1r)$$

$$P_{ji}(t)^2 + Q_{ji}(t)^2 \le \left(S_{ij}^{max}\right)^2 \qquad \forall (i,j) \in \mathcal{L} \qquad (2.1s)$$

$$P_{g,i}(t) + P_{w,i}(t) + r_{d,i}(t) - r_{c,i}(t) - P_{d,i}(t) = \sum_{(i,j)\in\mathcal{L}} P_{ij}(t) + \sum_{(j,i)\in\mathcal{L}} P_{ij}(t) + g_{sh,i}V_i(t)^2 \qquad \forall i \in \mathcal{N} \qquad (2.1t)$$

$$Q_{g,i}(t) - Q_{d,i}(t) = \sum_{(i,j)\in\mathcal{L}} Q_{ij}(t) + \sum_{(j,i)\in\mathcal{L}} Q_{ij}(t) + b_{sh,i}V_i(t)^2 \qquad \forall i \in \mathcal{N} \qquad (2.1u)$$

where the power injections equal zero when the corresponding device does not exist at a bus (e.g., $P_{g,i} = 0, \forall i \in \mathcal{N} \setminus \mathcal{G}$). Constraints (2.1b) and (2.1c) limit the active and reactive generation at conventional generators. Constraint (2.1d) limits the active power output of wind generators. Constraints (2.1e) and (2.1f) limit the charge and discharge rates, respectively, (2.1g) limits the maximum energy storage, and (2.1j) controls the state-of-charge evolution with boundary conditions set by (2.1h) and (2.1i). Constraint (2.1k) prevents simultaneous charging and discharging of the storage devices. See [28] for further details on this storage device model. Note that constraints (2.1e)-(2.1k) could be replaced with another storage model if desired; the proposed framework is not limited to this modeling choice. The voltage magnitude limits are enforced by (2.1l), and (2.1m) sets the reference angle. Constraints (2.1n)-(2.1q) define the active and reactive line flows at both ends of each branch in the network, where for each line $(i,j) \in \mathcal{L}$, $\theta_{ij} = \theta_i - \theta_j - \theta_{shift,ij}$, and $\theta_{ji} = \theta_j - \theta_i + \theta_{shift,ij}$. These line flows are used in (2.1r)-(2.1s) to enforce apparent power line flow limits. The power flow equations (2.1t) and (2.1u) relate the voltages and the power injections. Note that adding generator ramp rate limits to this formulation is straightforward; these constraints are excluded for simplicity.

The main technical challenge in solving this problem is due to the nonconvexity of constraints (2.1n)-(2.1s), (2.1t)-(2.1u), and (2.1k). A method for solving the nonconvex power balance and line flow constraints is given in Chapter III, while storage complementarity is addressed in Chapter IV.

CHAPTER III

AC-QP Solution Algorithm

The AC-QP OPF algorithm is employed in this work to solve Problem (2.1). It is a local solution method adopted from [1], which is summarized in Figure 3.1. Note that the nonconvex storage complementarity constraint (2.1k) is initially neglected in the development of this method. However, it is incorporated into the formulation in Chapter IV. The AC-QP algorithm begins by solving a separate AC power flow for each time period in the optimization horizon from an initial (possibly approximate) operating point. These solutions are used to linearize the nonconvex constraints in Problem (2.1). Define $G_a \in \mathbb{R}^{n_B \times n_G}$ to be the node-generator incidence matrix, $W_a \in \mathbb{R}^{n_B \times n_W}$ to be the node-wind incidence matrix, and $S_a \in \mathbb{R}^{n_B \times n_S}$ to be the node-storage incidence matrix. Here n_B, n_G, n_W, and n_S represent the numbers of buses, generators, wind nodes, and storage nodes in the network, respectively. As such, $G_a(i,j) = 1$ if generator j is located at bus i; otherwise $G_a(i,j) = 0$. W_a and S_a are defined similarly. Given the Jacobian of the power flow equations at each time $t \in \mathcal{T}$, $\mathbf{J}(t)$, constraints (2.1t)-(2.1u) can be replaced with their first order approximation

$$\mathbf{J}(t)\Delta x(t) = \Delta S(t), \tag{3.1}$$

where

$$\mathbf{J}(t) = \begin{bmatrix} \frac{\partial P}{\partial \theta}(t) & \frac{\partial P}{\partial V}(t) \\ \frac{\partial Q}{\partial \theta}(t) & \frac{\partial Q}{\partial V}(t) \end{bmatrix}, \qquad \Delta x(t) = \begin{bmatrix} \Delta\theta(t) \\ \Delta V(t) \end{bmatrix}$$

$$\Delta S(t) = \begin{bmatrix} G_a \Delta P_g(t) - S_a\big(\Delta r_c(t) - \Delta r_d(t)\big) + W_a \Delta P_w(t) \\ G_a \Delta Q_g(t) \end{bmatrix}.$$

Likewise, the sensitivity factors of the flow on each line $(i,j) \in \mathcal{L}^*$ with respect to the voltage

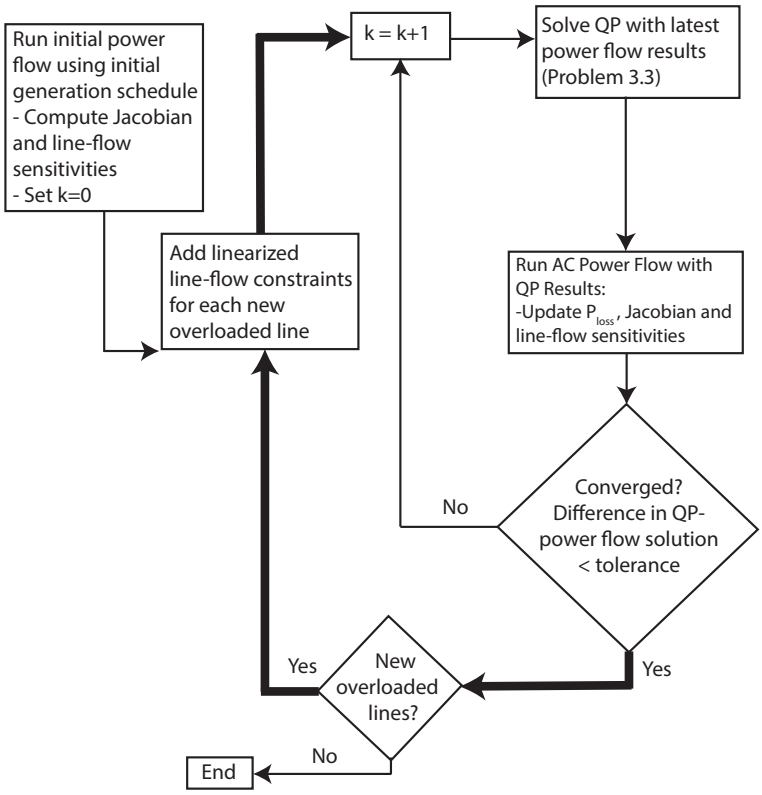

Figure 3.1: Flowchart for the base AC-QP OPF algorithm, (adapted from [1], [44]).

angle and magnitude of each node $k \in \mathcal{N}$ at each time $t \in \mathcal{T}$, denoted $\frac{\partial S_{ij}}{\partial \theta_k}(t)$ and $\frac{\partial S_{ij}}{\partial V_k}(t)$, can be calculated from the power flow solutions. These are then used to linearize constraints (2.1n)-(2.1s):

$$S_{ij}^{\circ}(t) + \sum_{k \in \mathcal{N}} \frac{\partial S_{ij}}{\partial \theta_k}(t) \Delta\theta_k(t) + \sum_{k \in \mathcal{N}} \frac{\partial S_{ij}}{\partial V_k(t)} \Delta V_k(t) \leq S_{ij}^{max} \qquad \forall\, (i,j) \in \mathcal{L}^* \tag{3.2a}$$

$$S_{ji}^{\circ}(t) + \sum_{k \in \mathcal{N}} \frac{\partial S_{ji}}{\partial \theta_k}(t) \Delta\theta_k(t) + \sum_{k \in \mathcal{N}} \frac{\partial S_{ji}}{\partial V_k(t)} \Delta V_k(t) \leq S_{ij}^{max} \qquad \forall\, (i,j) \in \mathcal{L}^*. \tag{3.2b}$$

Note that in these constraints, $S_{ij}^{\circ}(t)$ and $S_{ji}^{\circ}(t)$ are the line flows on each line $(i,j) \in \mathcal{L}^*$ calculated from the power flow solution. Again neglecting constraint (2.1k) and using these linearized constraints, Problem (2.1) can be approximated as a QP.

The QP is then solved to find a generation schedule that minimizes the generation cost while enforcing (linearized) power balance and line flow equations. The QP solution provides new generation and voltage schedules that are used in the next set[1] of AC power flows.

In the QP, the notation Δ is used to denote a change in the corresponding variable from the

[1] A separate power flow is required for each time step.

previous power flow solution. These are the decision variables in the problem. The superscript '$\circ$' denotes quantities obtained from the AC power flow, which are fixed parameters in the optimization problem. These are updated after each QP–(power flow) iteration. The QP solved at each iteration is formulated as follows:

$$\min_{\substack{\Delta P_g(t),\Delta Q_g(t),\Delta\theta(t),\Delta V(t),\\ \Delta P_w(t),e(t),\Delta r_c(t),\Delta r_d(t)}} \quad \sum_{t\in\mathcal{T}}\sum_{i\in\mathcal{G}} C_i\big(P^{\circ}_{g,i}(t)+\Delta P_{g,i}(t)\big) \tag{3.3a}$$

subject to $\forall t \in \mathcal{T}$ (3.1), (3.2)

$$P^{min}_{g,i} \le P^{\circ}_{g,i}(t)+\Delta P_{g,i}(t) \le P^{max}_{g,i} \qquad \forall i\in\mathcal{G} \tag{3.3b}$$

$$Q^{min}_{g,i} \le Q^{\circ}_{g,i}(t)+\Delta Q_{g,i}(t) \le Q^{max}_{g,i} \qquad \forall i\in\mathcal{G} \tag{3.3c}$$

$$\Delta\theta_{slack}(t) = 0 \tag{3.3d}$$

$$-\pi \le \theta^{\circ}_i(t)+\Delta\theta_i(t) \le \pi \qquad \forall i\in\mathcal{N}\backslash slack \tag{3.3e}$$

$$V^{min}_i \le V^{\circ}_i(t)+\Delta V_i(t) \le V^{max}_i \qquad \forall i\in\mathcal{N} \tag{3.3f}$$

$$0 \le P^{\circ}_{w,i}(t)+\Delta P_{w,i}(t) \le W^{max}_i(t) \qquad \forall i\in\mathcal{W} \tag{3.3g}$$

$$T_s\left(\eta_c\left(r^{\circ}_{c,i}(t)+\Delta r_{c,i}(t)\right)-\left(r^{\circ}_{d,i}(t)+\Delta r_{d,i}(t)\right)/\eta_{d,i}\right) = e_i(t+1)-e_i(t) \qquad \forall i\in\mathcal{S} \tag{3.3h}$$

$$e_i(0) = e^{init}_i \qquad \forall i\in\mathcal{S} \tag{3.3i}$$

$$e_i(T) = e^{term}_i \qquad \forall i\in\mathcal{S} \tag{3.3j}$$

$$0 \le r^{\circ}_{c,i}(t)+\Delta r_{c,i}(t) \le R^{max}_{c,i}(t) \qquad \forall i\in\mathcal{S} \tag{3.3k}$$

$$0 \le r^{\circ}_{d,i}(t)+\Delta r_{d,i}(t) \le R^{max}_{d,i}(t) \qquad \forall i\in\mathcal{S} \tag{3.3l}$$

$$0 \le e_i(t) \le E_i \qquad \forall i\in\mathcal{S} \tag{3.3m}$$

The QP–(power flow) iterations continue until the difference between the QP and power flow solutions is within a specified tolerance (10^{-3} p.u. provides sufficient accuracy). At that point, the inner loop of the method in Figure 3.1 is terminated, and the nonconvex constraints (2.1t)-(2.1u) are satisfied with sufficient accuracy.

In practice, it has been observed that only a small subset of line flow constraints are binding at optimality. Noting this, the linearized line-flow constraints (3.2a)-(3.2b) are initially enforced for all lines that are at or above 95% of their line-flow limit after the first AC power flow, the set of which is denoted $\mathcal{L}^*$. This set is updated at the beginning of each outer loop of the AC-QP algorithm (bolded in Figure 3.1). Introducing line limit constraints in this iterative manner generally reduces the number of branch flow constraints that must be explicitly modeled in the QP, which improves the solution time of each QP. This reduction is particularly noticeable in realistically large networks having several thousand nodes. The outer loop ensures that the nonconvex line flow constraints

Algorithm 1 Trust-region step of the AC-QP OPF algorithm

1: Calculate the predicted change in system losses from the QP solution at each time $t \in \mathcal{T}$ according to (3.5).
2: Calculate the actual change in system losses from the power flow solution at each time $t \in \mathcal{T}$ according to (3.4).
3: Update QP decision variable limits at the next iteration:
4: **if** $\max_{t\in\mathcal{T}} |\Delta P^k_{loss\_act}(t) - \Delta P^k_{loss\_pred}(t)| <$ tolerance
5: The linearization is considered accurate.
6: Increase decision variable limits at next iteration by a scaling factor: $d(k+1) = \min(2 \times d(k), 1)$.
7: **else**
8: The linearization is considered inaccurate.
9: Reduce decision variable limits at next iteration by a scaling factor: $d(k+1) = Sc \times d(k)$.
10: **end if**

(2.1n)-(2.1s) are satisfied with acceptable accuracy at convergence. It should also be noted that in the worst case, all line flow constraints will be added to the QP, as in a typical OPF formulation.

The convergence of this method depends on the accuracy of the linearization at each iteration, which is generally only valid for small changes. To improve convergence, a "trust-region" step, based on the formulation in [44], is included in the algorithm after each set of AC power flows to check the accuracy of the linearization before the next QP is solved. The implementation of the trust-region step is summarized in Algorithm 1, and the updated AC-QP algorithm with this step is given in Figure 3.2.

The actual change in the total losses,

$$\Delta P^k_{loss\_act}(t) = P^k_{loss}(t) - P^{k-1}_{loss}(t), \qquad \forall t \in \mathcal{T}, \tag{3.4}$$

is computed after the power flow step, where superscript k indicates the k^{th} iteration of the AC-QP algorithm. The actual change in losses is compared with that predicted from the QP solution,

$$\Delta P^k_{loss\_pred}(t) = \sum_{i\in\mathcal{N}} \sum_{j\in\mathcal{N}} \left[\Big(\frac{\partial P_i}{\partial \theta_j}(t)\Big)^{k-1} \Delta\theta^k_j(t) + \Big(\frac{\partial P_i}{\partial V_j}(t)\Big)^{k-1} \Delta V_j(t)^k \right]. \tag{3.5}$$

If the difference between the predicted and actual losses at each time $t \in \mathcal{T}$ is within a specified tolerance (a suitable value being 10%), the linearization is considered sufficiently accurate. Otherwise, the linearization is of questionable accuracy, and all decision variable limits in the QP at the next iteration are reduced by a scaling factor, denoted $d(k)$ for iteration k. If after the next QP–(power flow) iteration the linearization is again insufficiently accurate, the scaling factor $d(k)$

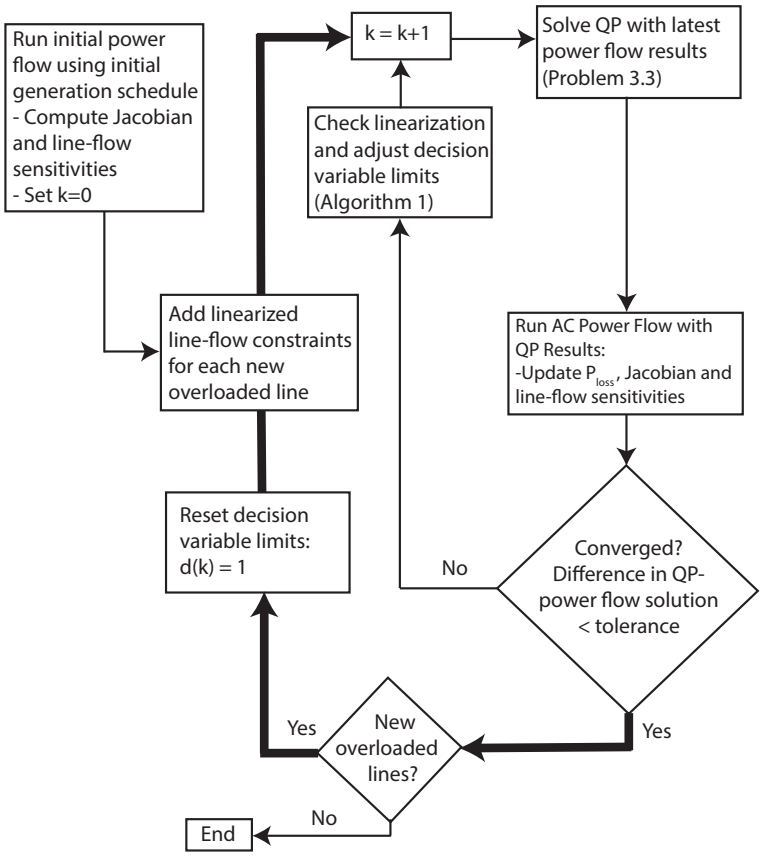

Figure 3.2: Flowchart for the AC-QP OPF algorithm with a trust region step.

is further reduced by a constant, denoted Sc in Algorithm 1. (A value of $Sc = 0.5$ was used in this work.) If the linearization provides acceptable accuracy though, $d(k)$ is increased according to $d(k+1) = \min(2 \times d(k), 1)$.

This process reduces the magnitude of the changes from the previous AC power flow solution that can be scheduled by the QP. As the decision variable step size at each iteration shrinks until the linearization is sufficiently accurate, this improves the convergence of the inner loop of the method. If the outer loop is required because new lines become overloaded, decision variable limits are reset to their original values (i.e. $d(k) = 1$) and the process repeats.

Often convergence can be further improved by reducing the range of values that appear in the admittance matrix. This is achieved by removing low-impedance lines (i.e., lines with impedance less than 1×10^{-3} pu) by merging the connected buses; the method described in [45] was used in this work. This is similar to the preprocessing steps used in many commercial software packages, for example [46].

The traditional AC-QP OPF solution method has been extended to a multiperiod setting to

include both renewable generation and energy storage devices. The algorithm is used to solve Problem (2.1), including the nonconvex power balance and line flow constraints. Moreover, a trust region step has been developed to improve the convergence rate of the proposed method. An improved initialization method to further improve the convergence of this algorithm, as well as the optimality of the final solution, is proposed in Chapter V. This formulation is extended in Chapter IV, which presents a technique for solving the nonconvex storage complementarity constraint in Problem (2.1).

CHAPTER IV

Enforcing Storage Complementarity

From an optimization perspective, the addition of storage devices into power system models presents unique challenges that must be addressed. One issue of particular importance that is addressed in this work is complementarity between charging and discharging of storage devices. There are situations where simultaneous charging and discharging would reduce overall operating costs. In particular, such a cost reduction would be achieved by allowing simultaneous charging and discharging whenever a storage device was located at a bus with a negative "Locational Marginal Price" (i.e., a negative-valued Lagrange multiplier associated with the active power balance constraint (2.1t)). From a purely mathematical point of view, producing solutions that result in devices simultaneously charging and discharging is not a problem. However, such solutions are not physically meaningful. Explicitly enforcing this complementarity in the OPF problem would require adding constraint (2.1k) for every storage device in the network, which would require integer variables in implementation.

Storage charging and discharging complementarity within the QP in Chapter III is an example of a broader class of problems, namely quadratic programs with complementarity constraints (QPCCs) [47]. This set of problems has been widely researched, and many algorithms have been developed to solve them. If the problem has m complementarity constraints, a straightforward but inefficient way to solve the problem is through full enumeration of the possible constraint values satisfying complementarity. However, practical solution techniques seek to avoid such enumeration. One possibility is to use a semidefinite programming heuristic to find a suitable subset of the 2^m possible quadratic programs to solve, and select an optimal solution from the results of that subset [48]. Another broad class of solution methods often used for these problems include sequential quadratic programming [49]. Still others include a modified logical Benders' decomposition to generate cuts of

the feasible region, sparsification to form a quadratic relaxation of the original QPCC, and penalty function methods that maintain convexity but satisfy complementarity at optimality [50].

Instead, an iterative approach that does not require the use of integer variables and does not increase the complexity of the original QP is proposed. Moreover, because the AC-QP OPF is already an iterative algorithm, the proposed approach does not change the type of problem being solved or nature of the method (iterative as compared to non-iterative). However, the resulting solutions are physically meaningful, and reveal at optimality the charging/discharging patterns for storage devices.

The initial (dis)charging status of each storage device $i \in \mathcal{S}$ at each time step $t \in \mathcal{T}$ is determined by the net value of charging/discharging in the initial storage (dis)charging schedule. When in charging mode, the status is enforced in the QP by setting the discharging limit $R_{d,i}^{max}(t)$ to zero, with $R_{c,i}^{max}(t)$ taking its proper value. Adding this check after the first iteration enforces complementarity between storage charging and discharging explicitly, ensuring physically meaningful solutions. However, this assignment of a device's charge/discharge status at the first iteration may not be optimal for subsequent iterations. To account for the fact that in subsequent iterations it may be optimal for a storage device to switch its status, additional checks are added.

If the QP solves to a non-zero value of $r_{c,i}(t)$, the status remains unchanged for the next AC-QP iteration. If, however, the QP solves to the zero limit $r_{c,i}(t) = 0$ and the Lagrangian multiplier corresponding to that lower inequality constraint is positive[1] then the status is changed to discharging for the next iteration of the AC-QP algorithm. Likewise for transitioning from discharging to charging.

This algorithm enforces complementarity explicitly, due to the fact that at every iteration exactly one of the device charging or discharging upper limits is modified to force the corresponding variable to zero. Additionally, the algorithm allows for device status switching between iterations. Therefore this algorithm produces optimal solutions to the OPF problem but maintains linearity of the constraints in the problem being solved. Thus, constraint (2.1k) is enforced in an iterative manner. A more detailed discussion of this process can be found in [51]. Figure 4.1 shows the AC-QP OPF algorithm with this additional processing step to enforce storage complementarity.

[1] A positive Lagrangian multiplier indicates that the cost would be reduced by moving beyond the limit.

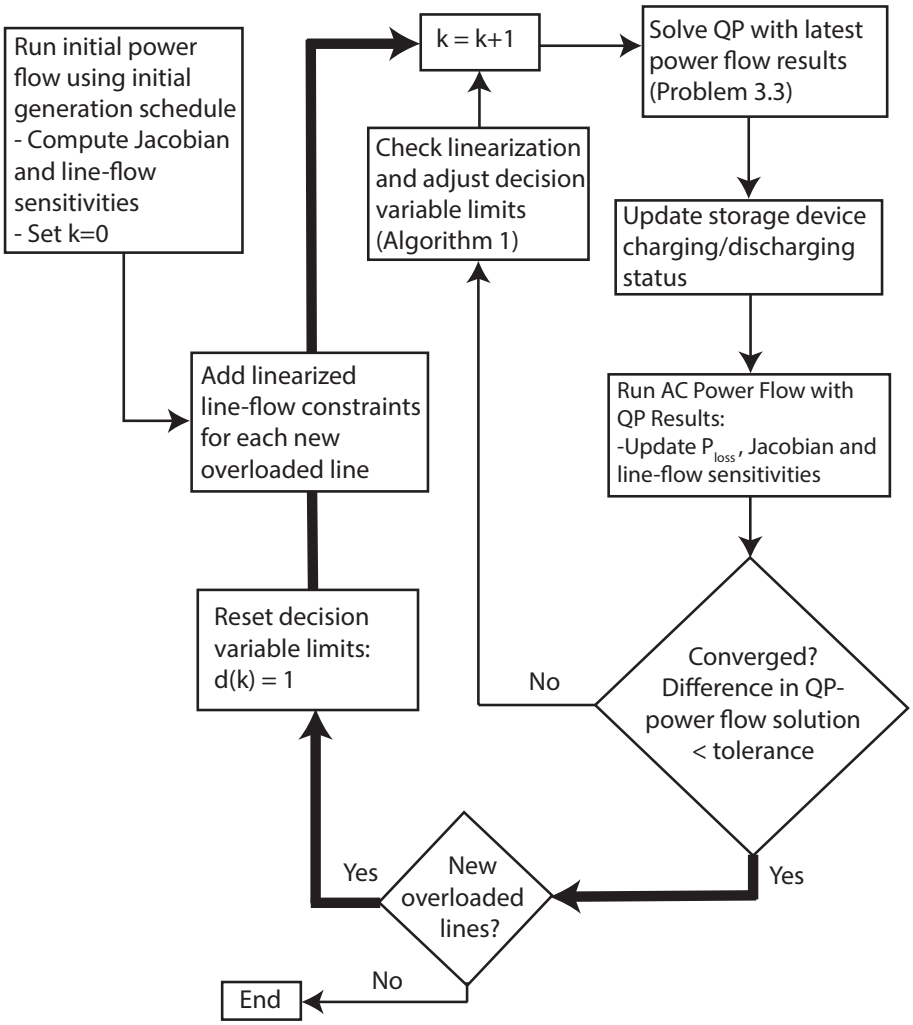

Figure 4.1: Flowchart for the AC-QP OPF algorithm enforcing storage complementarity.

4.1 An Indicative Example

The proposed method for enforcing storage complementarity was tested on a modified RTS-96 system [52]. The RTS-96 system is comprised of three symmetric areas with 73 nodes and 120 lines. Significant wind generation was added to area 1 of the system, with lesser wind added in areas 2 and 3. Correspondingly, traditional generators were removed from service in area 1 and to a lesser extent in area 2. In total, 19 wind locations were added in the system. Four storage devices were also added at locations throughout the system.

The test case assumes that a unit commitment (UC) has previously been run using day-ahead demand and wind forecasts. This UC produces a schedule of generators that are in service. The OPF then runs every 15 minutes or so, using up-to-date forecasts of demand and wind to establish

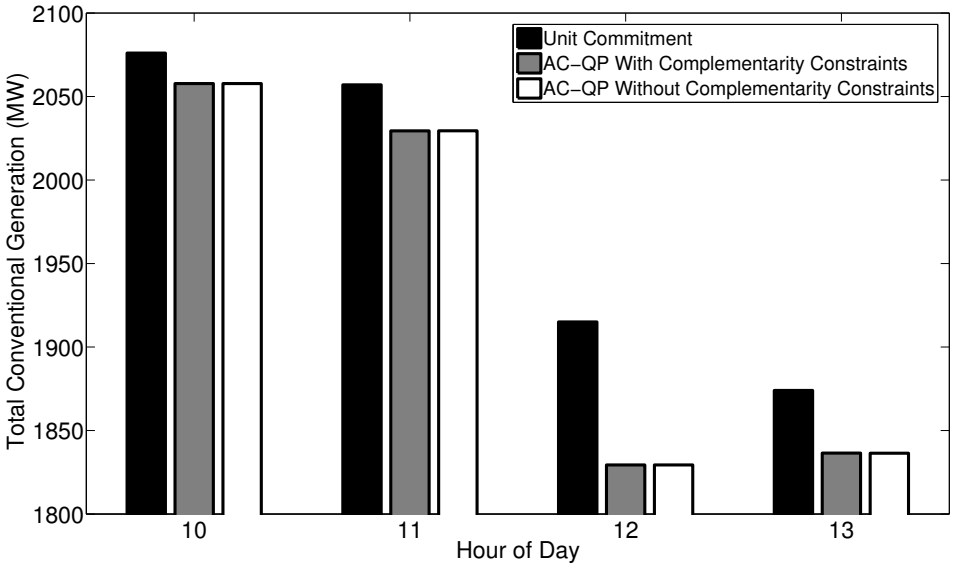

Figure 4.2: Total Conventional Generation.

the most economical real-time operating conditions.

The AC-QP OPF algorithm was run with and without storage complementarity being enforced, to explore how the solution quality might change. Figures 4.2 to 4.4 show the results for hours 10-13 of day 1 of the RTS-96 system data. Online generation is scheduled as shown in Figure 4.2, storage devices are scheduled as in Figures 4.3 and 4.4, and available wind generation is scheduled to maintain power balance. Figure 4.3 shows the total change in state-of-charge across all devices at each hour, and Figure 4.4 shows the total net power demand for all storage devices at each hour. Figure 4.2 shows the effect on the scheduling of conventional generation, and therefore total cost, of adding storage complementarity constraints. It should be noted that there is a negligible effect on the generation schedule when complementarity is enforced. However, the solution is only physically realizable with this additional consideration.

Figures 4.3 and 4.4 highlight an important phenomenon that can occur when simultaneous charging and discharging is observed. Examining the results in Figure 4.3, with and without complementarity enforced, the change in state-of-charge at each hour is nearly equal. However, the corresponding results in Figure 4.4 indicate that for the same change in state-of-charge, storage devices appear to the network as much larger loads when simultaneous charging and discharging occur. In other words, when complementarity is not enforced, solutions that undergo simultaneous charging and discharging will always underestimate the state-of-charge, as proven in [53].

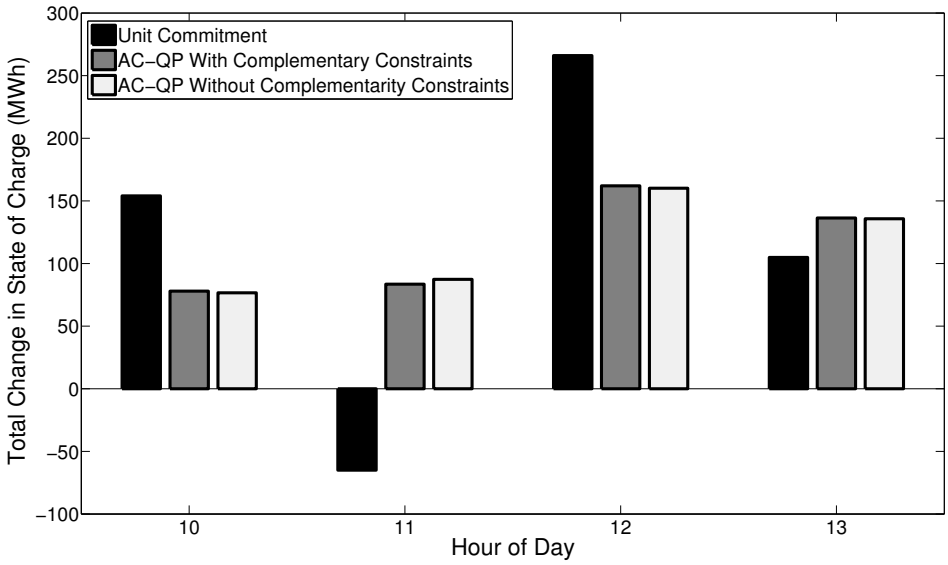

Figure 4.3: Total Change in State of Charge.

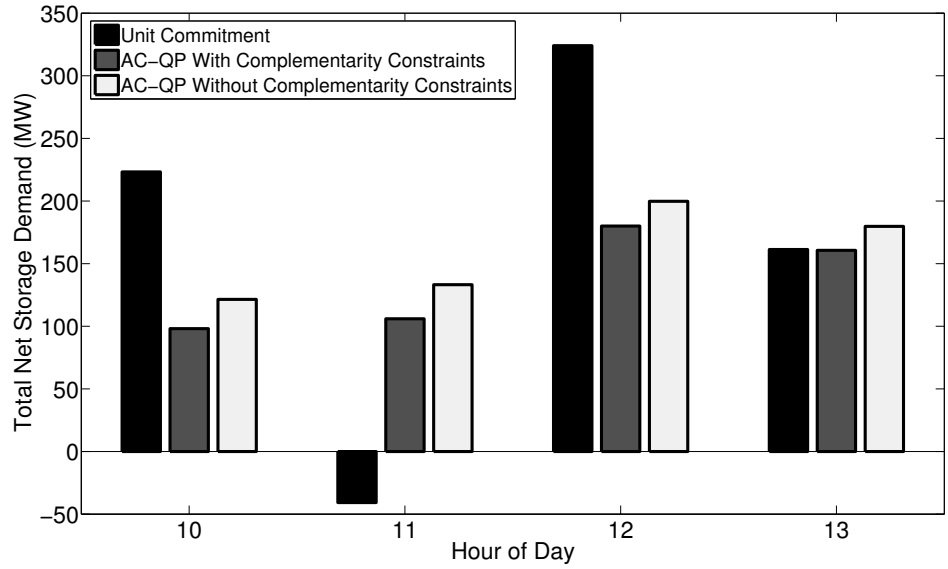

Figure 4.4: Total Storage Demand.

4.2 Conclusions

The AC-QP algorithm from Chapter III has been extended to address the challenges associated with adding storage in OPF formulations, namely including temporal coupling over the time

horizon and complementarity between storage charging and discharging. The latter ensures that solutions obtained from this solution method are physically realizable. Compared with other solution methods used for quadratic programs with complementarity constraints (QPCCs), the proposed method is simple to implement and does not increase the complexity of the original OPF problem. Moreover, the proposed method maintains the convergence properties of the AC-QP problems. The current implementation relies upon a single choice of the optimization horizon, $\mathcal{T}$. The sensitivity of the optimality of the OPF solution and of the total execution to the choice of this horizon is examined in Chapter VI.

CHAPTER V

Improved AC-QP Initialization with an SOCP Relaxation

The performance of the AC-QP algorithm in Chapter IV is greatly improved by an initialization near the global optimum. One such initialization comes from the solution of a second order cone program (SOCP) relaxation of the OPF problem. The SOCP solution provides the power injections $P_g(t)$, $Q_g(t)$, $P_w(t)$, $r_c(t)$, $r_d(t)$ and voltage magnitudes that are used for the initial power flow. Additionally, voltage angle differences across each line in the network are calculated from the apparent power line flows and voltage magnitudes. Based on those angle differences, a least-squares problem then establishes a best fit for the voltage angles at all nodes in the network. This provides an initialization for voltage angles. The voltage magnitude and angle schedules from the SOCP initialization are particularly useful when applying the AC-QP algorithm to large systems, where obtaining a converged AC power flow can be challenging. Moreoever, as the SOCP relaxation that follows lower bounds the optimal objective value of (2.1), it forms a convenient measure of the AC-QP solution quality.

5.1 SOCP Relaxation of the Multiperiod OPF Problem

Recall that the multiperiod OPF problem in (2.1) is a nonconvex optimization problem due to the nonlinear power flow equations (2.1t) and (2.1u) as well as the complementarity constraint (2.1k) that prevents simultaneous charging and discharging of the storage devices. This section addresses both sources of nonconvexity to form a convex relaxation of (2.1).

5.1.1 SOCP Relaxation of the Power Flow Equations

Recent research efforts have developed a diverse variety of convex relaxations of the power flow equations, with trade-offs in computational tractability and tightness. In order to initialize the

AC-QP algorithm, a convex relaxation with fast computational speed is desired. Therefore the "branch-flow model" (BFM) relaxation of the power flow equations from [54] was selected. The BFM relaxation has beneficial numerical characteristics relative to another SOCP relaxation based on a "bus-injection model" [55] and is faster than other convex relaxations based on semidefinite programming (e.g., [11, 12, 14, 18]).

The BFM approach in [54] relaxes the DistFlow equations [56], which formulate the power flow equations in terms of active power, reactive power, and squared current magnitude flows, $P_{ij}(t)$, $Q_{ij}(t)$, and $L_{ij}(t)$, respectively, out of terminal i for each line $(i,j) \in \mathcal{L}$ as well as squared voltage magnitudes $V_i(t)^2$ at each bus $i \in \mathcal{N}$ and time $t \in \mathcal{T}$. Note that the time dependence of the rest of the equations in this section is suppressed for brevity.

To derive the BFM relaxation, begin with the relationship between the active and reactive line flows and the squared current magnitude (see Figure 2.1):

$$L_{ij}V_i^2 = (P_{ij})^2 + (Q_{ij})^2 . \tag{5.1}$$

To form an SOCP, (5.1) is relaxed to an inequality constraint:

$$L_{ij}V_i^2 \geq (P_{ij})^2 + (Q_{ij})^2 . \tag{5.2}$$

Using $(\cdot)^*$ to denote the complex conjugate operator, the current flow on the series impedance of the Π-circuit model is:

$$I_\pi = \left(\frac{P_{ij} - \mathbf{j}Q_{ij}}{\tilde{V}_i^*}\right)\left(\tau_{ij}e^{-\mathbf{j}\theta_{shift,ij}}\right) - \mathbf{j}\frac{b_{sh,ij}\tilde{V}_i}{2\tau_{ij}e^{\mathbf{j}\theta_{shift,ij}}}. \tag{5.3}$$

The relationship between the terminal voltages is:

$$\frac{\tilde{V}_i}{\tau_{ij}e^{\mathbf{j}\theta_{shift,ij}}} - I_\pi\left(R_{ij} + \mathbf{j}X_{ij}\right) = \tilde{V}_j. \tag{5.4}$$

Taking the squared magnitude of both sides of (5.4) and using (5.1) and (5.3) yields:

$$V_j^2 = \frac{V_i^2}{\tau_{ij}^2} - 2\left(X_{ij}Q_{ij} + R_{ij}P_{ij}\right) - V_i^2 X_{ij}\frac{b_{sh,ij}}{\tau_{ij}^2} + \left(R_{ij}^2 + X_{ij}^2\right)\left(Q_{ij}b_{sh,ij} + \tau_{ij}^2 L_{ij} + \frac{b_{sh,ij}^2 V_i^2}{4\tau_{ij}^2}\right). \tag{5.5}$$

Active and reactive line losses are:

$$P_{loss,ij} = R_{ij}\tau_{ij}^2 L_{ij} + \frac{R_{ij}b_{sh,ij}^2}{4\tau_{ij}^2}V_i^2 + Q_{ij}R_{ij}b_{sh,ij} \tag{5.6a}$$

$$Q_{loss,ij} = X_{ij}\tau_{ij}^2 L_{ij} + \Big(\frac{X_{ij}b_{sh,ij}^2 - 2b_{sh,ij}}{4\tau_{ij}^2}\Big)V_i^2. \tag{5.6b}$$

The active and reactive injections at bus k are:

$$P_k^{SOCP} = \sum_{(k,j)\in\mathcal{L}} P_{kj} + \sum_{(i,k)\in\mathcal{L}} \big(P_{loss,ik} - P_{ik}\big) + g_{sh,k}V_k^2 \tag{5.7a}$$

$$Q_k^{SOCP} = \sum_{(k,j)\in\mathcal{L}} Q_{kj} + \sum_{(i,k)\in\mathcal{L}} (Q_{loss,ik} - Q_{ik}) + b_{sh,k}V_k^2. \tag{5.7b}$$

5.1.2 Relaxation of the Charging/Discharging Complementarity Condition

As discussed in Chapter IV, the complementarity constraint (2.1k) prevents simultaneous charging and discharging of storage devices, which would lead to "fictitious" consumption of energy in devices with non-ideal efficiencies (i.e., $\eta_{c,i}, \eta_{d,i} < 1$). The feasible region for constraint (2.1k) is defined by the red dashed lines on the axes in Figure 5.1. In this work, a convex relaxation of this space is used, which is given by the blue region in Figure 5.1. Mathematically, this constraint is given by (2.1e) and (2.1f) augmented with:

$$r_{c,i}(t) \leq -\Big(\frac{R_{c,i}^{max}}{R_{d,i}^{max}}\Big)r_{d,i}(t) + R_{c,i}^{max} \qquad \forall i \in \mathcal{S}, t \in \mathcal{T}. \tag{5.8}$$

While this formulation allows some degree of simultaneous charging and discharging (i.e., points in the blue region that are not on the red lines in Figure 5.1), it is the most straightforward way to approximate the complementarity constraint. Other techniques for enforcing this constraint have been proposed, including modifying the OPF objective to include a cost for storage (dis)charging, which can be shown to strictly enforce complementarity under certain conditions [57], [58]. Since conditions resulting in simultaneous charging and discharging are relatively rare, the convex relaxation typically provides good initializations and close lower bounds, as demonstrated by the results in Section 5.2.[1]

[1]The complementarity constraint is enforced in the AC-QP algorithm, so the final solution cannot have simultaneous charging and discharging.

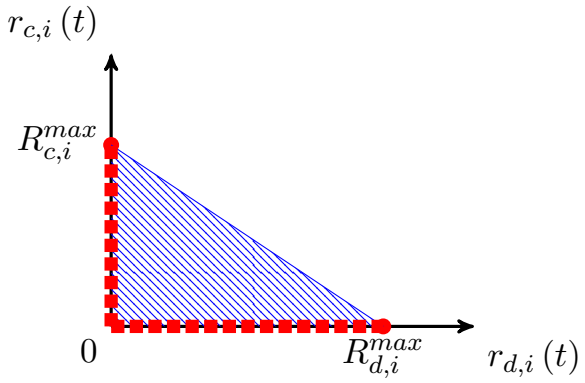

Figure 5.1: Charging/discharging characteristic. The complementarity constraint (2.1k), with feasible space denoted by the red dashed lines, prevents simultaneous charging and discharging. The blue region shows the convex relaxation of the complementarity constraint (5.8) that is used in the SOCP relaxation.

5.1.3 Formulation of the SOCP Relaxation of the Multiperiod OPF Problem

The SOCP relaxation of the multiperiod OPF problem is given by combining the relaxations of the power flow equations and the complementarity constraint:

$$\min_{\substack{w(t),P_g(t),Q_g(t),V(t),P_{ij}(t),Q_{ij}(t),\\ L_{it}(t),P_w(t),r_d(t),r_c(t),e(t)}} \quad \sum_{t\in\mathcal{T}}\sum_{i\in\mathcal{G}} \omega_i\,(t) \qquad \text{subject to } (\forall t \in \mathcal{T}) \tag{5.9a}$$

Eqns. (2.1b)–(2.1j), (2.1m), (5.2), (5.6)–(5.8)

$$1 - c_{1,i}P_{g,i}\,(t) - c_{0,i} + \omega_i\,(t) \geq \left\| \begin{bmatrix} 1 + c_{1,i}P_{g,i}(t) + c_{0,i} - \omega_i(t) \\ 2\sqrt{c_{2,i}}\,P_{g,i}(t) \end{bmatrix} \right\|_2 \qquad \forall i \in \mathcal{G} \tag{5.9b}$$

$$(V_i^{min})^2 \leq V_i(t)^2 \leq (V_i^{max})^2 \qquad \forall i \in \mathcal{N} \tag{5.9c}$$

$$S_{ij}^{max} \geq \left\| \begin{bmatrix} P_{ij}(t) \\ Q_{ij}(t) \end{bmatrix} \right\|_2 \qquad \forall (i,j) \in \mathcal{L} \tag{5.9d}$$

$$S_{ij}^{max} \geq \left\| \begin{bmatrix} P_{loss,ij}(t) - P_{ij}(t) \\ Q_{loss,ij}(t) - Q_{ij}(t) \end{bmatrix} \right\|_2 \qquad \forall (i,j) \in \mathcal{L} \tag{5.9e}$$

$$P_{g,i}\,(t) + P_{w,i}\,(t) + r_{d,i}\,(t) - r_{c,i}\,(t) - P_{d,i}\,(t) = P_i^{SOCP}\,(t) \qquad \forall i \in \mathcal{N} \tag{5.9f}$$

$$Q_{g,i}\,(t) - Q_{d,i}\,(t) = Q_i^{SOCP}\,(t) \qquad \forall i \in \mathcal{N} \tag{5.9g}$$

where $\|\cdot\|_2$ denotes the two-norm. Note that the line-flow limits (5.9d)–(5.9e) and the squared current equation (5.2) are implemented with second-order cone constraints. The quadratic objective is implemented with the auxiliary variables $\omega_i\,(t)$, $i \in \mathcal{G}$, $t \in \mathcal{T}$ and the SOCP constraint (5.9b). The remainder of the constraints are linear. Thus, (5.9) is an SOCP.

Table 5.1: Descriptions of Test Cases

Test Network	**Number of Buses, Lines**	**Number Wind Buses**	**Number Storage Buses**	**Renewable Penetration (%)**
PL-3012wp	2292, 2851	70	300	8.4
30-bus loop	30, 30	5	3	0.0049
PL-2383wp	2177, 2690	60	238	7.3
PEGASE-2869	2487, 4164	70	287	1.3
PL-3120sp	2314, 2886	70	312	10.0
PL-2737sop	2183, 2715	35	274	12.2
WECC	4259, 5868	531	10	45.2

Without consideration of the complementarity constraint (2.1k), the SOCP relaxation is *exact* (i.e., yields the globally optimal solution) for radial networks that satisfy certain non-trivial technical conditions [54]. However, for more general networks such as those considered in the following examples, the relaxation is usually not exact.

5.2 Results and Discussion

Both the SOCP relaxation and AC-QP algorithm have been applied to a variety of test cases. This section presents detailed results for two of these test cases: modified versions of the Polish 3012wp test case [59] and a 30-bus loop network [60]. The scalability of these methods is further demonstrated using five other large test cases (the Polish 2383wp, 2737sop and 3120sp cases [59], the 2869-bus PEGASE network representing portions of the European power system [61], and a 4259-bus model of the Californian region of WECC). A summary of the details of each test case is provided in Table 5.1.

It has been observed that for realistically large-scale networks and a time horizon exceeding 16 time steps, the AC-QP OPF is likely to require solution times longer than 5 minutes, which is a reasonable time limit for on-line applications. Moreover, as will be discussed further in Chapter VI, a moderate horizon of 4 hours (8 step with $T_s = 30$ minutes) is sufficient to obtain the economic benefits of operating storage with renewable generation. All test cases therefore consider a horizon of 4 hours with a time-step of $T_s = 30$ minutes, for a total of 8 time steps. Because renewable generation may change more rapidly than this 30-minute time step, in an operational setting this algorithm could be re-run frequently (every 5 to 10 minutes) using a receding horizon strategy [62] to account for deviations in measured and forecast generation.

Storage and wind generation were added to each test network at randomly chosen buses. As the

focus of this work is to provide an improved initialization for the AC-QP OPF method, the purpose of adding storage and wind in these cases is to exercise the multiperiod OPF formulation. It should be noted that the only temporal coupling in this problem is due to the presence of energy storage. Without such devices, a multiperiod formulation is unnecessary. The available wind $W_i^{max}(t)$ at each wind bus was chosen from a uniform random distribution over the range 1 to 100 MW. The corresponding renewable penetration of each test case, which is calculated as the total available wind generation as a percentage of total conventional generation capacity, is given in the final column of Table 5.1. This forecast of available wind at each location is assumed to be perfect, as this work relies upon a deterministic OPF formulation.[2] Storage device power ratings were chosen from a uniform distribution of 1–5 MW, and storage device energy ratings were chosen from a uniform distribution of 1–20 MWh. Table 5.1 provides additional details for these test cases.

Three initialization approaches for the AC-QP algorithm were tested. The first used the generation and voltage schedules provided in the test case description. With this method, storage and wind are unused in the initialization (i.e., no charging or discharging and full wind curtailment). The second is a DC OPF that approximates total system losses as 3% of total load (i.e., the DC power balance constraint at each bus is modified to include an additional 3% of the demand and storage charging at that bus to account for system losses). The final initialization method is the SOCP relaxation.[3] Note that the first step of the AC-QP method is to solve a power flow using this initial operating point. The algorithm thus begins from a full AC power flow solution, regardless of the choice of initialization.

The formulations were implemented in MATLAB R2012a and solved on a MacBook Pro with a quad-core Intel i7 2.3 GHz processor with 16 GB of 1600 MHz DDR3 RAM using MOSEK version 7.0 to solve the SOCP programs and Gurobi version 5.6.3 to solve the quadratic programs. A Newton algorithm was used to solve the power flows.

The results in this section demonstrate the computational tractability and solution quality for the proposed approach of using the SOCP initialization with the AC-QP algorithm.

[2]Note that this deterministic OPF can be embedded in a receding horizon strategy to account for variability and uncertainty. Furthermore, such deterministic OPF problems form the basis of many stochastic OPF formulations. Integrating the proposed approach into stochastic OPF methods is discussed in Chapter VII.

[3]In an on-line environment, the state estimator solution would be available to initialize the OPF. As a surrogate, an initialization based on the single-time-step OPF solution at $t = 0$, copied to each later time step, was also considered. The results indicated that this approach was generally inferior to the initialization from the SOCP relaxation in both computation time and solution quality. Inferiority of the single-step initialization is attributable to the fact that it does not consider the forecast of future wind availability and the corresponding changes in storage utilization, both of which are available to other initialization methods.

5.2.1 Case 1: Polish 3012wp Network

The convergence and computation time of the AC-QP algorithm are substantially improved by accurately predicting which line-flow constraints need to be explicitly enforced in the QP (i.e., determining the set $\mathcal{L}^*$ in Problem (3.3)). The initial set of line-flow constraints is highly dependent on the choice of initialization. This first test case emphasizes an important benefit of the SOCP initialization method: compared to the other initializations, the power flow solution resulting from the SOCP initialization more accurately predicts the set of line-flow constraints that must be included in the QP. Consequently, fewer outer loops of the AC-QP algorithm (the bold path in Figure 4.1) are required, reducing the number of QP–(power flow) iterations and hence the computation time.

The results of the Polish 3012wp test case are summarized in Tables 5.2–5.3. For each initialization method, the second column of Table 5.2 gives the line index for line-flow constraints that are added to the QP. The lines shown in parentheses were not identified from the initial power flow, but were added through additional outer loops as they became overloaded in subsequent iterations of the AC-QP algorithm. Compared with the other methods, the SOCP initialization performs better in two aspects: 1) it requires the fewest number of explicitly enforced line-flow constraints, which reduces the time required to solve the QP at each iteration, and 2) the initial set of line-flow constraints is sufficient throughout the AC-QP iterations (i.e., no additional outer loops of the AC-QP algorithm are required). The third column of Table 5.2 demonstrates that regardless of the initialization procedure, the same line constraints are binding in the final solution for this test case. Only the SOCP initialization yields a superset of the binding line-flow constraints.

Table 5.2: PL-3012wp: Explicitly Enforced Line-Flow Constraints

Initialization Method	**Initial Lines (Additional Lines)**	**Line Limits Binding at Soln.**
Case description	324, 331, 529, 813, 1411, 1412, 1436, 1833, 2225, (231), (495), (1367), (1388), (1519), (2829)	231, 495, 529, 1367, 1388, 1519, (2829)
DC OPF	231, 495, 542, 813, 1367, 1388, 1519, 1718, 1833, 1878, 2233, 2473, 2608, 2829, (529)	231, 495, (529), 1367, 1388, 1519, 2829
SOCP	231, 495, 529, 542, 813, 1367, 1388, 1519, 1833, 2233, 2473, 2829	231, 495, 529, 1367, 1388, 1519, 2829

Table 5.3: PL-3012wp: Convergence and Execution Time

Initialization Method	**Number of QP–(power flow) iterations**	**Init. Time (sec)**	**AC-QP Time (sec)**	**Total Time (sec)**
Case Description	7	–	111	111
DC OPF	7	18	107	124
SOCP	4	19	58	77

Table 5.3 indicates that the SOCP initialization offers appreciable performance improvements over the other forms of initialization. The SOCP method eliminates the need for additional outer loops to add line-flow constraints not initially identified, thus reducing the total number of iterations, as shown in the second column. Explicitly enforcing fewer inequality constraints reduces the QP's solution time at each iteration. These two factors greatly reduce the solution time of the AC-QP algorithm, as demonstrated in the fourth column of this table. The fifth column shows that SOCP initialization results in a total computation time that is substantially less than the other methods. These timing results also highlight the scalability of these methods for large networks.

The objective value of the SOCP relaxation lower bounds the generation cost, thus providing a useful metric for assessing the quality of the solution obtained from the AC-QP algorithm. For this example, the SOCP gave a lower bound of 13.602 M$ on the cost of generation. All three initialization processes resulted in convergence to the same total cost of generation of 13.618 M$, implying a relaxation gap of at most 0.12%. Thus, the AC-QP solution is at least very close to being globally optimal, and may, in fact, be the global optimum.[4] Even though all initialization methods resulted in equivalent dispatches, the choice of initialization process significantly affected the solution time and the number of iterations required to reach that solution.

5.2.2 Case 2: 30-Bus Loop Network

The SOCP initialization is also useful for cases where the AC-QP algorithm finds a local solution rather than the global optimum. The AC-QP algorithm provides neither a guarantee of finding a global solution nor a metric for assessing solution quality. As shown in [60], OPF problems may have multiple locally optimal solutions. Tables 5.4–5.5 provide results for a modified multiperiod version of the 30-bus loop test case from [60] that demonstrate the utility of the SOCP initialization for both finding a global solution and providing a metric of solution quality.

[4]This gap can be at least partially attributed to relaxations of the power flow equations (5.9f),(5.9g) and the simultaneous charging/discharging constraint (5.8). For several test cases, solutions to the relaxation (5.9) exhibited simultaneous charging and discharging at some buses.

Table 5.4: 30-Bus Loop: Generation Cost

Initialization Method	SOCP Lower Bound ($)	AC-QP Cost ($)	% Cost Difference
Case description	23,840	31,577	32.5 %
DC OPF	23,840	26,759	12.2 %
SOCP	23,840	23,840	0.0011 %

Table 5.5: 30-Bus Loop: Total Generation and Losses

Initialization Method	AC-QP Total Generation (MW)	AC-QP Total Losses (MW)
Case description	15,788	3,937.5
DC OPF	13,380	1,526.5
SOCP	11,920	69.3

As shown in Table 5.4, initializing the AC-QP algorithm using the case description or the DC OPF results in solution costs that are significantly higher than the SOCP lower bound, while the SOCP initialization gives a cost that is within 0.0011% of the lower bound.[5] Using the lower bound from the SOCP relaxation as an indicator of solution quality, it is reasonable to assert that the solution resulting from the SOCP initialization is sufficiently close to the global optimum, while the other two solutions are locally optimal solutions.

In this example, the suboptimal solutions resulting from the DC OPF and case description initializations have power circulating around the loop while the global solution does not. As shown in Table 5.5, this circulating power results in greatly increased losses. Substantially more generation is required, incurring higher cost. Moreover, as each branch has a relatively small angle difference, identifying such local optima may be difficult in more general problems. Similar phenomena have been observed in actual systems, as described in [63].

The example demonstrates the value of the SOCP relaxation: 1) it provides a sufficient condition for quickly assessing whether a solution to the AC-QP algorithm has an objective value that is close to the globally optimal value, and 2) SOCP initialization results in a globally optimal solution for this case.

5.2.3 Other Large Test Cases

The AC-QP algorithm with its various initializations was also applied to other large test cases, including a 4259-bus model of the WECC system, to assess performance on networks of various

[5]The SOCP relaxation does not always yield a lower bound that is close to the global optimum (e.g., the lower bound from the SOCP relaxation of the nine-bus system in [60] is 11% below the global optimum identified in [15]).

sizes and topologies. An 8-step time horizon was used in all cases. The details of these test cases are given in Table 5.1, and the results are summarized in Tables 5.6–5.9. Tables 5.6 and 5.7 show the convergence results of each test case and each initialization method. In each case, the SOCP initialization method improves the convergence rate of the AC-QP algorithm, requiring a smaller number of iterations and achieving the fastest total execution time. The computational improvement is particularly significant for the PEGASE-2869 and PL-3120sp test cases. It is important to note that these execution time improvements are achieved by changing only the initialization procedure.

Initialization of the WECC case is particularly challenging. The initial power flow of the AC-QP algorithm did not converge when initialized using the case description or the DC OPF. This resulted in failure of the AC-QP algorithm. In contrast, SOCP initialization provides close-to-feasible initial conditions that result in convergence of the initial power flow (and subsequently of the AC-QP algorithm). Note that the execution time for the WECC case is fast enough for use in a practical on-line setting, although including other features, such as contingency constraints, requires further work.

Table 5.8 gives the total cost of generation while Table 5.9 provides the corresponding percent difference in generation cost between the lower bound of the SOCP relaxation and the AC-QP solution. In all cases, the SOCP initialization yields the AC-QP solution with generation cost closest to the SOCP lower bound. It therefore provides a more economic operating point than those resulting from the other two initializations. Note, however, that the small differences in Table 5.9 may be due in part to the termination criterion used in the AC-QP algorithm.

The case PL-2383wp is of particular interest due to larger cost variations among the different initialization methods. Figure 5.2 shows the total storage (dis)charging across all storage devices, as well as the total wind generation across all wind nodes at each time step in the OPF horizon. Taking the AC-QP solution initialized with the SOCP as a reference, the results presented are normalized to show the difference in each solution for the various initialization algorithms. Looking at the storage (dis)charging results over the 8-step horizon, the solution from the DC OPF initialization generally makes less use of storage. As a consequence, less wind generation can be used to meet demand, resulting in higher cost of operation. This highlights the economic value of optimally scheduling storage in conjunction with renewable generation.

Table 5.6: Number of Iterations for Test Cases

Test Network	Case Description Init.	DC OPF Init.	SOCP Init.
PL-2383wp	8	5	5
PEGASE-2869	8	8	4
PL-3120sp	11	7	5
PL-2737sop	6	6	3
WECC	–	–	4

Table 5.7: Total Execution Time (Seconds)

Test Network	Case Description Init.	DC OPF. Init.	SOCP Init.
PL-2383wp	97	77	78
PEGASE-2869	127	149	87
PL-3120sp	159	126	98
PL-2737sop	81	94	62
WECC	–	–	128

Table 5.8: Total Cost of Generation for Test Cases

Test Network	SOCP Lower Bound (M$)	Case Description Init. (M$)	DC-OPF Init. (M$)	SOCP Init. (M$)
PL-2383wp	8.58	8.61	8.65	8.60
PEGASE-2869	0.875	0.882	0.879	0.878
PL-3120sp	11.2	11.2	11.2	11.2
PL-2737sop	6.44	6.47	6.47	6.47
WECC	0.208	–	–	0.208

Table 5.9: Percent Cost Difference (%) for Test Cases

Test Network	Case Description Init.	DC-OPF Init.	SOCP Init.
PL-2383wp	0.40	0.82	0.23
PEGASE-2869	0.72	0.43	0.27
PL-3120sp	0.30	0.30	0.30
PL-2737sop	0.37	0.37	0.37
WECC	–	–	0.03

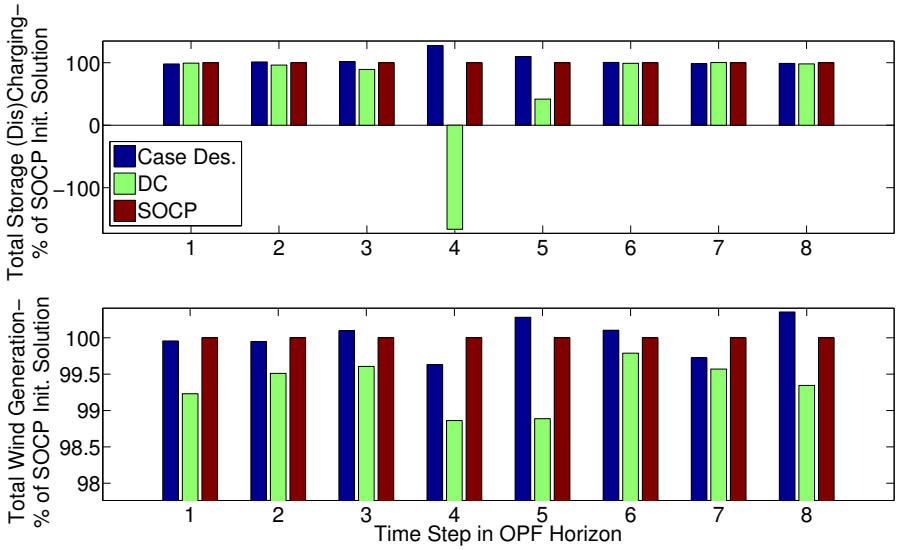

Figure 5.2: An example of differing use of storage and wind resulting in local minima.

5.3 Conclusions

An AC OPF solution method that uses an SOCP relaxation to initialize an AC-QP successive linearization algorithm has been proposed. The SOCP provides initial values for the decision variables (traditional and renewable generation, and energy storage charge/discharge values) along with approximate values for all voltage magnitudes and angles across the network. These values are particularly useful for achieving convergence of the initial power flow in the AC-QP algorithm. The resulting initial solution often lies in the vicinity of the globally optimal solution.

The proposed SOCP initialization offers several benefits over other approaches. The SOCP relaxation often provides an accurate prediction of the subset of line-flow constraints that require explicit representation in the QP. This reduces both the total number of iterations needed in the AC-QP algorithm as well as the number of inequality constraints in the QP. These factors improve the solution time of the AC-QP algorithm. The SOCP initialization reduces the likelihood of the AC-QP algorithm converging to a local optimum that is far from the global solution. Furthermore, the lower bound on the OPF objective given by the SOCP relaxation provides an indication of the quality of the AC-QP solution. A small "gap" between the SOCP lower bound and the AC-QP solution indicates that a nearly globally optimal outcome has been achieved.

The algorithm has been applied to a variety of multiperiod OPF test cases that incorporate wind and storage resources. The results indicate that this approach scales well, with tractability demonstrated for large-scale test cases up to 4259 buses and 8 time-steps. This choice of the number of time steps used in the OPF formulation is explored further in Chapter VI.

CHAPTER VI

Choice of Optimization Horizon

Without constraint (2.1i) on the final state-of-charge, the OPF problem will typically use storage in a greedy manner, fully discharging the storage device to minimize operational cost within the time horizon. This is of particular importance for shorter horizon choices, which may suffer from their short-sighted nature. This chapter explores one method for implementing constraint (2.1i) and choosing e_i^{term}, as well as its impact on solution quality.

6.1 Avoiding the Greedy Use of Storage

A penalty term is added to the generation cost term of the OPF objective to avoid the greedy use of storage and enforce constraint (2.1i) as a soft constraint. The modified objective is then given by,

$$\min_{\substack{\Delta P_g(t),\Delta Q_g(t),\Delta\theta(t),\Delta V(t),\\ \Delta P_w(t),e(t),\Delta r_c(t),\Delta r_d(t)}} \quad \sum_{t\in\mathcal{T}}\sum_{i\in\mathcal{G}} C_i\big(P_{g,i}^0(t)+\Delta P_{g,i}(t)\big) + \gamma\sum_{i\in\mathcal{S}} \|e_i(T) - e_i^{term}(T^{term})\|_2^2 \quad (6.1)$$

Note that the constraints in the QP solved at each iteration of the AC-QP algorithm are those given in Problem 3.3, with constraint (3.3j) removed. The intuitive use of storage is to charge devices during low demand and high renewable periods of the day, and then discharge them during high demand and low renewable periods to achieve peak shaving and reduce the total operating cost. However, shorter horizons may not achieve this desirable behavior, as the valley and peak periods are not visible within the reduced optimization horizon.

To address this problem, a reference storage usage pattern can be determined by solving a

higher level problem, such as unit commitment, that performs an optimization over a sufficiently long horizon. The approach adopted has been to establish this reference trajectory by solving a higher-level, approximate, storage allocation problem using six 4-hour time steps.

The multiperiod OPF seeks to minimize the total generation cost over the horizon of interest. To do so, it can use storage freely, and only incurs a penalty cost if the state of charge of each storage device at the end of the horizon deviates from the reference usage pattern. This terminal penalty also ensures fair usage of storage devices over the entire day. As storage devices begin the 24 hours charged to half of their energy rating, they should be returned to that initial value at the end of the 24-hour period. This is achieved by varying the penalty coefficient γ throughout the 24 hours, depending on the time at the end of the OPF horizon (denoted T^{term}), according to the following scheme:

$$\gamma = \begin{cases} 10^2, & T^{term} \in [1, 15] \\ 10^3, & T^{term} \in (15, 17] \\ 10^4, & T^{term} \in (17, 19] \\ 10^5, & T^{term} \in (19, 21] \\ 10^6, & T^{term} \in (21, 24] \\ 10^2, & T^{term} > 24. \end{cases} \tag{6.2}$$

This coefficient is relatively low for the first part of the day and then gradually increases as the day progresses. The specific values given above are designed such that the largest coefficient is of the same order of magnitude as the cost of conventional generation. Additionally, including several steps to increase this penalty coefficient ensures a relatively smooth transition to return storage energy levels at the end of the 24 hours to their initial values. Moreover, the very large coefficient over the last few hours ensures that if it is feasible to do so, the state of charge of each storage device will be returned to its initial value. While this policy ensures fair usage of storage devices, it may impact the optimality of the final solution.

6.2 Test Cases

Two test cases are presented to assess the performance of the proposed method. They are both based on a modified version of the Polish 3012wp network from [59]. This system has been augmented with both wind nodes and storage devices. Three hundred storage devices were placed

at randomly chosen locations within the network. The maximum (dis)charging rating and energy rating of each device were then chosen from a uniform random distribution over the ranges 1–5 MW and 1–20 MWh, respectively. One hundred wind locations were randomly chosen within the network. The available wind at those locations was likewise chosen from a uniform random distribution over the range 1–100 MW. To create a demand profile over 24 hours, the hourly load data provided in the RTS-96 test case description for a summer weekend was used [52]. Both cases are assumed to begin at 7 p.m., just after the midday peak demand period has occurred. Additionally, it is assumed that storage devices begin each 24-hour period charged to half of their maximum energy ratings, and must be returned to that value by the end of the 24-hour period to maintain a fair usage policy. The demand and wind profiles assumed in this case over the course of 24 hours are given by the solid lines in Figure 6.1.

Both test cases presented use the same network description, as well as randomly chosen wind and storage device locations and ratings. The difference between the two cases is in the assumption of load and wind forecast accuracy. Initially, results are presented assuming perfect wind and load forecasts. This test case is used to assess the computational scalability of the method and to demonstrate the sensitivity of the total cost of generation to the OPF horizon chosen. The second test case introduces an event such that the load forecast has significant error, as shown by the dotted line in Figure 6.1. This case highlights the sensitivity of the OPF solution to forecast errors, and considers the effect of horizon length.

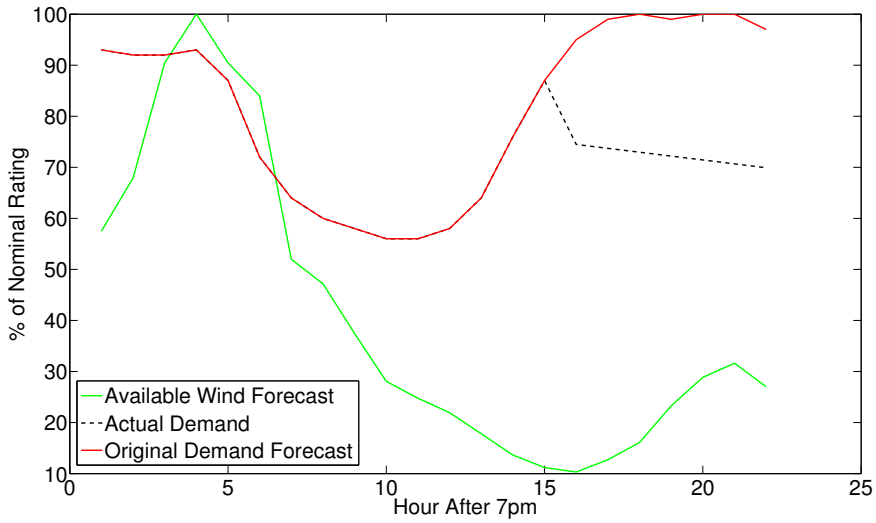

Figure 6.1: Demand and Wind Profiles Used in Both Test Cases

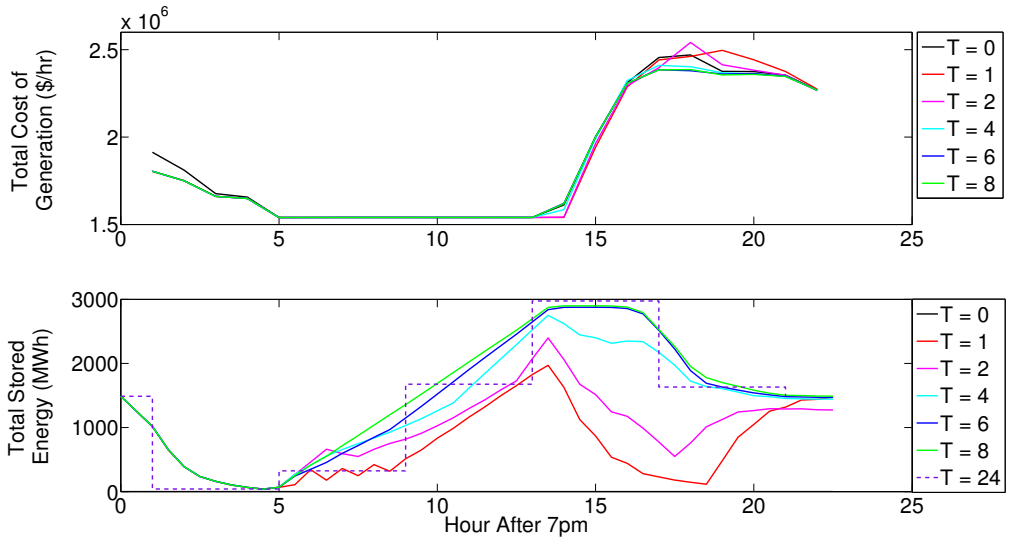

Figure 6.2: Case 1: Cost of Generation and Total Stored Energy Results

6.3 Results and Discussion

6.3.1 Test Case 1: Perfect Wind and Load Forecasts

The results of the first test case are given in Figures 6.2–6.7. Note that the x-axis in these plots gives the hour after 7 pm. As such, this time axis begins with the overnight period at the far left of the plots. Both the total cost of generation and total stored energy of all 300 storage devices over the 24-hour period considered are given in Figure 6.2. The storage state of charge reference pattern over the entire day, denoted by T=24 in the lower figure, establishes the terminal value that is used in the penalty term in the OPF objective function (6.1).

Figure 6.2 demonstrates the improved performance of the longer OPF horizons in scheduling storage (dis)charging. Shorter horizons, such as 1 or 2 hours, result in storage charging over the valley period (hours 7–13) being insufficiently scheduled, such that during the peak demand period (hours 15–24) less storage is available to achieve lower peak operating costs. This highlights the short-sighted nature of these horizons that are unable to anticipate the upcoming peak demand. It should also be observed that these shorter horizons not only charge storage devices to a lower state of charge, but also begin discharging several hours before the peak demand period, contributing to a higher cost of operation. Conversely, longer horizons, such as 4, 6 or 8 hours, successfully charge storage devices to a higher state of charge level before the peak demand period. Storage can then be discharged during the peak periods, resulting in significant cost savings.

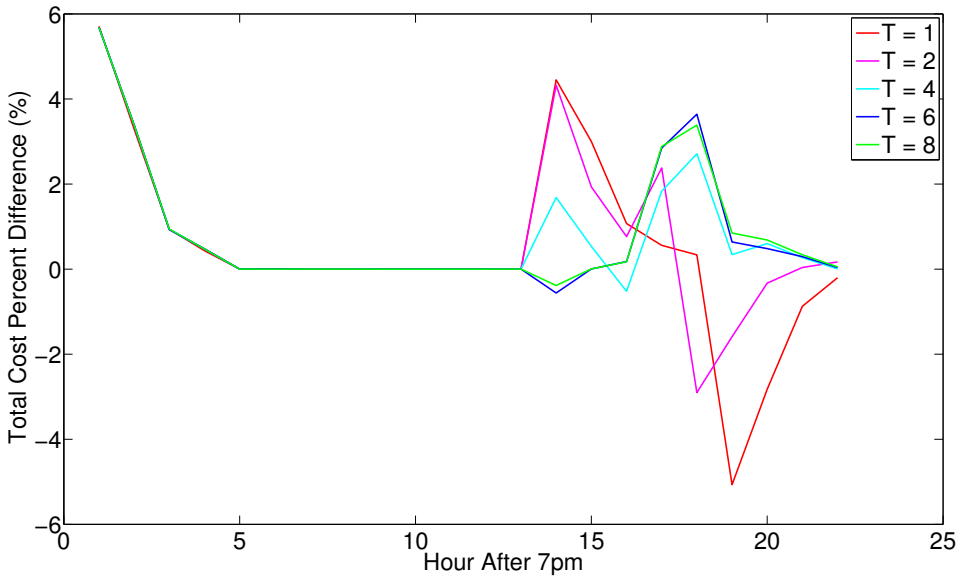

Figure 6.3: Case 1: Hourly Percent Savings Compared to No Storage Case

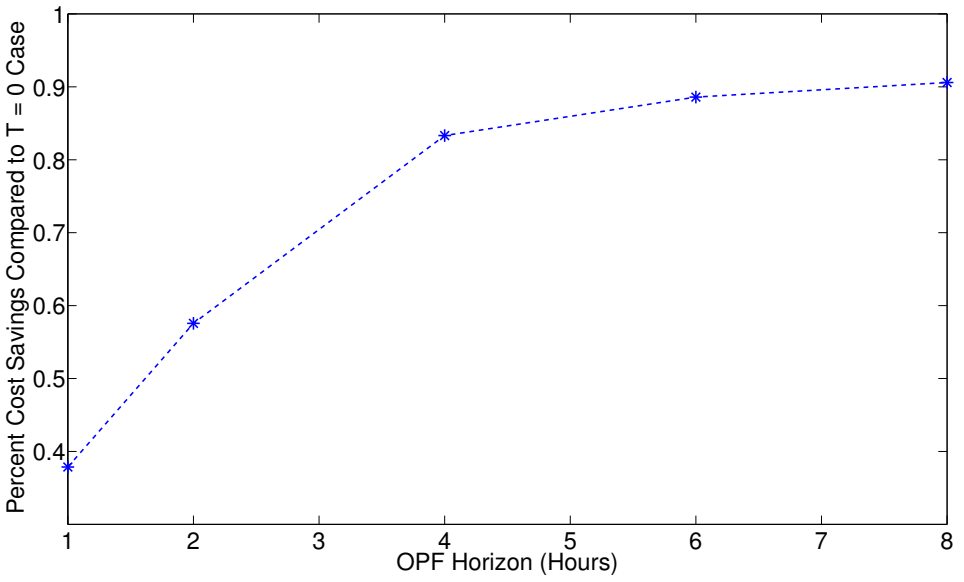

Figure 6.4: Case 1: Total Cost Percent Savings Over 24 Hours for Various Horizons

Figure 6.3 highlights the economic improvement for each horizon tested, relative to the cost of operation with no storage in the network. Both the 1- and 2-hour horizons achieve some cost savings during hours 14–16, but also incur higher cost during the high-demand hours of 19–21, as storage must be charged to return to its initial state of charge. However, using a longer horizon,

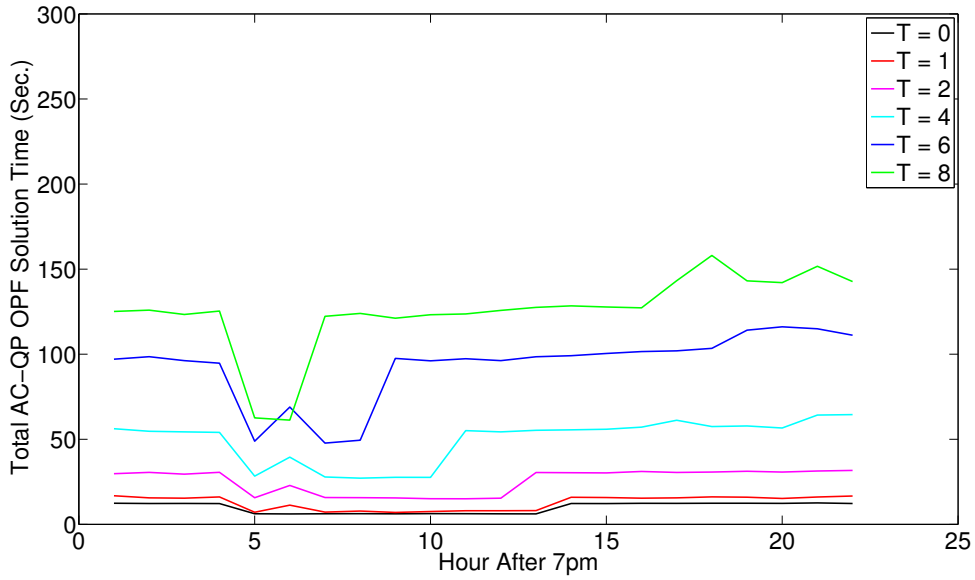

Figure 6.5: Case 1: AC-QP OPF Timing Results

such as 4, 6, or 8 hours, avoids this issue and can achieve cost savings up to 4% during peak demand periods in this case. Figure 6.4 shows the improved cost savings over an entire day that result from optimally scheduling storage (dis)charging. The savings can be up to 0.9% per day in this case. While longer horizons produce higher cost savings, there is a diminishing benefit as the length of the OPF horizon is increased.

Figures 6.5–6.6 show the computation time for various OPF horizons. For real-time OPF applications, an execution time target of 5 minutes is assumed. While longer horizons can schedule storage devices more economically, the computation time of the AC-QP OPF method increases significantly as the horizon increases, as shown in Figure 6.5. Moreover, when the initialization time to solve the SOCP OPF relaxation given in Chapter V is considered in the total computation time, as shown in Figure 6.6, the increase in total time for longer OPF horizons is even more pronounced. Horizons longer than 8 hours have not been considered as they are likely to exceed the 5 minute target assumed for real-time applications. Computation time must be carefully addressed when choosing an appropriate horizon, especially considering the diminishing cost benefits achieved with longer horizons.

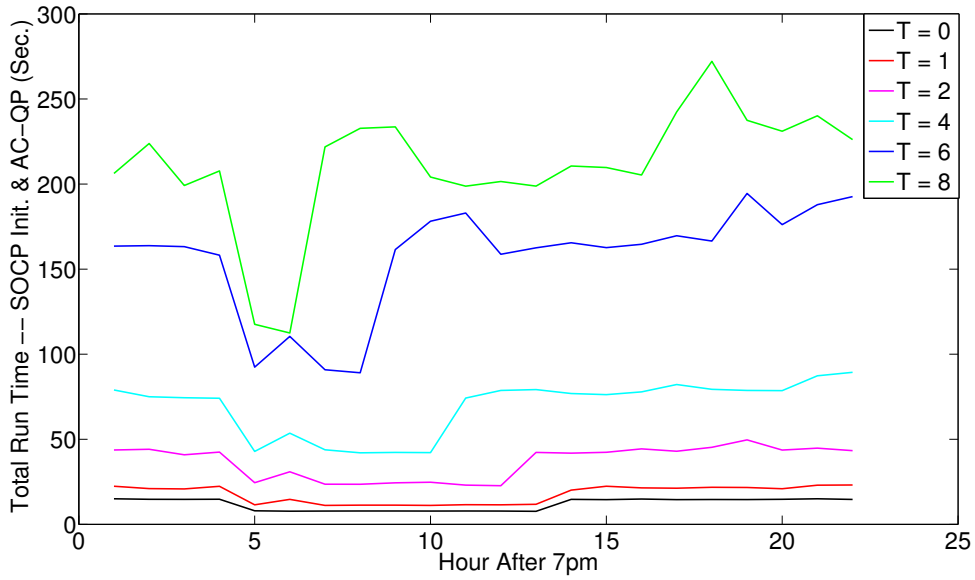

Figure 6.6: Case 1: SOCP Initialization and AC-QP Total Timing Results

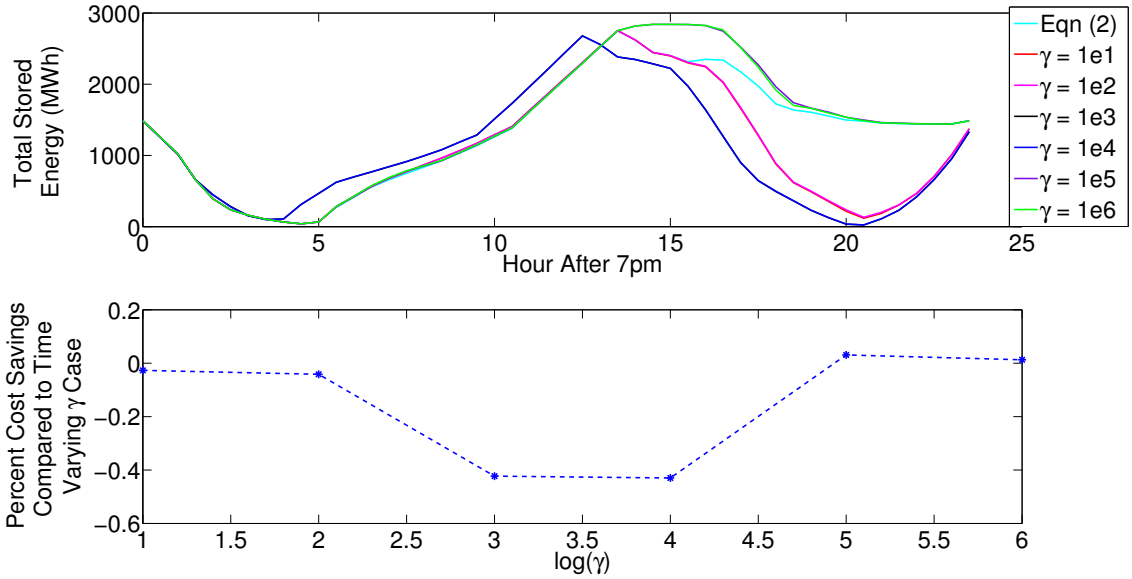

Figure 6.7: Case 1: Total Energy and Cost Comparison - Constant γ, $T = 4$

Figure 6.7 shows the sensitivity of these results to the choice of the storage terminal penalty coefficient γ. The first test case is repeated for a constant choice of γ throughout the day and a horizon of 4 hours. When γ is less than 10^4, storage is discharged before the peak demand period. This short-sighted operation of storage leads to a higher operating cost over the entire day,

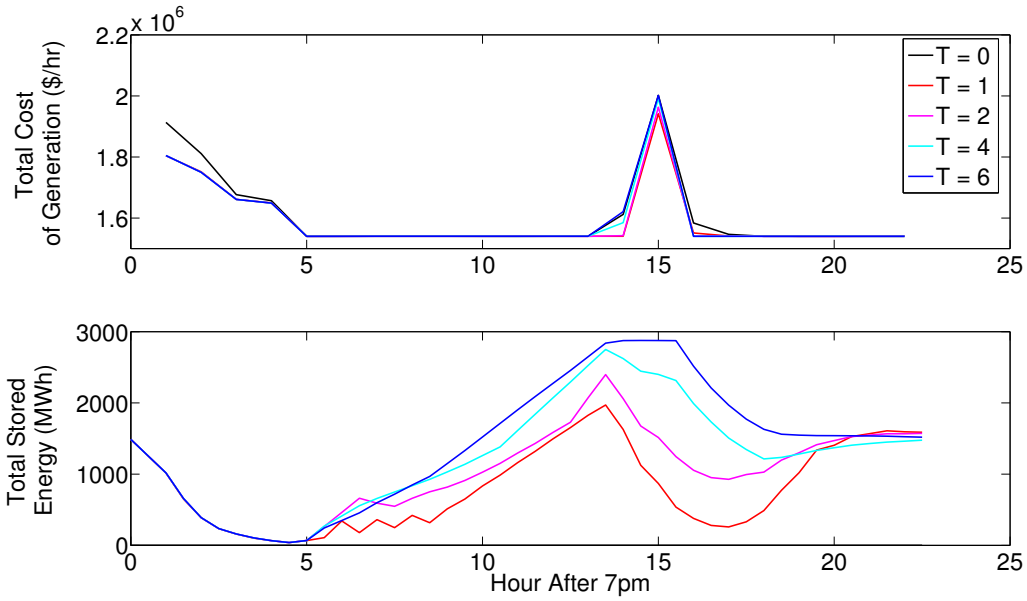

Figure 6.8: Case 2 Cost of Generation and Total Stored Energy Results

compared to the time-varying scheme proposed. Conversely, when γ is increased to 10^5 or 10^6, the storage usage pattern matches the reference pattern more closely. This leads to a slightly lower cost of operation compared to the time-varying scheme. However, this result relies upon the assumption of having a perfect demand forecast.

6.3.2 Test Case 2: Introducing Load Forecast Error

The second test case, the results of which are summarized in Figures 6.8–6.11, explores the impact of significant forecast errors on the quality of solutions for various OPF horizons. As the day begins, the wind and demand forecasts are those given by the solid lines in Figure 6.1. Then, at hour 16, a new demand forecast is received, which is shown by the dotted curve in Figure 6.1. Comparing the original forecast and actual demand curves, it it observed that there is significant error in the original forecast. In particular, the actual demand lacks the peak demand period that was originally anticipated. The degree to which this forecast error impacts the quality of the solutions achieved by the AC-QP OPF depends on the horizon chosen, as shown in Figure 6.8.

As in the first case, storage devices begin charging at hour 5. The longer horizons (4 and 6 hours) charge those devices more rapidly, and have them more fully charged by hour 14. This is due to the fact that those horizons are sufficiently long for the peak demand at hour 16 to be anticipated. However, the shorter horizons (1 and 2 hours) begin charging, but at a lower rate, as

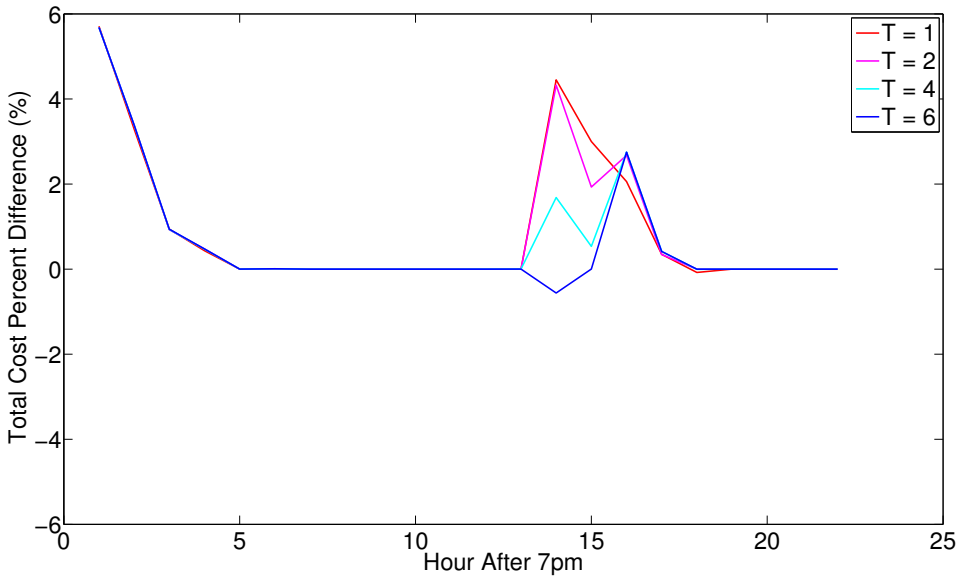

Figure 6.9: Case 2 Hourly Percent Savings Compared to No Storage Case

the peak demand has not yet been taken into account. As in the first case, the shorter horizon results are short-sighted, and so begin discharging storage devices at hour 14. In this case, however, the demand forecast for which the storage (dis)charging pattern was planned was in error. An event occurs at hour 16 such that a large portion of the anticipated demand does not eventuate, and load continues to decrease over the rest of the day. Consequently, the original peak demand period never occurs. The longer horizons have already incurred the extra cost of charging storage to a higher level in planning for that peak, which results in a higher cost compared to the shorter horizon results. This is just one example where relying upon a longer horizon, which is more economic given a reliable forecast, leaves operations vulnerable to forecast error and actually results in a higher cost solution.

Figure 6.9 emphasizes the impact that forecast error may have on the cost savings achieved by adding storage to a network. Compared to the case without any storage in the network, all horizons achieve similar cost savings until hour 14. At that time, the longer horizons incur a cost to charge storage to a higher energy level, while the shorter horizons achieve cost savings up to 4.5% in this case, as they have already begun returning power from storage devices to the network. Then, after the unanticipated load-reduction event at hour 16, all horizons use the available storage to return power to the network. It is again clear that shorter horizons may be beneficial in scenarios with less reliable forecasts.

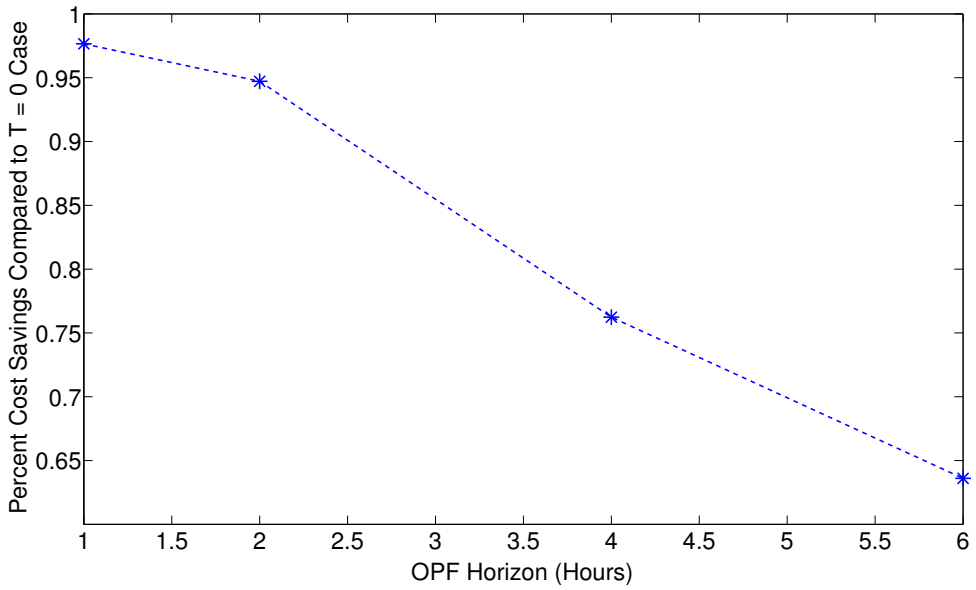

Figure 6.10: Case 2 Total Cost Percent Savings Over 24 Hours for Various Horizons

Considering the cost of operation over the entire 24-hour period, Figure 6.10 emphasizes the significance of forecast error on the quality of the solution. This plot shows that the difference in cost of operation between a 1-hour and 6-hour horizon is approximately 0.3%. In the presence of significant error, using a 1-hour horizon could save almost 1% per day. Forecast errors should also be taken into account when choosing appropriate values for γ. Figure 6.11 shows the results of this second case study for a constant γ throughout the day. In the presence of significant forecast errors, choices of γ that are less than 10^4 achieve the same use of storage and cost of operation as the time-varying scheme (6.2). However, when γ is increased to 10^5 or 10^6, while the use of storage more closely matches the reference pattern, the cost of operation is higher compared to the time-varying scheme. Placing such large penalties on deviation from terminal state of charge reduces the flexibility of the storage to adapt to forecast errors.

Taken together, these figures reveal that the degree of confidence placed in a demand or wind forecast must be assessed carefully, as that accuracy can have a significant impact on the choice of horizon length. Finally, as in the first test case, Figure 6.12 demonstrates the scalability of this method for a realistically large network, as all cases are within the 5-minute limit set for real-time applications. It should also be noted that if large forecast errors are a concern and shorter horizons are implemented, significant execution time savings can be achieved.

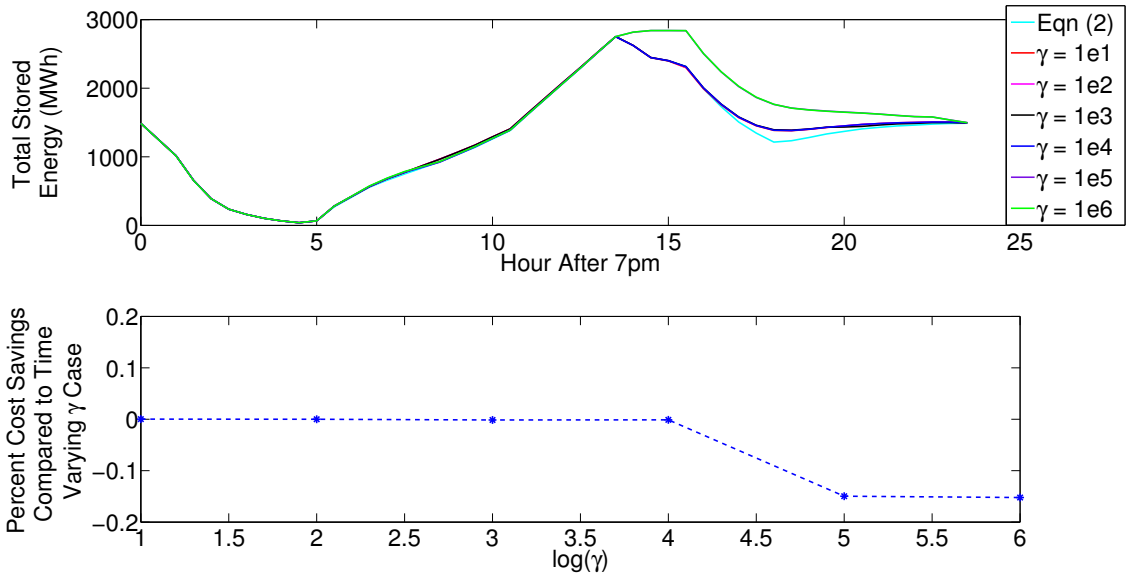

Figure 6.11: Case 2 Total Energy and Cost Comparison - Constant γ, $T = 4$

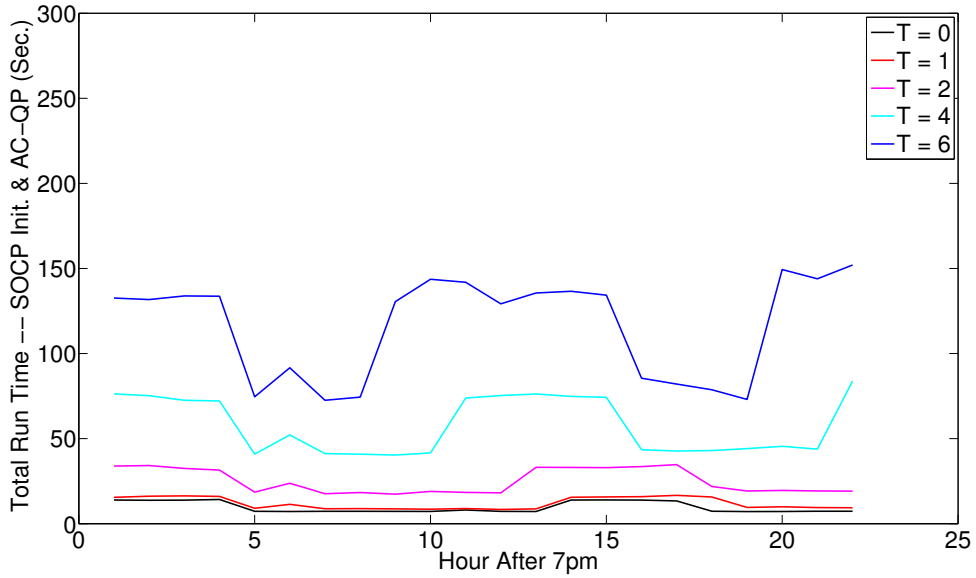

Figure 6.12: Case 2 SOCP Initialization and AC-QP Total Timing Results

6.4 Conclusions

Several factors influencing the choice of OPF horizon used in the multiperiod AC-QP formulation from Chapter V have been explored. First, when forecasts are accurate, longer horizons offer significant benefits in reducing operational costs. Conversely, when large forecast errors are anticipated, choosing a longer horizon may increase the operational cost, while shorter horizons can achieve greater cost savings. Together, these investigations demonstrate that optimal scheduling is reliant upon matching the horizon length to the forecast quality. The scalability of the proposed approach has also been demonstrated on a realistically large network and timing results fall within a reasonable (5-minute) operation time limit. The AC-QP algorithm is extended to consider wind forecast uncertainty in Chapters VII-X.

CHAPTER VII

Introducing Renewable Generation Uncertainty

As demonstrated in Chapter VI, forecast quality can have a significant impact on the economic operation of power systems. Due to its variable nature, renewable generation is a main source of uncertainty in power systems. Accurate methods for mitigating such uncertainty are crucial for the reliable operation of power systems. This chapter extends the AC-QP OPF method to a stochastic setting that includes wind generation uncertainty.

7.1 Introducing scenarios into the AC-QP OPF

The solution of the AC-QP OPF formulation presented in previous chapters is deterministic in the sense that it does not take into account the uncertainties of the system. In this section, wind power uncertainty is considered, and the algorithm shown in Figure 4.1 is reformulated to provide a solution that is robust over a finite set of possible wind generation scenarios. This results in a probabilistic AC-QP OPF algorithm (AC-QP pOPF). The base case generation dispatch will satisfy the network constraints for a particular wind forecast. Any wind power scenario differing from the forecast will introduce a generation-load mismatch, driving the system to a new operating point. This active power mismatch is assumed to be compensated according to a linear policy, adjusting the power of each generator based on a distribution (or participation) vector as in [34], [1]. Let P_g represent the base case generation dispatch corresponding to a particular wind forecast, P_w. If a wind scenario, denoted P_w^m, is then encountered, the base case generation dispatch is adjusted according to a distribution vector, d:

$$P_g^m = P_g - d \sum_{k \in \mathcal{W}} \left(P_{w,k}^m - P_{w,k} \right). \tag{7.1}$$

Note that the nonnegative entries of d describe the contribution of each generator in alleviating the forecast error. As each scenario will also incur different losses in the network, generation must also be adjusted in a similar manner to cover this variation. It is assumed in this work that the generator voltage magnitude setpoints remain constant through deviations from the wind power forecast.

The robust (over the scenarios) reformulation is based on a series of iterations between an AC power flow and a QP, as in the deterministic algorithm shown in Figure 4.1. The initialization of the first set of AC power flows is provided by a reformulation of the SOCP relaxation given in Chapter V. In this modified SOCP, each new scenario requires additional variables for the voltage magnitude at load buses ($V_i \ \forall i \in pq$), the active and reactive flows on each line (P_{ij}, Q_{ij} $\forall (i,j) \in \mathcal{L}$), the square current magnitude flows ($L_{ij} \ \forall (i,j) \in \mathcal{L}$), and generator reactive power output ($Q_{g,i} \ \forall i \in \mathcal{G}$). The network constraints in Problem 5.9 are duplicated within the SOCP for each new operating point due to a scenario. The coupling between the base case and each scenario is maintained through the generator active power output linear policy and common voltage magnitude setpoints.

A QP is then solved to schedule changes from the initial power flow solutions to alleviate constraint violations and satisfy the objective. A separate linearization is formed for each scenario in the QP using the solution of the corresponding power flow. Separate AC power flows are then solved for the base case and each scenario, and these iterations continue until the power flow and QP solutions agree within an acceptable tolerance.

The objective and constraints for the base case wind forecast are those given in Problem (3.3), with three modifications. First, a single period OPF formulation is considered (i.e. $\mathcal{T} = 1$), so the time dependence of all constraints is suppressed in the formulations that follow. Second, no storage has been added in the network, so constraints (3.3h)-(3.3m) are omitted from the base case description. Finally, while the base case wind generation, P_w, is a decision variable in Problem 3.3, it is considered a fixed parameter in this formulation. Likewise, the wind generation in each scenario is a fixed parameter in the optimization problem. The set of wind scenarios to be considered in the pOPF problem is denoted $\mathcal{S}$ and is indexed by the variable m. A scenario in this context is defined by a vector of wind generation values. For example, if the base case forecast of one wind generator is 100 MW, a possible scenario could be that it produces only 95 MW instead of its forecasted value. For every scenario $m \in \mathcal{S}$, the set of operational constraints (7.2b)-(7.2h), which are in line with the base case description, is added to the optimization problem. The QP solved at

each iteration of the AC-QP pOPF algorithm is then as follows:

$$\min_{\substack{\Delta P_g, \Delta Q_g, \Delta\theta, \Delta V, \alpha^m, \\ \Delta P_g^m, \Delta Q_g^m, \Delta\theta^m, \Delta V^m}} \quad \sum_{i\in\mathcal{G}} C_i\left(P_{g,i}^{\circ} + \Delta P_{g,i}\right) \tag{7.2a}$$

subject to $\quad (3.1), (3.2), (3.3b) - (3.3d), (3.3f)$

$\forall m \in \mathcal{S}$:

$$\mathbf{J^m}\Delta x^m = \Delta S^m \tag{7.2b}$$

$$P_{g,i}^{min} \leq P_{g,i}^{\circ,m} + \Delta P_{g,i} + \alpha^m d_i \leq P_{g,i}^{max} \qquad \forall i \in \mathcal{G} \tag{7.2c}$$

$$Q_{g,i}^{min} \leq Q_{g,i}^{\circ,m} + \Delta Q_{g,i}^m \leq Q_{g,i}^{max} \qquad \forall i \in \mathcal{G} \tag{7.2d}$$

$$\Delta\theta_{slack}^m = 0 \tag{7.2e}$$

$$V_i^{min} \leq V_i^{\circ,m} + \Delta V_i^m \leq V_i^{max} \qquad \forall i \in \mathcal{N} \tag{7.2f}$$

$$\Delta V_i = \Delta V_i^m \qquad \forall i \in \mathcal{G} \tag{7.2g}$$

$$S_{ij}^{\circ,m} + \sum_{k\in\mathcal{N}} \frac{\partial S_{ij}}{\partial \theta_k}^m \Delta\theta_k^m + \sum_{k\in\mathcal{N}} \frac{\partial S_{ij}}{\partial V_k}^m \Delta V_k^m \leq S_{ij}^{max} \qquad \forall\,(i,j) \in \mathcal{L}^{*,m} \text{ and } \forall\,(j,i) \in \mathcal{L}^{*,m}. \tag{7.2h}$$

The modified linearization for each scenario is given by

$$\Delta x^m = \begin{bmatrix} \Delta\theta^m \\ \Delta V^m \end{bmatrix}, \Delta S^m = \begin{bmatrix} G_a[\Delta P_g + \alpha^m d] \\ G_a \Delta Q_g^m \end{bmatrix},$$

where G_a is the node-generator incidence matrix defined in Chapter III.

Each scenario m introduces extra variables, namely the reactive power output of each generator (ΔQ_g^m) and the complex voltage at each bus (ΔV^m, $\Delta\theta^m$). Note that the term $\alpha^m d$ has been added to the definition of ΔS^m and to constraint (7.2c), where α^m represents the difference in total active power losses between the base case and scenario m. In a distributed slack manner, this accounts for the the fact that total system losses will differ between the base case and each scenario. The deviation of the active power generation, ΔP_g, is forced to take the same value for the base case and all scenarios. Recall the linear policy given in (7.1) that is used to run the AC power flows of the base case and each scenario. The parameter P_g° in the QP represents the active power generation from the base case power flow solution. It is thus P_g adjusted for the actual system losses in a distributed slack manner. Likewise, $P_g^{\circ,m}$ is obtained from the power flow solution of scenario m, and is P_g^m adjusted for the actual network losses. As such, the mismatch introduced by each scenario is already taken into account in the corresponding generation dispatch, $P_g^{\circ,m}$, obtained from the previous AC power flow. The same generator voltage magnitude setpoints are

enforced in the base case and each scenario through constraint (7.2g).

Once the algorithm has converged, the final solution guarantees that the operating point of the base case and the operating points for the considered scenarios will satisfy the nonconvex AC power flow constraints with sufficient accuracy. However, there is no guarantee that the constraints will be satisfied for any arbitrary scenario that may be encountered in actual operation. To achieve such generalization properties, a randomized optimization technique is applied, which is the topic of Section 7.3.

7.2 Improving the scalability of the AC-QP pOPF

The previous section presented the pOPF for the general case where a finite number of wind power scenarios are considered. To improve the scalability of the method with respect to the number of scenarios that can be incorporated in the pOPF problem, the modified algorithm shown in Figure 7.1 is proposed. This algorithm is based on ranking the scenarios according to the absolute value of the difference between the scenario and the forecast, $|\sum_{i\in\mathcal{W}}(P^m_{w,i} - P_{w,i})|$. This updated method adds only the highest ranked wind scenario to the pOPF at the beginning of each outer loop. Then, if the solution results in constraint violations for any of the remaining scenarios, one more scenario from those with violations is added in the same way to the pOPF at the next iteration. In practice, it has been observed that relatively few of these outer loops are necessary to satisfy the constraints for even a very large number of scenarios. In other words, a solution satisfying the constraints for a very large set of possible scenarios is found by explicitly including only a small fraction of them in the pOPF problem. Limiting the size of the subset of wind power scenarios explicitly modeled in the pOPF problem reduces the number of variables and constraints in the QP, making the AC-QP pOPF faster to achieve a feasible solution for all considered scenarios. It is this iterative approach of introducing scenarios that makes the proposed AC-QP method highly scalable with respect to the number of scenarios considered in the pOPF problem.

7.3 Providing a-posteriori probabilistic guarantees

The proposed algorithm provides a method for selecting a subset of scenarios to include in the pOPF problem to generate a solution that is feasible for a much larger set of scenarios. As such, the solution resulting from optimizing over a very small number of scenarios is an identical feasible solution to the pOPF problem considering the entire (potentially much larger) set of scenarios. The

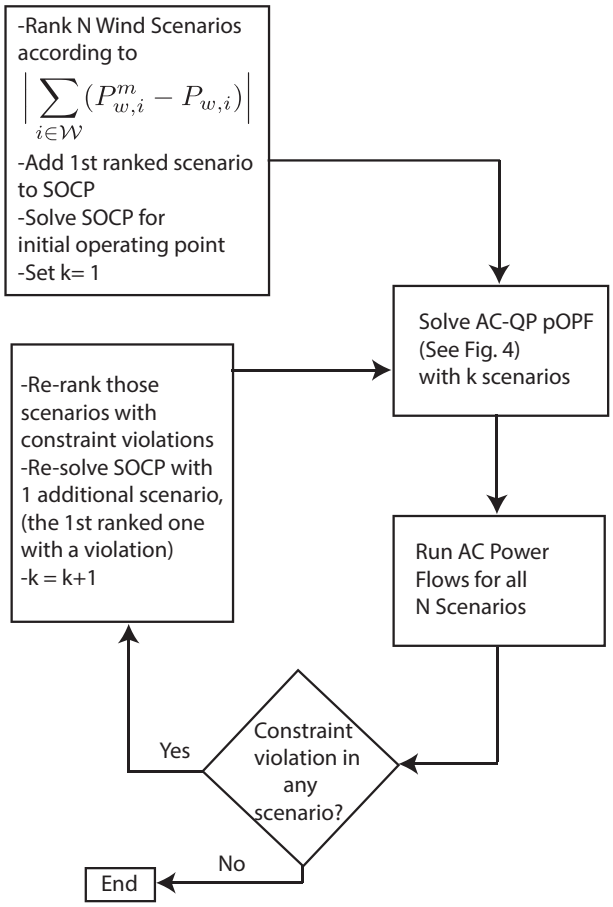

Figure 7.1: AC-QP pOPF algorithm for N scenarios.

crucial criterion of this algorithm is that the solution satisfies the constraints for all other scenarios, even though they were not used explicitly in the solution method [64].

The framework in [42] is then employed to find a-posteriori probabilistic guarantees to accompany the solution of the nonconvex problem. This method is applicable to any algorithm that takes as an input a particular set of scenarios and provides a feasible solution of the problem. The critical point is the definition of the support set, also known as a compression scheme in [64], which is the set of scenarios that support the solution. In other words, if the solution of the problem using a set of N scenarios, $\mathcal{S}_N$, is considered, and an identical solution can be achieved given a subset $\mathcal{S}_k$ of $\mathcal{S}_N$ that contains only k scenarios, then the set $\mathcal{S}_k$ is a support set of the problem with N scenarios.

With the cardinality k of the support set of the problem associated with N scenarios identified, a theoretical upper bound on the probability of constraint violation is provided by the formula

from [42]:

$$\epsilon(k) = \begin{cases} 1, & \text{if } k = N \\ 1 - \sqrt[N-k]{\frac{\beta}{N\binom{N}{k}}}, & \text{otherwise} \end{cases} \tag{7.3}$$

where $\beta \in (0, 1)$ is a design parameter representing the probability that the upper bound ϵ will be violated. In other words, β is the probability that the probability of constraint violation will be greater that ϵ. A choice of β that is sufficiently small (e.g. $\beta = 10^{-4}$) will ensure that the calculated upper bound ϵ will hold with "very high confidence".

It is important to note that there are only two assumptions required for this bound to be valid. First, the algorithm must map the scenario set to a 'unique' solution satisfying the constraints for all the scenarios in the set. Second, the solution must be invariant to any permutation of the scenarios taken into account. These requirements are both satisfied for the proposed algorithm.

The provided theoretical guarantees are a-posteriori, as the cardinality of the support set can only be identified after the solution is obtained. Moreover, the result will be less conservative if a support set of minimum cardinality is found. The algorithm proposed in Section 7.2 can then be used to obtain a solution and identify the cardinality of the support set. The previously defined theoretical probabilistic bound is then validated via Monte Carlo simulation.

7.4 Results and Discussion

7.4.1 An indicative example of the AC-QP pOPF

A first test case that uses the IEEE 14-bus network and unit commitment [59] is presented to demonstrate the progression of this method when 1500 scenarios are considered in the pOPF problem, and how the resulting support set for this problem is identified. The network has been augmented with two wind generators at nodes 9 and 3; 40 MW of available wind power is assumed at each node in the base case forecast. This corresponds to a renewable penetration (calculated as the ratio of total available wind generation to total generation capacity) of 9.4%. The AC-QP method described in Figure 7.1 is used to solve the pOPF problem considering 1500 scenarios. The results of this first example are shown in Figure 7.2.

The method begins by randomly choosing 1500 scenarios from a set of 10,000 possible scenarios. These 1500 scenarios are then ranked according to the criterion established in Section 7.2, the absolute value of the total forecast error. An SOCP relaxation is solved including only the first

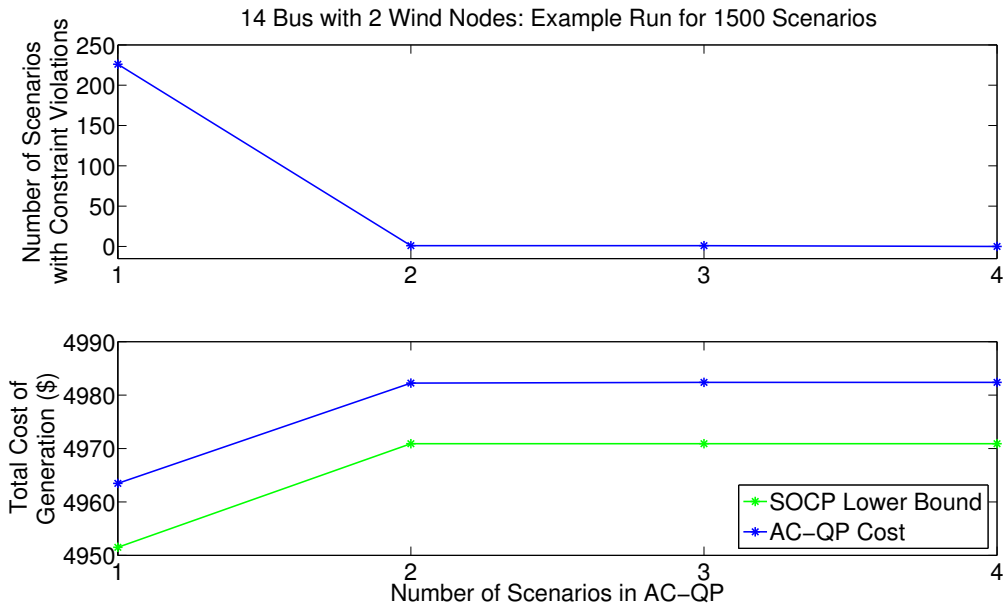

Figure 7.2: Solving pOPF with 1500 scenarios.

scenario, which corresponds to the scenario with the largest total mismatch, to initialize the AC-QP algorithm. That single scenario is also included in the QP of the AC-QP algorithm. After the AC-QP method has terminated, the solution is feasible for the base case forecast and the first scenario introduced into the problem. An AC power flow is then solved for the remaining 1499 scenarios being considered, and the set of scenarios with constraint violations is identified.

After the AC-QP method terminates with only one scenario included, the AC power flow solutions corresponding to the remaining 1499 scenarios reveal that there are 226 scenarios with constraint violations. This is shown as the initial point at the leftmost portion of the x-axis in the upper plot of Figure 7.2. These 226 scenarios are again sorted with respect to the absolute mismatch criterion, and the first ranked scenario (again corresponding to the scenario with the largest mismatch that has constraint violations) is now added to the set of scenarios included in the pOPF problem. The SOCP relaxation is solved again with two scenarios to reinitialize the AC-QP algorithm. This process repeats, introducing a single scenario into the AC-QP in each outermost loop of the algorithm. In this way, a very small number of scenarios that must be explicitly included in the AC-QP such that constraints are satisfied for all 1500 scenarios is identified.

In this particular example, only 4 scenarios out of the 1500 possibilities needed to be included in the AC-QP such that the resulting solution satisfied the constraints for all 1500 scenarios. In other words, using only those 4 scenarios provides an identical feasible solution to the problem

that incorporates all 1500 scenarios. Moreover, this implies that those 4 scenarios comprise a support set for the problem associated with the larger set of 1500 scenarios. The resulting solution is accompanied with a-posteriori probabilistic guarantees, calculated using (7.3). As a feasible solution for the 1500 scenarios is found, and because the same feasible solution exists for the problem including only 4 of those scenarios, it can be claimed with very high confidence (choosing $\beta = 10^{-4}$) that the solution of this algorithm will satisfy the AC OPF constraints with probability of at least 97.2% over any possible realization of the wind power. In fact, Monte-Carlo simulation revealed that the empirical probability of violation in this case is only 0.23%. The empirical violation probability is evaluated by checking the violation of the constraints for 10,000 scenarios. The scenarios are generated by a Markov Chain Monte Carlo (MCMC) mechanism that builds a transition probability matrix that suggests with what probability the uncertain variables will move from one value to another in time [65]. Normalized hourly measured wind power data, both forecasts and actual values, for the total wind power infeed of Germany over the period from 2006-2011 was used to train the model.

In addition to its feasibility, the optimality of the pOPF solution must also be considered. The lower plot of Figure 7.2 shows the AC-QP cost and corresponding SOCP lower bound after each additional scenario is added. These results demonstrate the inherent tradeoff between reliability and optimality: each additional scenario increases the cost of operation, until constraints have been satisfied for all 1500 scenarios and no further scenarios need be included in the pOPF. Additionally, notice that the AC-QP cost results are sufficiently close to the lower bound established by the objective value of the SOCP solution. The AC-QP solution can therefore be claimed to be sufficiently close to the globally optimal solution.

7.4.2 Extended results

The previous example using the modified IEEE 14-bus network is now expanded to assess the performance of the proposed AC-QP pOPF method as the number of scenarios considered in the pOPF problem (the value of N in Figure 7.1) is increased from 10 to 1500[1]. The choice of 1500 scenarios here is sufficiently large to explore the impact on the empirical probability of violation of increasing numbers of scenarios considered in the pOPF problem. As in the previous example, the quality of solution from the AC-QP pOPF algorithm is assessed via Monte Carlo simulation using 10,000 possible scenarios. For each scenario, an AC power flow is run and the violation of any

[1]Recall that an example for N=1500 case was presented in Chapter 7.4.1.

constraint is checked. Out of those 10,000 scenarios, those that result in any constraint violations (including generator active and reactive power limits, voltage magnitude limits, and line flow limits) are recorded to provide an empirical probability of constraint violation. For each choice of N, the number of scenarios considered in the pOPF, 500 repeated trials are then performed. Each trial differs in the specific set of N randomly chosen wind power scenarios that are considered in the problem. These results are gathered in boxplots which give several statistical quantities of interest for each set of 500 trials, given the number of scenarios to be considered in the pOPF: the central line inside the box shows the median over all 500 trials; the bottom and top edges of each box show the 25% and 75% percentiles respectively; and the vertical lines show the extreme values.

The generation cost and corresponding empirical probability of constraint violation results for increasing N are shown in Figure 7.3(a) and Figure 7.4, respectively. These figures demonstrate the inherent tradeoff between reliability and optimal cost of operation. As more scenarios are included in the pOPF problem, the cost of operation increases, resulting in a less economic operating point. However, with an increasing number of scenarios added to the algorithm, the solution is more robust and fewer scenarios create constraint violations. Thus, although less economic, operating points that consider larger numbers of scenarios in the pOPF are more reliable. Furthermore, Figure 7.3(b) validates the quality of solution of these results: the cost of generation in all cases is within 0.26% of the SOCP lower bound, and is thus sufficiently close to the globally optimal solution.

The empirical probability of violation in Figure 7.4 decreases significantly as the number of scenarios included in the pOPF algorithm increases. Notice that with only 50 scenarios included in the pOPF problem, the empirical probability of violation is already below 5% for 75% of the trials.

Based on the theory discussed in Section 7.3, the solution of the proposed algorithm should satisfy the a-posteriori probabilistic guarantees. To verify this, the cardinality of the support set for each trial is identified and the corresponding theoretical upper bound on constraint violation based on (7.3) is calculated. Figure 7.5 summarizes the cardinality of the support set for each trial. As these results show, a very small number of scenarios, on average around 2, need to be explicitly enforced in the AC-QP problem for all constraints to be satisfied for the remaining scenarios. Noting that the median values in these results are somewhat biased, Figure 7.6 gives individual histograms of the data summarized by the boxplots for $N = 10, 200, 600$ and 1500 for completeness. For the cases considering 10 and 200 scenarios, this distribution is heavily weighted at 2-3 support scenarios. However, when N is increased to 1500, it is slightly more evenly distributed between 1-3

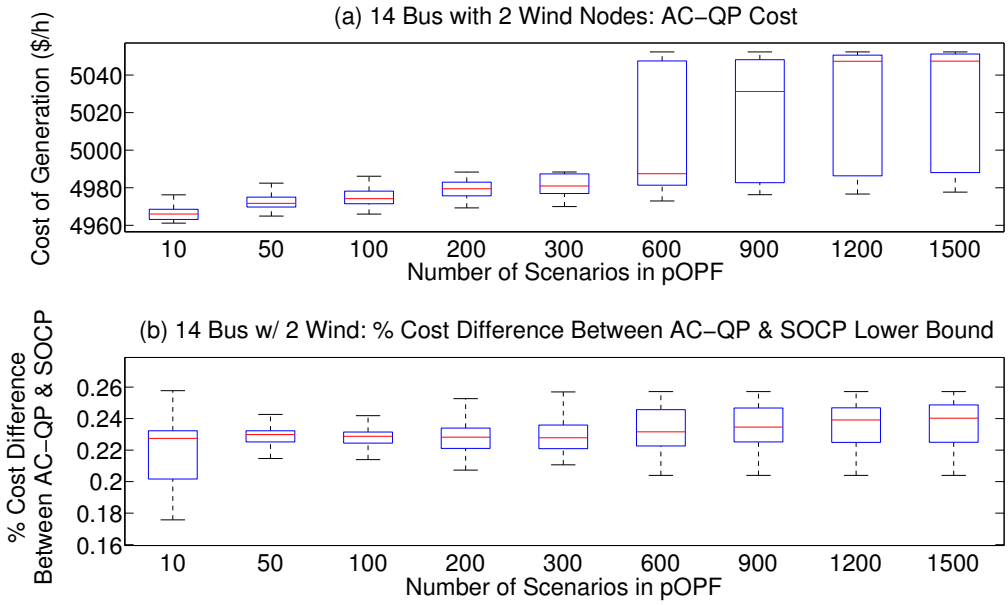

Figure 7.3: (a) Cost of generation, (b) Distance from SOCP lower bound results.

support scenarios.

A comparison between the empirical and theoretical violation results is provided in Figure 7.7. The y-axis of this plot gives the theoretical minus the empirical probability of violation. Note that this difference is positive, which highlights the fact that the solution of the AC-QP pOPF algorithm results in an empirical probability of violation that satisfies the theoretical bounds in all trials.

To ensure the reliability of a system, large numbers of scenarios may need to be included in the pOPF problem. The scalability of any proposed algorithm is therefore an important factor that must be assessed. For the purposes of real-time operation, a threshold of 5 minutes (300 seconds) is assumed to be an acceptable limit on total execution time. Figure 7.8 summarizes the timing results for the proposed AC-QP pOPF algorithm. As demonstrated in these results, the timing requirement is satisfied in all trials, even those considering 1500 scenarios, which have a median solution time less than 20 seconds. This suggests that the proposed method scales well with respect to the number of scenarios included in the pOPF problem.

7.5 Conclusions

The AC-QP OPF solution method in Chapter III has been extended to include wind power uncertainty, captured through the addition of a finite number of possible wind scenarios. The

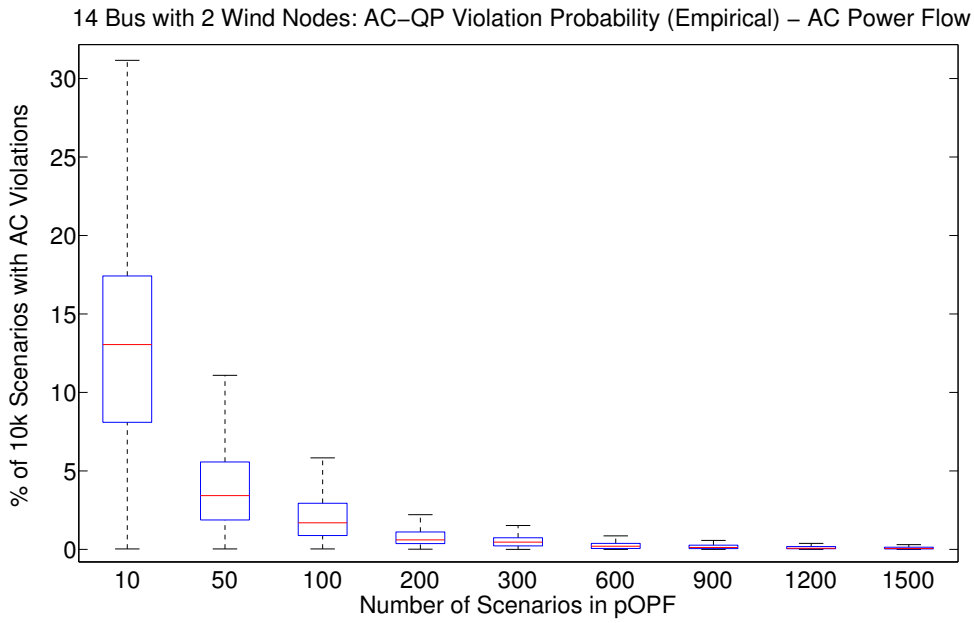

Figure 7.4: AC-QP empirical violation.

scalability of this algorithm with respect to large numbers of scenarios has been demonstrated, and the timing results support its utility for real-time applications. Randomized optimization techniques are then applied to characterize the solution with a-posteriori theoretical probabilistic guarantees. The empirical reliability of the solution has been evaluated to assess the quality of the AC-QP solution and verify the theoretical bound.

The proposed algorithm offers several advantages compared to other approaches. It does not rely upon model approximations as in DC OPF formulations. Moreover, it produces an AC feasible solution, where convex relaxations may not be tight. It also maintains scalability with respect to the number of scenarios to be optimized over, which is a limitation of convex relaxations. Finally, it provides a probabilistically robust solution with a-posteriori probabilistic violation guarantees.

The objective of this formulation is to minimize the cost of conventional generation. However, significant generator reserve capacity may be necessary to maintain reliability standards in the presence of large forecast errors. As this is a relatively expensive service for generators to provide, it should be included in the objective of the pOPF problem. The cost of generator reserves is incorporated in the pOPF problem in Chapter VIII. Moreover, while this work relies upon a fixed wind generation forecast, it is extended in Chapters IX and X to determine the maximum wind penetration that can be introduced in a network while maintaining reliability standards.

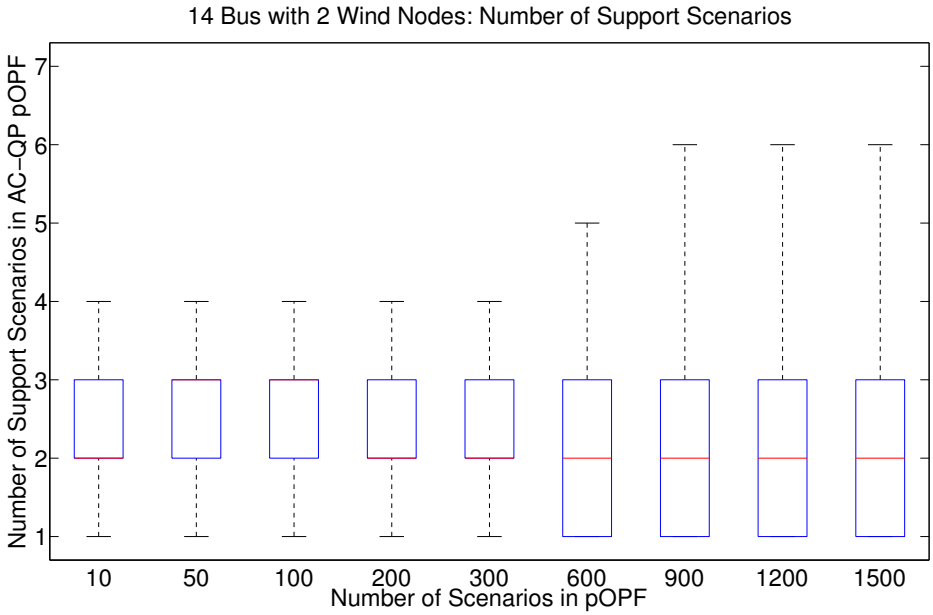

Figure 7.5: Number of support scenarios.

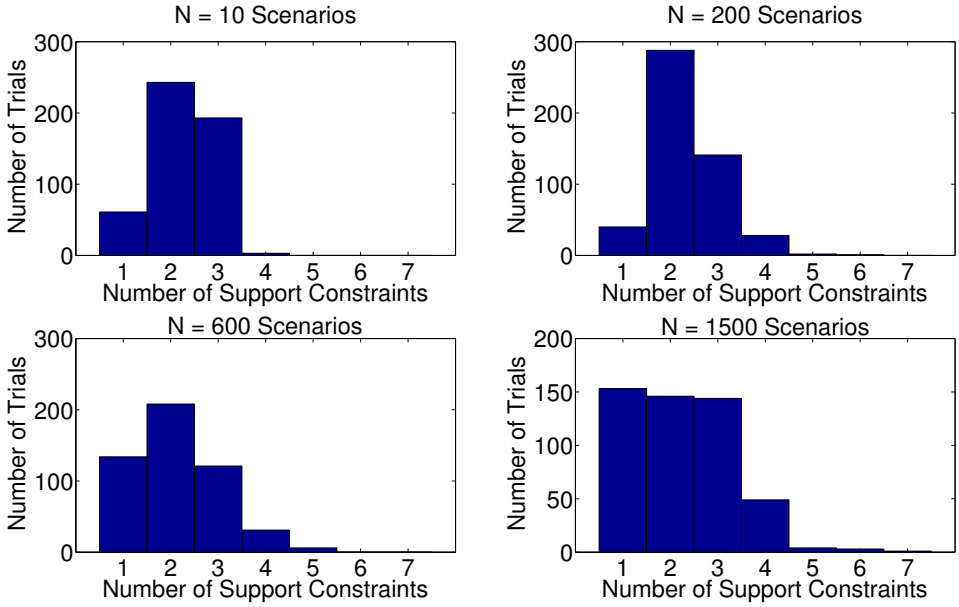

Figure 7.6: Histograms of number of support scenarios for N=10,200,600,1500.

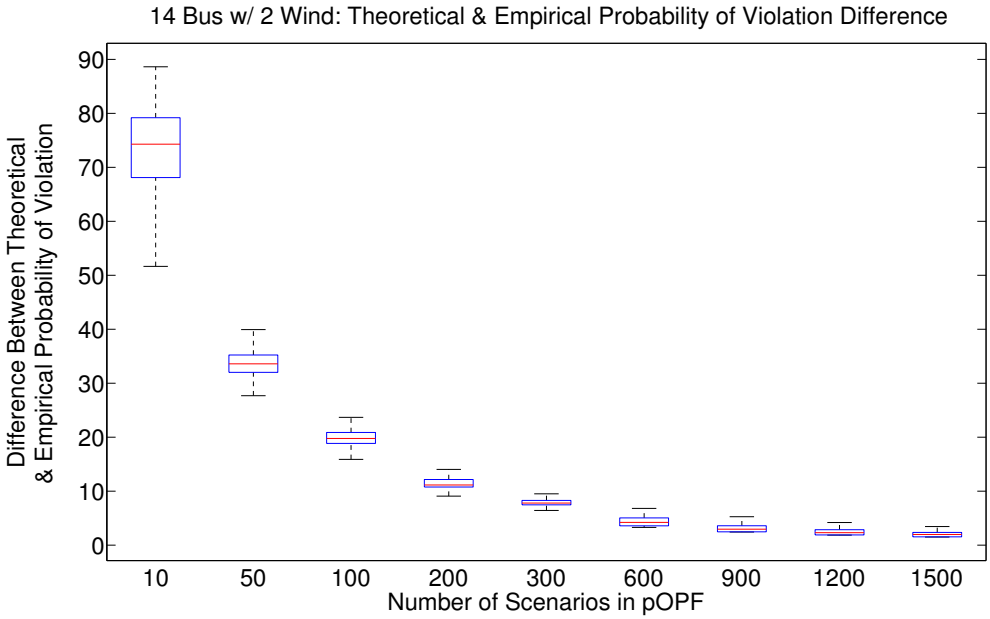

Figure 7.7: Empirical violation compared to a-posteriori theoretical violation.

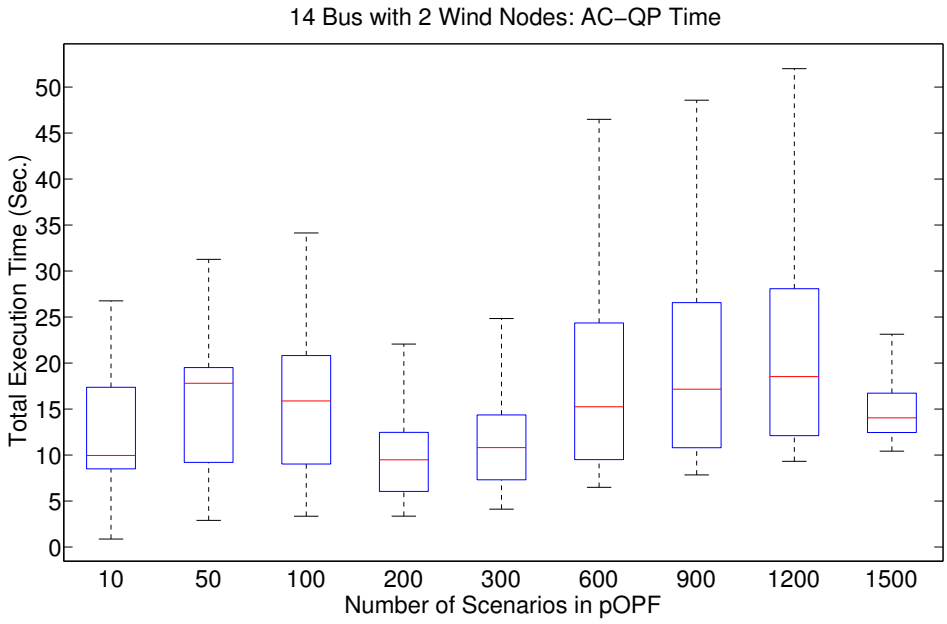

Figure 7.8: AC-QP timing results.

CHAPTER VIII

Optimizing the Cost of Generator Reserve Capacity While Considering Uncertainty

The formulation in Chapter VII is suitable for an operational setting to schedule conventional generation in an economic manner such that reliability standards are maintained in the presence of significant wind generation forecast error. To do so, generators must maintain sufficient reserve capacity to respond to the generation-load mismatch introduced by wind variability. Compared to the cost of conventional generation, reserve capacity is a relatively expensive service to provide. Another important operational problem is thus optimally allocating generator reserve capacity. Accurately solving this problem can have significant economic impacts on the operation of power systems. This chapter extends the AC-QP pOPF method to include the cost of generator reserve capacity. It also motivates the need for the increased accuracy provided by an AC OPF formulation, compared to one relying upon a DC OPF.

8.1 Adapted AC-QP Algorithm

The AC-QP pOPF algorithm shown in Figure 7.1 is reformulated to provide a solution that is robust over a finite set of possible wind generation scenarios, while minimizing both the cost of conventional generation and the cost of generator reserve capacity. It is assumed that the vector of generator distribution factors, d, is a fixed input parameter, and that the linear policy (7.1) describes how generators respond to wind forecast errors. As in the previous pOPF formulation, scenarios are modeled as vectors of wind generation values. The modified QP solved at each iteration of the AC-QP in Figure 4.1 that includes the cost of generator reserves is formulated as follows.

$$\min_{\substack{R_g,\Delta P_g,\Delta Q_g,\Delta\theta,\Delta V,\\ \alpha^m,\Delta P_g^m,\Delta Q_g^m,\Delta\theta^m,\Delta V^m}} \quad \sum_{i\in\mathcal{G}} C_i\big(P^{\circ}_{g,i}+\Delta P_{g,i}\big)+\sum_{i\in\mathcal{G}}\tilde{C}_i\big(R_{g,i}\big) \tag{8.1a}$$

subject to (3.3b) − (3.3d), (3.3f), (3.2a) − (3.2b), (7.2d) − (7.2h)

$$\mathbf{J}\Delta x=\Delta S \tag{8.1b}$$

$\forall m\in\mathcal{S}$:

$$\mathbf{J^m}\Delta x^m=\Delta\hat{S}^m \tag{8.1c}$$

$$P^{min}_{g,i}\le P^{\circ,m}_{g,i}+\Delta P_{g,i}+\alpha^m d_i\le P^{max}_{g,i} \qquad \forall i\in\mathcal{G} \tag{8.1d}$$

$$-R_{g,i}\le\alpha^m d_i-d_i\sum_{k\in\mathcal{W}}(P^m_{w,k}-P_{w,k})\le R_{g,i} \qquad \forall i\in\mathcal{G} \tag{8.1e}$$

where

$$\Delta S=\begin{bmatrix}G_a\Delta P_g\\ G_a\Delta Q_g\end{bmatrix},\qquad \Delta\hat{S}^m=\begin{bmatrix}G_a[\Delta P_g+\alpha^m d]\\ G_a\Delta Q_g^m\end{bmatrix}$$

In this problem, the second term of the objective is the cost of generator reserve capacity. Constraint (8.1e) models the reserve capacity each generator can provide as a function of the distribution vector, d, the total active power mismatch introduced by all scenarios, and the change in total system losses. This constraint captures the greatest (among all scenarios) reserve capacity that generators would be required to provide. Note that as in the formulation in Chapter VII, the term $\alpha^m d$ has been added to the definition of $\Delta\hat{S}^m$ and to constraint (8.1d). In a distributed slack manner, this accounts for the the fact that total system losses will differ between the base case and each scenario. While prior work [66], [67] has focused on solving these types of problems using a DC approximation or convex relaxations, there is a need for more accurate methods to optimally schedule these reserve services. This need results from the fact that the DC approximation is subject to modeling errors, and there are no guarantees that convex relaxations will be tight for arbitrary networks.

8.2 An Indicative Example

This need for more accurate methods can be seen even on small networks, such as the IEEE 14-bus network. A modified version of that network has been augmented with 2 wind nodes, each of which has a rated capacity of 40 MW. The AC-QP pOPF method described in Chapter VII was then applied to solve Problem (8.1). The cost and empirical violation results of the AC-

QP algorithm are given in Figures 8.1 and 8.3. These results are also compared to those from a stochastic DC OPF, in which a scenario approach is also used. The results of this method are given in Figures 8.2 and 8.4. As in Chapter VII, boxplots are used to summarize each of these results. Recall the statistical quantities of interest for each set of 500 trials that these include: the central line inside the box shows the median over all 500 trials; the bottom and top edges of each box show the 25% and 75% percentiles respectively; the vertical lines extend to the 99% percentile; and the dots represent statistical outliers.

Comparing Figures 8.1 and 8.2, two observations can be made. First, the natural tradeoff between increasing numbers of scenarios considered in the pOPF problem and the cost of operation is observed. Note that this cost of operation includes both the cost of conventional generation, as well as the cost of generator reserve capacity. As the number of scenarios considered in the pOPF problem increases, the resulting solution should theoretically be feasible for a winder range of arbitrary scenarios that may be encountered in operation. However, this increased reliability results in a higher cost of operation. Second, the DC approximation results in a slightly lower cost of operation than the AC-QP method. This cost reduction is likely a result of the fact that the DC pOPF solution will not necessarily satisfy the nonconvex AC OPF constraints.

Figures 8.3 and 8.4 give the empirical probability of violation, which is determined by checking the pOPF solutions with the power flow solutions of 10,000 possible wind scenarios. The AC-QP results in Figure 8.3 reveal that the probability of violation is below 10% after 100 scenarios have been included in the problem. The DC pOPF results are checked with an AC power flow, as well as with a DC power flow. Figure 8.4 shows that while the DC power flow results have an empirical probability of violation below 10% after 300 scenarios are added to the problem, the AC power flow results do not follow this trend. In fact, the probability of violation remains close to 100% even after 1500 scenarios have been considered in the problem. This is due to the model mismatch introduced by the DC approximation. This example clearly motivates the need for accurate optimization methods, such as the AC-QP pOPF algorithm, in reserve scheduling under forecast uncertainty.

Expanded results for the proposed AC-QP method are included in Figures 8.5-8.7. The scalability of the proposed method is highlighted by the timing results in Figures 8.5. The total execution time is less than 180 seconds (3 minutes) in 99% of all trials, which is acceptable for a real-time operation setting. Moreover, the number of scenarios considered in the pOPF problem has a minimal effect on the median solution time. Thus, this approach is of particular interest for solving pOPF problems that consider very large sets of possible wind scenarios.

The timing results in Figure 8.5 are directly related to the number of support scenarios in each trial. Recall that these are the scenarios that must be explicitly included in the pOPF problem. These results are included in Figure 8.6. The median number of support scenarios in this case is only 2 scenarios, regardless of the size of the set of scenarios being considered in the problem. In fact, in 99% of all trials, the number of support scenarios is less than or equal to 4. This further demonstrates the scalability of the proposed algorithm for optimally allocating the generator reserve capacity that is needed to maintain reliability standards.

As described in Chapter VII, the a-posteriori theoretical probability of violation can be calculated using the number of support scenarios in each trial, along with (7.3). The difference between these theoretical upper bounds and the empirical results given in Figure 8.3 are summarized in Figure 8.7. As this difference is nonnegative in all trials, the calculated upper bound on the probability of violation is always satisfied. Furthermore, the empirical results converge to the calculated theoretical upper limits as N increases.

8.3 Conclusions

The AC-QP pOPF method from Chapter VII has been adapted to optimally allocate generator reserve capacity, while also minimizing the total cost of conventional generation. An example has been developed that clearly demonstrates the need for the increased accuracy provided by an AC pOPF formulation, to ensure that reliability standards are maintained. The scalability of the algorithm with respect to the number of scenarios considered in the problem has been demonstrated, and the total execution time has been shown to be suitable for real-time operational settings. This formulation assumed a fixed value for the generator distribution vector, d. However, determining which generators will respond to the active power mismatch, as well as how much each will contribute in reserves, is a natural component of the reserve scheduling problem. This formulation will be extended in Chapters IX and X to include d as a decision variable in the pOPF problem.

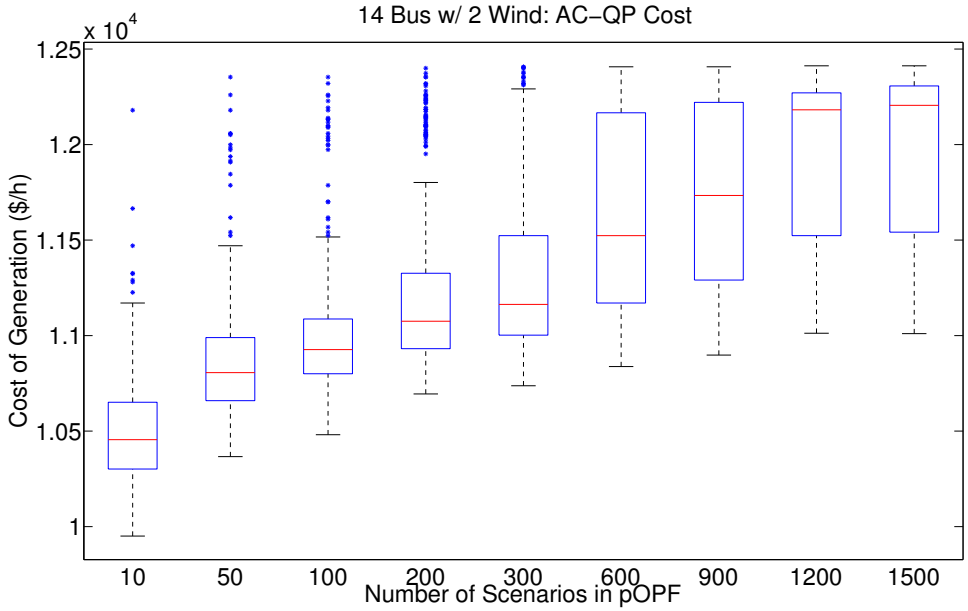

Figure 8.1: AC-QP pOPF Generation Cost Results

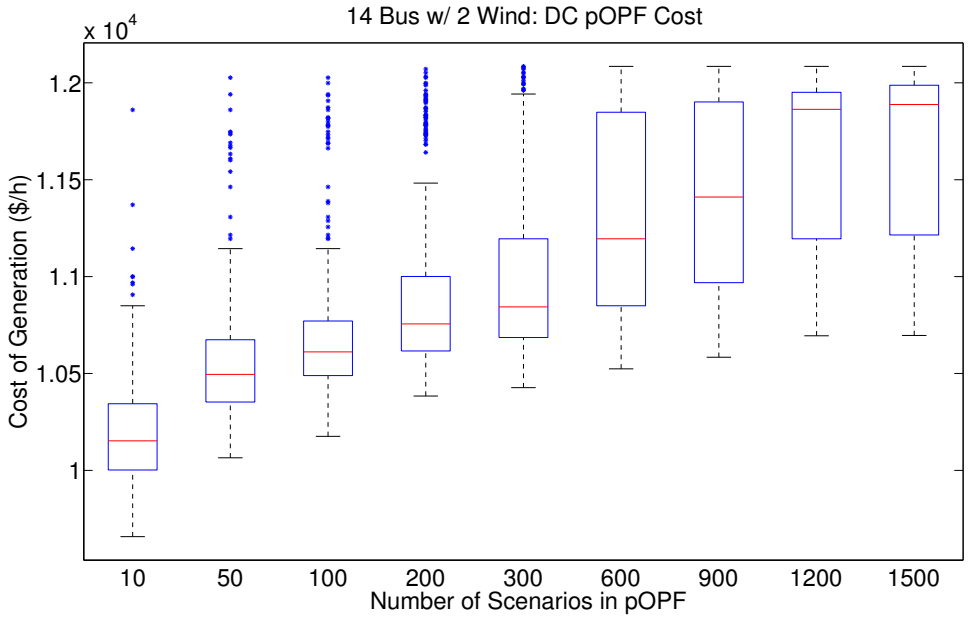

Figure 8.2: DC pOPF Generation Cost Results

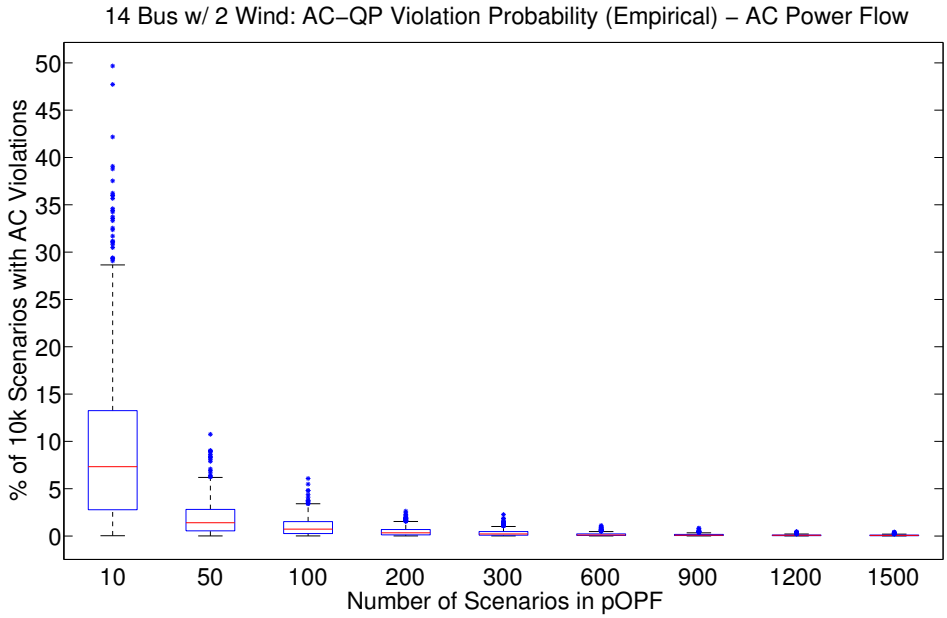

Figure 8.3: AC-QP pOPF Empirical Probability of Violation Results

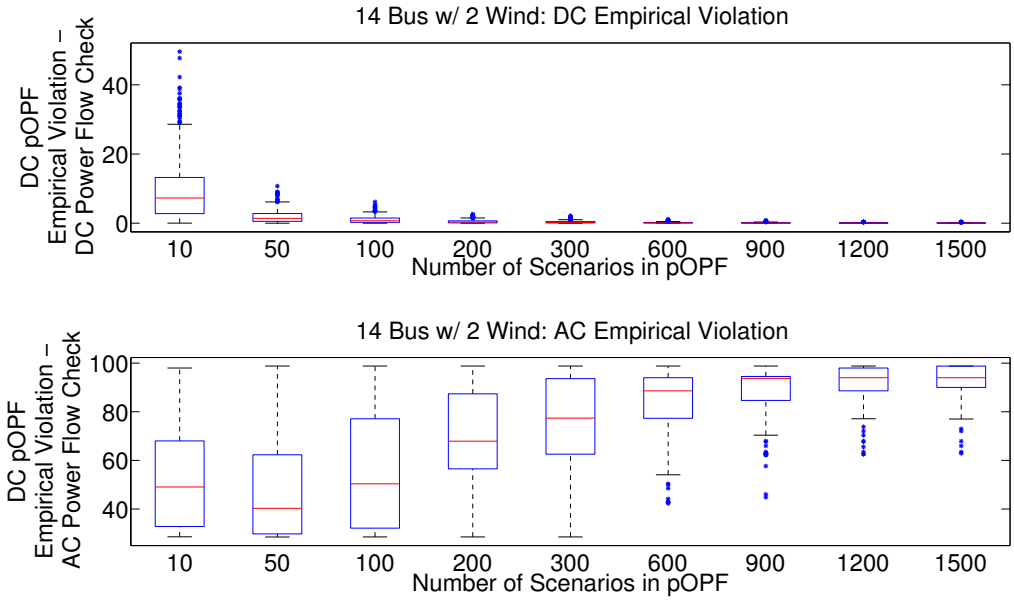

Figure 8.4: DC pOPF Empirical Probability of Violation Results

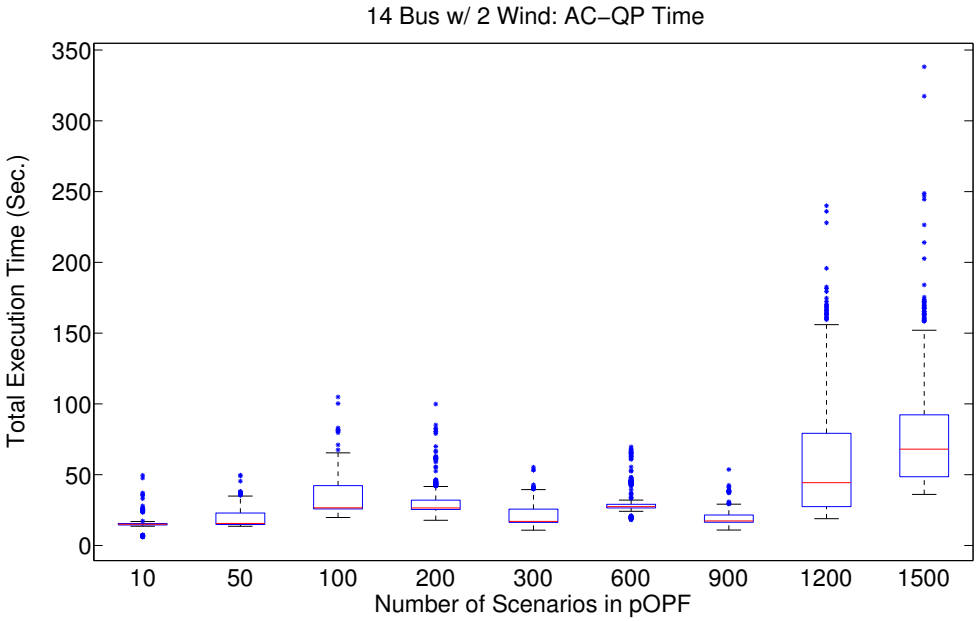

Figure 8.5: AC-QP pOPF Time Results

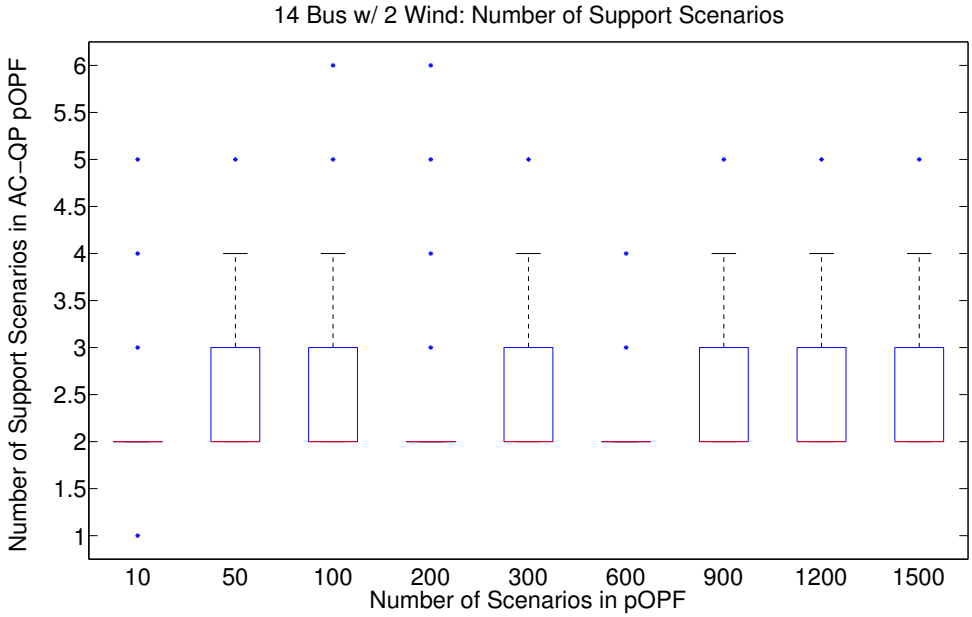

Figure 8.6: AC-QP pOPF Number of Support Scenarios Results

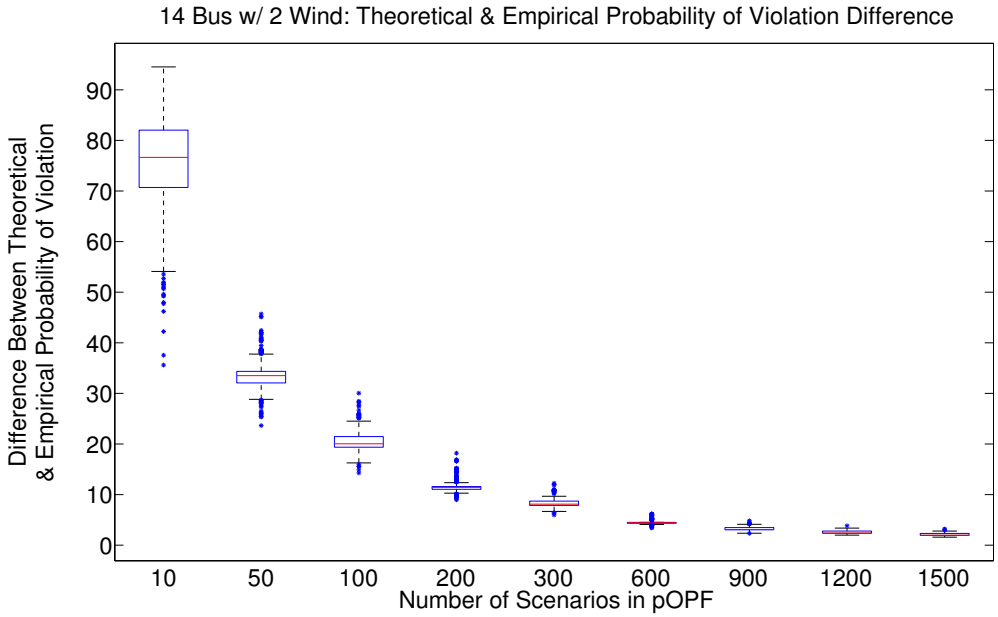

Figure 8.7: AC-QP pOPF Empirical Violation Compared to A-posteriori Theoretical Violation Results

CHAPTER IX

Optimizing Wind Penetration While Considering Uncertainty

The pOPF formulations in Chapters VII and VIII rely upon having a base case wind forecast and are designed for an operational setting. However, determining the base case wind generation for which the operation of conventional generation can be reliably scheduled for a wide range of possible wind scenarios is a challenging problem. Given a set of potential wind locations within a network, determining the maximum wind capacity that should be installed at each is thus an important planning problem. While the base case forecast was a fixed input parameter in the formulation in Chapter VII, the base case wind generation is a decision variable in this planning problem. Solution methods have been developed for this problem in the stochastic DC optimal power flow (OPF) context, as in [43]. While such formulations address the uncertainty of wind generation, the DC approximation may result in solutions that do not satisfy the AC power flow equations, as demonstrated in Chapter VIII. Such work must therefore be extended to the AC OPF setting, improving the accuracy of the network model in the OPF problem to ensure reliability standards are maintained.

9.1 Updated AC-QP OPF Formulation

The problem assumes that, as in the previous formulation in Chapter VII, two input parameters have been chosen: a set of wind node locations (denoted $\mathcal{W}$), and a set $\mathcal{S}$ of wind scenarios for each wind location to be considered in the pOPF problem. When the base case wind forecast is a fixed parameter (as in Chapters VII and VIII), each scenario is represented by a vector of wind generation values. However, in this context, the base case wind generation is itself a decision variable that is being maximized. Scenarios must therefore be represented differently to account for the fact that the base case is changing. Each scenario, indexed by the variable m, is characterized

by a vector E^m. Each nonnegative entry of this vector, E_i^m, gives the percentage of the base case wind generation taken at node i in scenario m. For example, if in scenario m the actual wind output at node i would be 95% of the base case value, then $E_i^m = 0.95$. It is possible that the value E_i^m takes may be greater than 1. While the maximum base case wind generation is constrained to a realistic value, it is possible in such cases that the value of wind generation in a given scenario will exceed this upper limit.

The problem is then solved in the following manner using a modified AC-QP algorithm. As in previous formulations, the AC-QP method is initialized from the solution of an SOCP relaxation of the AC OPF problem. It is assumed in the SOCP that there is no wind in the network. A value of the base case wind generation, denoted P_w°, is also required. In this work, it is assumed that $P_{w,i}^\circ = 0$ for all wind nodes $i \in \mathcal{W}$. Note that this choice is only used in the first QP-(power flow) iteration. The initial AC power flow for the base case is solved using P_w° and the generation schedule from the SOCP solution, P_g^{init}. The result of the power flow gives an updated generation schedule, P_g°, that has been adjusted to account for network losses. The initial power flow for each scenario can be run in a similar manner. The wind generation schedule in scenario m can be calculated as $P_w^{\circ,m} = \text{diag}\{E^m\}P_w^\circ$. The generation schedule for each scenario, $P_g^{init,m}$, is then found by adjusting the base case generation schedule according to the linear policy described by (7.1). It should be noted that the distribution vector in this policy is a decision variable in this optimization problem. The value of this vector that was used to solve the previous AC power flow will be represented in the QP by d°. An AC power flow is then solved for each scenario using $P_g^{init,m}$ and $P_w^{\circ,m}$. As in the base case, the power flow solution gives an updated generation schedule, $P_g^{\circ,m}$, that has been adjusted to account for the network losses. As such, the value of $P_g^{\circ,m}$ includes not only the total system losses in each scenario, but also the distributed wind forecast error determined by the base case wind generation and the scenario vectors E^m.

A QP is solved at each iteration of the algorithm to schedule changes from the power flow solutions. The values of P_g° and $P_g^{\circ,m}$ are then updated after each set of AC power flows. Likewise, the value of P_w° is updated at each iteration based on the value of ΔP_w in the QP solution. The QP that must be solved at each iteration to schedule changes from the previous power flow solution is as follows. The OPF objective is to maximize the total base case wind generation, $\sum_{i\in\mathcal{W}}(P_{w,i}^\circ + \Delta P_{w,i})$. The nonconvex power balance constraints are linearized through constraints (9.1b) and (9.1d). The lower bound of constraint (9.1c) ensures the feasibility of the base case wind forecast, while the corresponding upper limit is included to provide a realistic wind generation schedule that is reflective

of available technology. A value of 250 MW was used for $P_{w,i}^{max}$ in this work. Generator active power limits are enforced for each scenario through constraint (9.1e). Constraint (9.1f) enforces entries of the vector d to be nonnegative, while the sum of all entries is constrained to equal 100% through constraint (9.1g).

The QP solved at each iteration is then formulated as:

$$\max_{\substack{\Delta P_w, \Delta P_g, \Delta Q_g, \Delta\theta, \Delta V, \\ \alpha^m, d, \Delta Q_g^m, \Delta\theta^m, \Delta V^m}} \quad \sum_{i \in \mathcal{W}} \left(P_{w,i}^{\circ} + \Delta P_{w,i}\right) \tag{9.1a}$$

$$\text{subject to } (3.3\text{b}) - (3.3\text{d}), (3.3\text{f}), (3.2\text{a}) - (3.2\text{b}), (7.2\text{d}) - (7.2\text{h})$$

$$\mathbf{J}\Delta x = \Delta S \tag{9.1b}$$

$$0 \leq P_{w,i}^{\circ} + \Delta P_{w,i} \leq P_{w,i}^{max} \qquad \forall i \in \mathcal{W} \tag{9.1c}$$

$$\forall m \in \mathcal{S}:$$

$$\mathbf{J^m}\Delta x^m = \Delta \bar{S}^m \tag{9.1d}$$

$$P_{g,i}^{min} \leq P_{g,i}^{\circ,m} + \Delta P_{g,i} + \alpha^m d_i + d_i^{\circ} \sum_{k \in \mathcal{W}} (E_k^m P_{w,k}^{\circ} - P_{w,k}^{\circ})$$
$$- d_i \sum_{k \in \mathcal{W}} [\, E_k^m (P_{w,k}^{\circ} + \Delta P_{w,k}) - P_{w,k}^{\circ} - \Delta P_{w,k}] \, \leq P_{g,i}^{max} \qquad \forall i \in \mathcal{G} \tag{9.1e}$$

$$d_i \geq 0 \qquad \forall i \in \mathcal{G} \tag{9.1f}$$

$$\sum_{i \in \mathcal{G}} d_i = 1 \tag{9.1g}$$

where

$$\mathbf{J} = \begin{bmatrix} \frac{\partial P}{\partial \theta} & \frac{\partial P}{\partial V} \\ \frac{\partial Q}{\partial \theta} & \frac{\partial Q}{\partial V} \end{bmatrix}, \Delta x = \begin{bmatrix} \Delta\theta \\ \Delta V \end{bmatrix}, \Delta S = \begin{bmatrix} G_a \Delta P_g + W_a \Delta P_w \\ G_a \Delta Q_g \end{bmatrix}$$

As defined in Chapter III, G_a is the node-generator incidence matrix and W_a is the node-wind incidence matrix. As in previous formulations, the linearized line-flow constraints are initially enforced for all lines that are at or above 95% of their line-flow limit. This set is then updated at the beginning of each outer loop of the AC-QP algorithm to include any lines that are overloaded but have not yet been added to the set (bolded in Figure 4.1). Doing so limits the number of equality constraints that must be explicitly modeled in the QP. This has been demonstrated to improve the solution time of the AC-QP network, particularly for large networks [68].

The linearization for each scenario is then modeled as

$$\Delta x^m = \begin{bmatrix} \Delta\theta^m \\ \Delta V^m \end{bmatrix},$$

$$\Delta\bar{S}^m = \begin{bmatrix} G_a\{\Delta P_g + \alpha^m d + d^\circ \sum_{k\in\mathcal{W}}(E_k^m P_{w,k}^\circ - P_{w,k}^\circ) \\ -d\sum_{k\in\mathcal{W}}[\ E_k^m(P_{w,k}^\circ + \Delta P_{w,k}) - P_{w,k}^\circ - \Delta P_{w,k}]\}+ \\ W_a[\mathrm{diag}\{E^m\}\Delta P_w] \\ \\ G_a\Delta Q_g^m \end{bmatrix}. \tag{9.2}$$

In this linearization, the active power component of $\Delta\bar{S}^m$ has several terms. Applying a distributed slack formulation, the term $\alpha^m d$ introduces a degree of freedom to account for the fact that active power losses differ between the base case and each scenario. It should be noted that when the AC-QP method has converged, α^m takes a sufficiently small value, such that this difference in losses does not introduce any constraint violations. The change in conventional generator participation in the increased or decreased mismatch in scenario m is modeled by $d\sum_{k\in\mathcal{W}}[\ E_k^m(P_{w,k}^\circ + \Delta P_{w,k}) - P_{w,k}^\circ - \Delta P_{w,k}]$. Finally, as d is a decision variable in this problem, the term $d^\circ \sum_{k\in\mathcal{W}}(E_k^m P_{w,k}^\circ - P_{w,k}^\circ)$ is required to adjust the conventional generator dispatch for any changes in d. This is due to the fact that as defined in (7.1), $P_{g,i}^{\circ,m}$ includes the mismatch of scenario m that was based on the base case wind generation from the previous QP-(power flow) iteration.

Each scenario m requires extra variables for the reactive power output of each generator (ΔQ_g^m) and the voltage at each bus (ΔV^m, $\Delta\theta^m$). Note that both the deviation of the active power generation, ΔP_g, and the generator voltage magnitude setpoints are required to take the same value for the base case and all scenarios.

The algorithm provides a solution satisfying the nonconvex AC power flow constraints for the base case and all considered scenarios. The randomized optimization technique discussed in Chapter VII is then employed to provide probabilistic guarantees to accompany the solution.

9.2 Addressing the Bilinearity in the AC-QP pOPF Problem

As formulated, ΔP_w, α^m, and d are all decision variables in the pOPF problem. Bilinearities thus arise in the terms in constraint (9.1e) and definition (9.2) that contain the products of these variables. The pOPF including these bilinear terms is solved by replacing the QP with a two-stage iterative solution method, the details of which are as follow.

Stage 1: Maximizing Wind Generation

The goal of the first stage is to determine the maximum base case wind generation that can be added in the network, subject to the linearized network constraints. To do so, the pOPF problem is solved assuming that the vector d is a fixed parameter, while α^m and ΔP_w are decision variables. The QP solved in Stage 1 is then as follows.

$$\max_{\substack{\Delta P_w, \Delta P_g, \Delta Q_g, \Delta\theta, \Delta V, \\ \alpha^m, \Delta Q_g^m, \Delta\theta^m, \Delta V^m}} \quad \sum_{i \in \mathcal{W}} \left(P_{w,i}^{\circ} + \Delta P_{w,i}\right) \tag{9.3a}$$

$$\text{subject to } (3.3\text{b}) - (3.3\text{d}), (3.3\text{f}), (3.2\text{a}) - (3.2\text{b}), (7.2\text{d}) - (7.2\text{h}), (9.1\text{b}) - (9.1\text{c}), (9.1\text{d}) - (9.1\text{e})$$

$$\sum_{i \in \mathcal{W}} \Delta P_{w,i} \geq \sum_{i \in \mathcal{W}} \Delta P_{w,i}^{z} \tag{9.3b}$$

Constraint (9.3b) is added to improve the convergence of this iterative solution method. In this constraint, the variable z is used to index the Stage 1-Stage 2 iterations. As these iterations between the two stages proceed, this constraint enforces adding increasing amounts of wind into the network. The values of α^m and ΔP_w then become fixed parameters in Stage 2, in which an optimal value of d is determined.

Stage 2: Maximizing Generator Reserve Capacity

The second stage determines an optimal distribution vector, d, to increase the amount of wind that can be added in the network. The original objective of maximizing total wind generation (which is a fixed parameter in this stage) is replaced with the modified objective of maximizing total reserve capacity of all conventional generators. The intuition behind this modified objective is that if conventional generators have larger reserve capacity, more wind can be integrated in the network in the next stage, as generators have greater ability to respond to larger forecast errors. This is a consequence of the linear policy assumed for how conventional generators respond to the wind generator forecast error. The QP solved in Stage 2 is then as follows.

$$\max_{\substack{\Delta P_g, \Delta Q_g, \Delta\theta, \Delta V, \\ d, \Delta Q_g^m, \Delta\theta^m, \Delta V^m}} \quad \sum_{i \in \mathcal{G}} [\ (P_{g,i}^{max} - P_{g,i}^{\circ} - \Delta P_{g,i}) + (P_{g,i}^{\circ} + \Delta P_{g,i} - P_{g,i}^{min})] \tag{9.4a}$$

$$\text{subject to } (3.3\text{b}) - (3.3\text{d}), (3.3\text{f}), (3.2\text{a}) - (3.2\text{b}), (7.2\text{d}) - (7.2\text{h}), (9.1\text{b}) - (9.1\text{c}), (9.1\text{d}) - (9.1\text{g})$$

Stage 2 then provides an updated value of the vector d to Stage 1. These iterations repeat

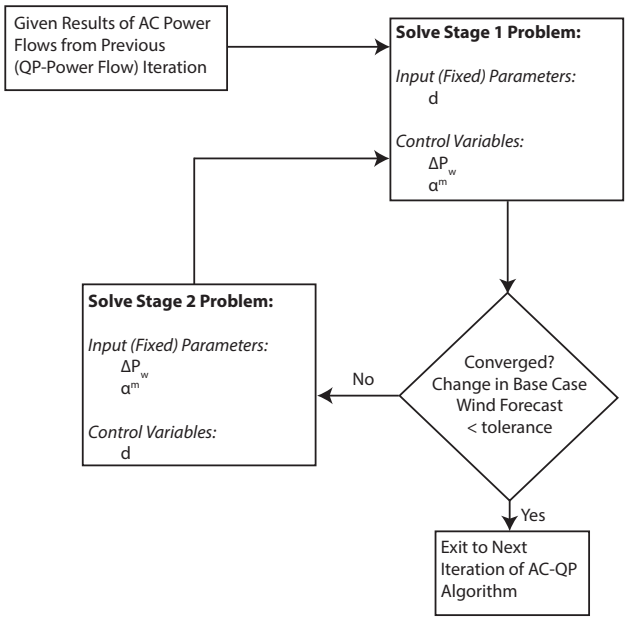

Figure 9.1: Iterative Solution Algorithm for Bilinear Terms in Constraints (9.1d) and (9.1e).

until the change in the total base case wind forecast, $\sum_{i \in \mathcal{W}}(P^{\circ}_{w,i} + \Delta P_{w,i})$, is within some small tolerance. The details of this iterative algorithm are summarized in Figure 9.1. Note that this iterative solution method replaces the "Solve QP with latest power flow results" box in Figure 4.1.

9.3 Identifying a Minimal Set of Support Scenarios

In the IEEE 14-bus test case discussed in Chapter VII, it was observed that when optimizing over a very large set of N wind scenarios, only a small subset of k scenarios were required to be explicitly modeled in the optimization problem for the resulting solution to be feasible for the remaining $(N-k)$ scenarios. This subset of k scenarios comprises the set of support scenarios associated with the problem optimizing over N scenarios, as including any of the remaining $(N-k)$ scenarios in the optimization problem will not change the solution. This property is of particular interest in the large-scale test case, as introducing a scenario into the pOPF problem requires duplicating the network constraints and introducing many additional decision variables. This has significant consequences when considering execution time for planning applications. Thus, identifying a minimal support set is beneficial to solve the pOPF problem in a reasonable time frame.

Moreover, this minimal set of support scenarios has important implications for deriving an a-posteriori probabilistic guarantee on the probability of violation to accompany the solution. Recall from (7.3) that this theoretical upper bound depends on the number of scenarios considered in the

pOPF problem (N), the cardinality of this set of support scenarios (k), and a design parameter (β). To be a meaningful upper bound, it should be as tight as possible. From the formula, it can be seen that this can be achieved in two ways: either optimizing over a larger set of scenarios (i.e. increasing N), or reducing the number of scenarios in the support set (reducing k). The latter is a topic to be examined in greater detail in future research.

The proposed formulation initially sorts the N scenarios to be considered according to the total difference between the scenario and the base case generation,

$$\sum_{i \in \mathcal{W}} (P_{w,i}^m - P_{w,i}). \tag{9.5}$$

Note that this calculation uses only the base case generation (and corresponding scenarios) used to initialize the AC-QP method. Initially, two scenarios are introduced into the pOPF problem. These scenarios are the first and last ranked ones, which correspond to the scenarios introducing the most positive and most negative mismatches, respectively. After the algorithm has converged, and a feasible solution for these two scenarios is found, AC power flows are solved to check the feasibility of the $(N-2)$ scenarios. One additional scenario is then introduced in the pOPF problem, corresponding to the scenario with the greatest number of constraint violations. The goal of iteratively introducing scenarios into the optimization, as in Chapter VII, is to arrive at a small[1] set of support scenarios.

9.4 Test Case Results and Discussion

The proposed method was tested on the IEEE 118-bus network [59] that has been augmented with 10 randomly chosen wind nodes. It was assumed that each potential wind site has a capacity of 250 MW. The results of this test case for increasing numbers of scenarios included in the pOPF problem (i.e. the value of N in Figure 7.1) are summarized in Figures 9.2-9.6. Boxplots are used to summarize the results of 500 repeated trials, where each trial differs in the specific set of N randomly chosen wind scenarios. Recall that these give several statistical quantities of interest for each set of 500 trials: the central line inside the box shows the median over all 500 trials; the bottom and top edges of each box show the 25% and 75% percentiles respectively; and the vertical lines show the extreme values. Statistical outliers are then marked by an asterisk.

[1] Note that ideally this small set should be a minimal set of support scenarios. However, this is not guaranteed.

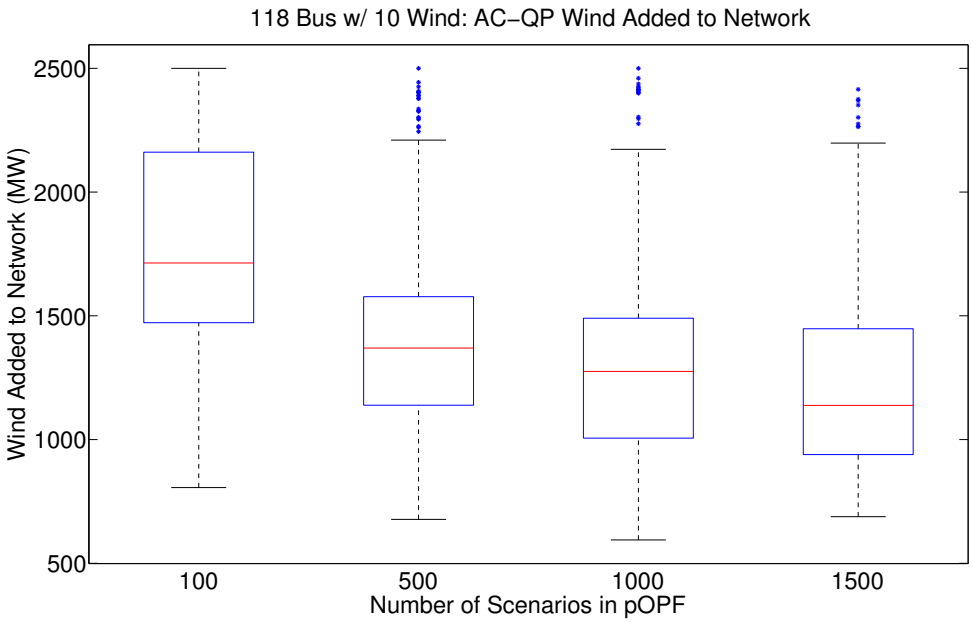

Figure 9.2: AC-QP Wind Added to Network.

Figure 9.2 shows the amount of wind that can be added in the network for various sets of N scenarios. These results demonstrate the need to account for the uncertainty of wind generation when planning how much wind to install at various network locations. If only 100 scenarios are considered, the median total wind generation added to the network is 1713 MW. However, the median total wind generation decreases to 1138 MW when 1500 scenarios are included in the optimization. As the number of scenarios considered in the pOPF increases, less wind can be added in the network to maintain reliability standards.

The scalability of the proposed method is highlighted by the results in Figure 9.3. In 99% of all trials, the AC-QP pOPF algorithm is solved within 18 minutes (1080 seconds), which is an appropriate time frame for planning problems. Moreover, due to the iterative manner in which scenarios are introduced into the problem, the execution time is only slightly affected by increasing N in the pOPF problem. Thus, the method is scalable with respect to network size and to the number of scenarios for which the resulting solution must be feasible.

Figure 9.4 shows the cardinality of the set of support scenarios identified in each trial. Denoted k in (7.3), this number is used to calculate the theoretical a-posteriori probability of violation for each trial (shown in Figure 9.5). While the number of support scenarios increases with larger numbers of scenarios considered in the problem, they remain a very small fraction of the much larger sets of N scenarios. This translates into reasonably low theoretical upper bounds on the probability

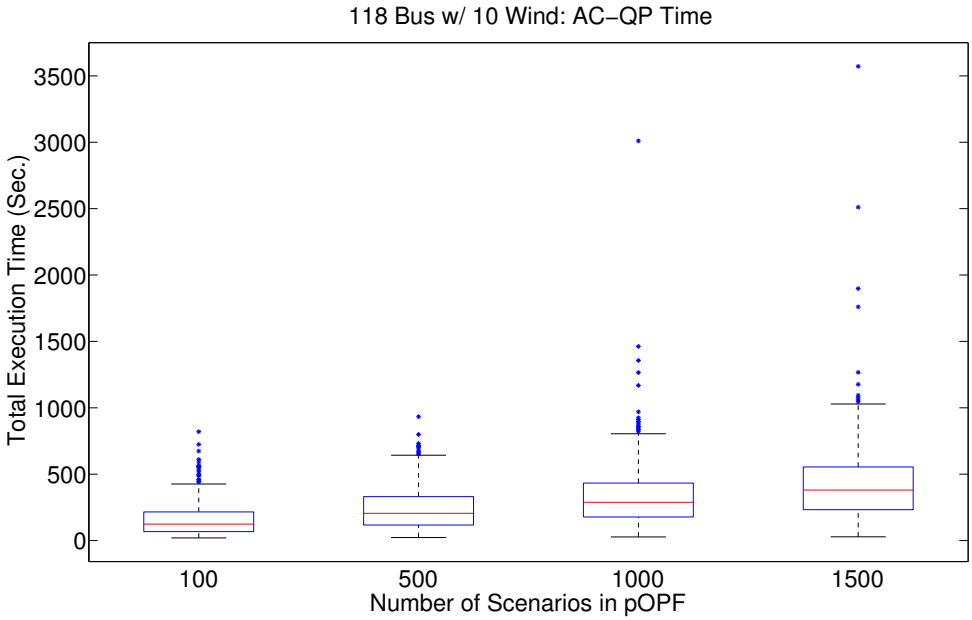

Figure 9.3: AC-QP Total Execution Time.

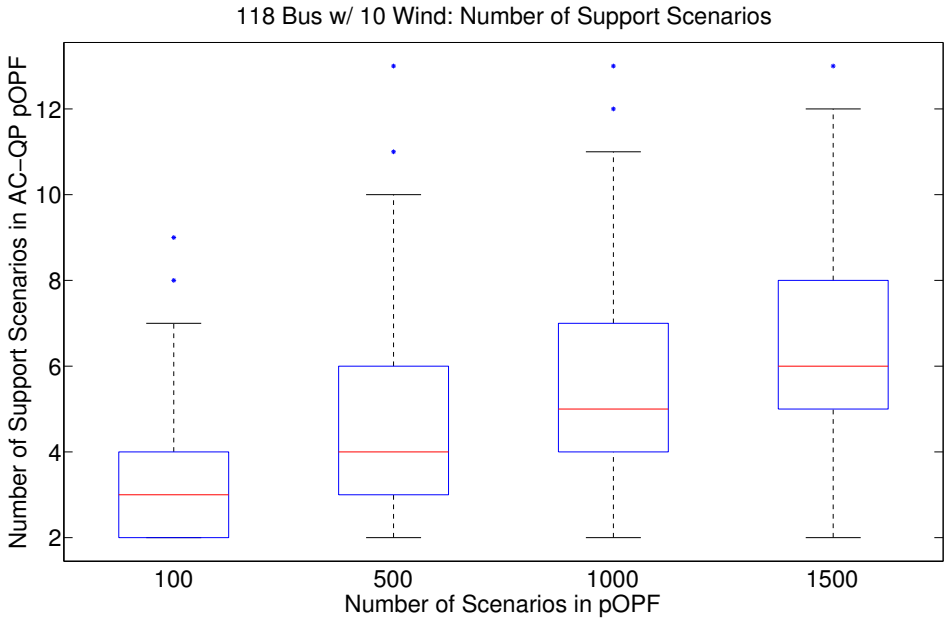

Figure 9.4: AC-QP Number of Support Scenarios.

of violation. As Figure 9.5 shows, the support set results correspond to theoretical upper bounds ranging from 20-33% when only 100 scenarios are considered in the problem. However, after N is increased to 1000 scenarios, the theoretical probability of any constraint violation is below 10%.

The empirical quality of solution from the AC-QP pOPF algorithm is assessed via Monte Carlo

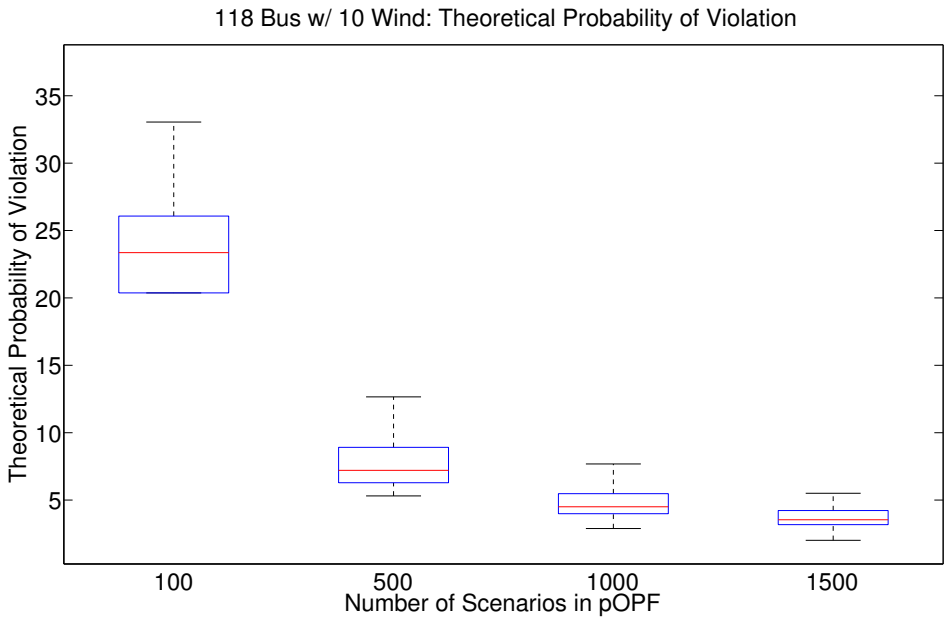

Figure 9.5: AC-QP A-Posteriori Theoretical Probability of Violation.

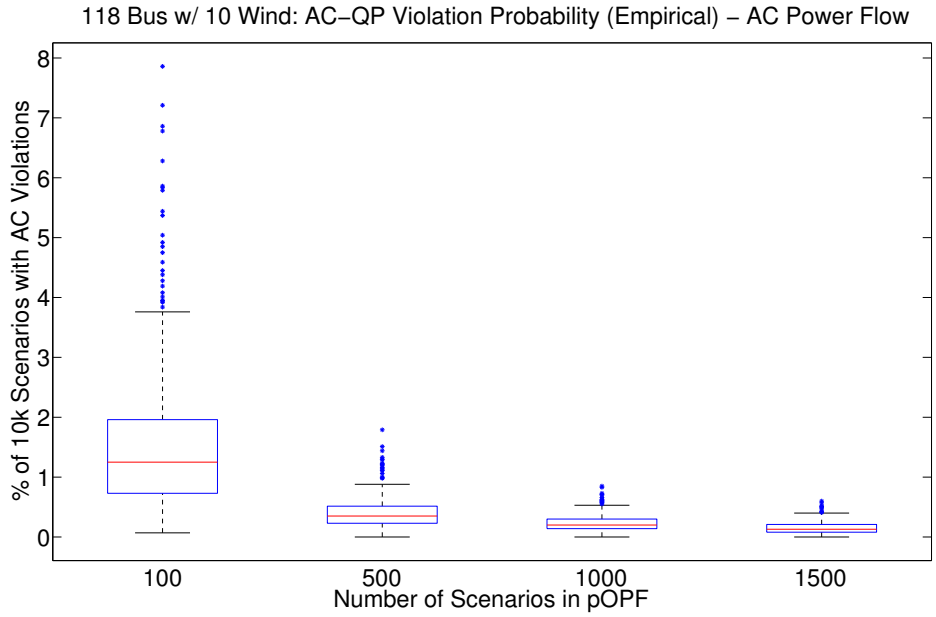

Figure 9.6: AC-QP Empirical Probability of Violation.

simulations using 10,000 possible scenarios. For each scenario, an AC power flow is run and the violation of any constraint is checked. Out of those 10,000 scenarios, those that result in any constraint violations (including generator active and reactive power limits, voltage magnitude limits, and line flow limits) are recorded to provide an empirical probability of constraint violation. The

results of these simulations are summarized in Figure 9.6. While the theoretical upper bound on the probability of violation is unacceptably high for the case of $N = 100$, the empirical results are more conservative. In this case, the empirical probability of violation is below 10% for all trials, and is less than 1% when N is increased to at least 1000 scenarios.

9.5 Conclusions

The stochastic AC-QP pOPF algorithm has been extended to a planning context to determine the maximum wind penetration that can be integrated in a network while maintaining reliability standards. The scalability of this method with respect to large numbers of wind scenarios and moderate network size has been demonstrated. The proposed algorithm does not rely upon model approximations and provides an AC-feasible solution, providing reliable wind installation solutions. Moreover, through the application of the scenario approach from the field of randomized optimization, the final solution is accompanied with theoretical a-posteriori guarantees on the probability of violation.

While this formulation focuses on maximizing the amount of wind that can be added in a network, it has not considered the cost of generator reserve capacity required to maintain reliability standards. As shown in Chapter VIII, the relatively expensive nature of this service can have a significant impact on the optimality of the final solution. It should therefore be included in the wind generation planning decisions as well. As such, the cost of generator reserves is incorporated in this formulation in Chapter X.

CHAPTER X

Co-Optimizing Wind Penetration and Reserve Capacity While Considering Uncertainty

As demonstrated in Chapter IX, determining the size of future wind generation at potential network locations to maximize the renewable penetration in a network is an important planning problem. Increasing the renewable generation in a network displaces conventional generation, reducing the operating cost. However, greater amounts of relatively expensive generator reserve capacity are necessary to maintain reliability standards as the wind penetration increases. The planning problem to decide on an optimal investment in wind generation must therefore consider such tradeoffs. The stochastic AC-QP pOPF solution algorithm presented in Chapter IX is modified to solve this problem.

10.1 Reformulated AC-QP OPF Problem

As in the previous formulation, the AC-QP pOPF is initialized from the solution of an SOCP relaxation of the AC OPF problem with no wind in the network. Recall that each scenario, indexed by m, is characterized by a vector E^m. Each nonnegative entry E_i^m gives the percentage of the base case wind generation taken at node i in scenario m. The initial value of wind generation in the base case is denoted P_w°, and the initial wind generation schedule in scenario m is calculated as $P_w^{\circ,m} = \text{diag}\{E^m\}P_w^\circ$. The initial AC power flow for the base case is solved using P_w° and the generation schedule from the SOCP solution, P_g^{init}. This provides an updated generation schedule, P_g°, that has been adjusted to account for network losses. Likewise, the initial power flow for each scenario is solved using $P_w^{\circ,m}$ and $P_g^{init,m}$, where the latter is the base case generation schedule adjusted to the linear policy (7.1). This gives an updated generation schedule, $P_g^{\circ,m}$ that has been adjusted to account for the network losses. As such, the value of $P_g^{\circ,m}$ includes not only the total

system losses in each scenario, but also the distributed wind forecast error determined by the base case wind generation.

A QP is then solved at each iteration of the algorithm to schedule changes from the power flow solutions. The values of P_g° and $P_g^{\circ,m}$ are then updated after each set of AC power flows. The QP that must be solved at each iteration to schedule changes from the previous power flow solution is as follows:

$$\min_{\substack{\Delta P_g, R_g, \Delta P_w, \Delta\theta, \Delta V, \Delta Q_g, \\ \alpha^m, d, \Delta Q_g^m, \Delta\theta^m, \Delta V^m}} \quad \xi_1 \left[\sum_{i \in \mathcal{G}} C_i\big(P_{g,i}^{\circ} + \Delta P_{g,i}\big) + \sum_{i \in \mathcal{G}} \tilde{C}_i\big(R_{g,i}\big) \right] - \xi_2 \sum_{i \in \mathcal{W}} \Delta P_{w,i} \tag{10.1a}$$

subject to (3.3b) – (3.3f), (3.2a) – (3.2b), (7.2d) – (7.2h)

$$\mathbf{J}\Delta x = \Delta\tilde{S} \tag{10.1b}$$

$$0 \le P_{w,i}^{\circ} + \Delta P_{w,i} \le P_{w,i}^{max} \qquad \forall i \in \mathcal{W} \tag{10.1c}$$

$\forall m \in \mathcal{S}$:

$$\mathbf{J^m}\Delta x^m = \Delta\breve{S}^m \tag{10.1d}$$

$$\begin{aligned} P_{g,i}^{min} \le P_{g,i}^{\circ,m} + \Delta P_{g,i} + \alpha^m d_i + d_i^{\circ} \sum_{k \in \mathcal{W}} (E_k^m P_{w,k}^{\circ} - P_{w,k}^{\circ}) \\ - d_i \sum_{k \in \mathcal{W}} [\ E_k^m (P_{w,k}^{\circ} + \Delta P_{w,k}) - P_{w,k}^{\circ} - \Delta P_{w,k}] \ \le P_{g,i}^{max} \qquad \forall i \in \mathcal{G} \end{aligned} \tag{10.1e}$$

$$-R_{g,i} \le \alpha^m d_i - d_i \sum_{k \in \mathcal{W}} (E_k^m (P_{w,k}^{\circ} + \Delta P_{w,k}) - P_{w,k}^{\circ} - \Delta P_{w,k}) \le R_{g,i} \qquad \forall i \in \mathcal{G} \tag{10.1f}$$

$$d_i \ge 0 \qquad \forall i \in \mathcal{G} \tag{10.1g}$$

$$\sum_{i \in \mathcal{G}} d_i = 1 \tag{10.1h}$$

where

$$\Delta\tilde{S} = \begin{bmatrix} G_a \Delta P_g + W_a \Delta P_w \\ G_a \Delta Q_g \end{bmatrix},$$

$$\Delta\breve{S}^m = \begin{bmatrix} G_a\{\Delta P_g + \alpha^m d + d^{\circ} \sum_{k \in \mathcal{W}} (E_k^m P_{w,k}^{\circ} - P_{w,k}^{\circ}) \\ -d \sum_{k \in \mathcal{W}} [\ E_k^m (P_{w,k}^{\circ} + \Delta P_{w,k}) - P_{w,k}^{\circ} - \Delta P_{w,k}]\} + \\ W_a[\mathrm{diag}\{E^m\}\Delta P_w] \\ \\ G_a \Delta Q_g^m \end{bmatrix}.$$

In this linearization, the active power component of $\Delta\breve{S}^m$ has several terms. Applying a distributed slack formulation, the term $\alpha^m d$ introduces a degree of freedom to account for the fact that active

power losses differ between the base case and each scenario. It should be noted that when the AC-QP method has converged, α^m takes a sufficiently small value, such that this difference in losses does not introduce any constraint violations. The change in conventional generator participation in the increased or decreased mismatch in scenario m is modeled by $d\sum_{k\in\mathcal{W}}[\ E_k^m(P_{w,k}^\circ+\Delta P_{w,k})-P_{w,k}^\circ-\Delta P_{w,k}]$. Finally, as d is a decision variable in this problem, the term $d^\circ\sum_{k\in\mathcal{W}}(E_k^m P_{w,k}^\circ - P_{w,k}^\circ)$ is required to adjust the conventional generator dispatch for any changes in d. This is due to the fact that $P_{g,i}^{\circ,m}$ already accounted for the mismatch in scenario m according to the linear policy when solving the previous AC power flow.

This problem seeks a solution that co-optimizes three objectives. The first is to minimize the total cost of conventional generation. The second is to minimize the total cost of generator reserve capacity. The final objective term is to maximize the total wind generation in the network. Increasing the amount of wind in a network displaces conventional generation, reducing the cost of conventional generation. Conversely, decreasing the cost of generator reserve capacity and increasing the total amount of wind in the network are competing objectives. The weighting factor of the third term in the objective function, relative to the first two terms, will thus influence the final solution. Placing a very high weight on this third term (i.e. choosing $\xi_2 \gg \xi_1$) will result in more wind being added to the network because the reserve capacity required to accommodate higher forecast errors is relatively cheap. Conversely, substantially decreasing the weight of this term ($\xi_2 \ll \xi_1$) places a relatively higher cost on reserve capacity, resulting in less wind being added to the network. Conducting a sensitivity study to explore this tradeoff is a topic of future research. In this work, weighting factors of $\xi_1 = 10^{-2}$ and $\xi_2 = \$1/\text{p.u.}$ were placed on the corresponding objective terms. The value of ξ_1 accounts for the fact that the units of the third objective term are in p.u., while the cost coefficients of the first two terms convert the p.u. arguments to MW. Moreover, the coefficient ξ_2 is used to convert the total base case wind generation to a monetary cost.

This is a planning problem, as it would be used to determine the optimal investment in wind generation that should be made at each potential wind location. It differs from the problems in Chapters VIII and IX in a few ways. This problem considers the generator distribution vector, d, as a decision variable, which is a fixed parameter in Chapter VIII. It is also different from the work in Chapter VIII, as the role of the wind forecast in previous formulations is replaced by the maximum base case wind generation, which is a decision variable in this problem. Compared to that in Chapter IX, this problem co-optimizes the cost of generator reserves and of conventional

generation.

Note that there are terms in constraints (10.1e)-(10.1f) and in the definition of $\Delta\breve{S}^m$ that involve the product of d and ΔP_w, as well as d and α^m. As these are all decision variables in the QP, several bilinear terms appear in the optimization problem. To solve this, the QP solved at each iteration of the AC-QP pOPF method is replaced with a two-stage iterative solution method, similar to that proposed in Chapter IX.

Stage 1: Maximizing Wind Generation

The first stage of this algorithm focuses on maximizing the wind penetration in the network, while simultaneously minimizing the total cost of conventional generation and the cost of generator reserve capacity. In this problem, ΔP_w and α^m are decision variables, while d is a fixed parameter. The QP solved in Stage 1 is then as follows.

$$\min_{\substack{\Delta P_g, R_g, \Delta P_w, \Delta\theta, \Delta V, \Delta Q_g, \\ \alpha^m, \Delta Q_g^m, \Delta\theta^m, \Delta V^m}} \quad \xi_1 \left[\sum_{i \in \mathcal{G}} C_i\big(P^\circ_{g,i} + \Delta P_{g,i}\big) + \sum_{i \in \mathcal{G}} \tilde{C}_i\big(R_{g,i}\big) \right] - \xi_2 \sum_{i \in \mathcal{W}} \Delta P_{w,i} \tag{10.2a}$$

subject to $(3.3\text{b}) - (3.3\text{f}), (3.2\text{a}) - (3.2\text{b}), (7.2\text{d}) - (7.2\text{h}), (10.1\text{b}) - (10.1\text{f})$

$\forall m \in \mathcal{S}$:

$$\sum_{i \in \mathcal{W}} \Delta P_{w,i} \geq \sum_{i \in \mathcal{W}} \Delta P^z_{w,i} \tag{10.2b}$$

In this formulation, constraint (10.2b) is added to improve the convergence of this iterative solution method. In this constraint, the variable z is used to index the Stage 1 - Stage 2 iterations. As these iterations between the two stages proceed, this constraint enforces adding increasing amounts of wind into the network.

Stage 2: Minimizing the Cost of Generator Reserve Capacity

The second stage receives as an input from the first stage the values of α^m and ΔP_w; these are thus fixed parameters in this stage. The objective of the second stage aims to minimize the cost of generator reserve capacity, while simultaneously minimizing the total cost of conventional generation. In this problem, d is a decision variable. The subsequent QP is solved in Stage 2 of the algorithm.

$$\min_{\substack{\Delta P_g, R_g, \Delta\theta, \Delta V, \Delta Q_g, \\ d, \Delta Q_g^m, \Delta\theta^m, \Delta V^m}} \quad \xi_1 \left[\sum_{i \in \mathcal{G}} C_i\big(P_{g,i}^{\circ} + \Delta P_{g,i}\big) + \sum_{i \in \mathcal{G}} \tilde{C}_i\big(R_{g,i}\big) \right] \tag{10.3a}$$

subject to (3.3b) − (3.3f), (3.2a) − (3.2b), (7.2d) − (7.2h), (10.1b) − (10.1f)

$$d_i \geq 0 \qquad \forall i \in \mathcal{G} \tag{10.3b}$$

$$\sum_{i \in \mathcal{G}} d_i = 1 \tag{10.3c}$$

In this problem, constraint (10.3b) ensures that all entries of the generator distribution vector are nonnegative, while constraint (10.3c) constrains their sum to equal 100%. The choice of this vector will impact how network losses (as well as wind forecast error) are allocated to each generator. Stage 2 initially determines d based on the active power losses from the previous AC power flow, which are incorporated in $P_g^{\circ,m}$, as well as the change in losses estimated by the value of α^m determined from Stage 1. With a new choice of d, Stage 1 is solved again, providing a new estimate of the change in losses by determining a new value of α^m. Once the two stages have converged, the actual impact on losses of this new distribution vector is updated through the new value of $P_g^{\circ,m}$ from the power flow solution.

At convergence, the maximum base case wind generation has been found, while minimizing the costs of conventional generation and of reserve capability. Moreover, as a scenario approach is applied to this stochastic AC OPF planning problem, the resulting solution is also accompanied with theoretical a-posteriori reliability guarantees. The details of this method are summarized in Figure 10.1. Note that this iterative solution method replaces the "Solve QP with latest power flow results" box in Figure 4.1.

10.2 Test Case 1: Assuming Generator Reserve Capacity is Four Times as Expensive as Cost of Conventional Generation

The proposed algorithm was tested on the IEEE 118-bus network that has been augmented with 10 randomly chosen wind nodes. It was assumed that each potential wind site has a capacity up to 250 MW (i.e. $P_{w,i}^{max} = 2.5$ p.u. in constraint (10.1c)). The results of this test case for increasing numbers of scenarios included in the pOPF problem are summarized in Figures 10.2-10.8. As in previous studies, bloxplots are used to summarize the results. The central line inside each box gives the median over all 500 trials; the bottom and top edges of each box show the 25% and 75%

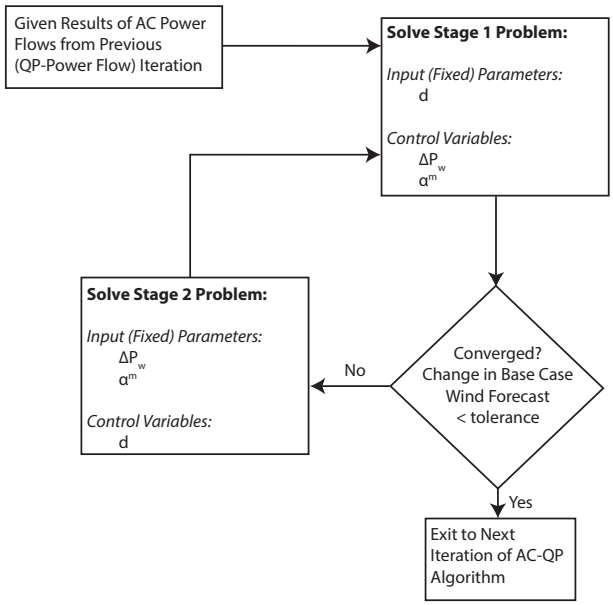

Figure 10.1: Iterative Algorithm to Solve Problem (10.1) with Bilinear Terms

percentiles respectively; and the vertical lines show the extreme values.

Figure 10.2 shows the value of each term in the objective function for various sets of N scenarios. As the number of scenarios considered in the pOPF increases, less wind can be added in the network to maintain reliability standards. This is reflected in the bottom subplot. Having less wind generation in the network results in a higher cost of conventional generation, as shown in the top subplot. Introducing greater amounts of wind in the network results in greater forecast errors considered, as demonstrated in Figure 10.3. The maximum absolute forecast error shown in this plot is calculated as $\max_{m\in\mathcal{S}} |\sum_{k\in\mathcal{W}}(E_k^m P_{w,k}^\circ - P_{w,k}^\circ)|$. As seen in constraint (10.1f), the value of this sum represents the forecast error that would be distributed to conventional generators. The maximum absolute value is thus directly related to the maximum amount of reserves required for the set of scenarios considered. Conventional generators must maintain larger reserve capacity to respond to these forecast errors. However, such reserve services are expensive to provide. Thus, the amount of wind added in the network and cost of generator reserves are directly related, as reflected in the middle subplot.

As reserves are assumed in this case to be significantly more expensive than the cost of conventional generation, there are many cases where no wind is added to the network. In these cases, the cost of generator reserve capacity is sufficiently high that it is more economical to supply demand using only conventional generation. Together, these results demonstrate the need to account for

the uncertainty of wind generation when planning how much wind to install at various network locations. Furthermore, they show the significant impact on the cost of operation that wind can have.

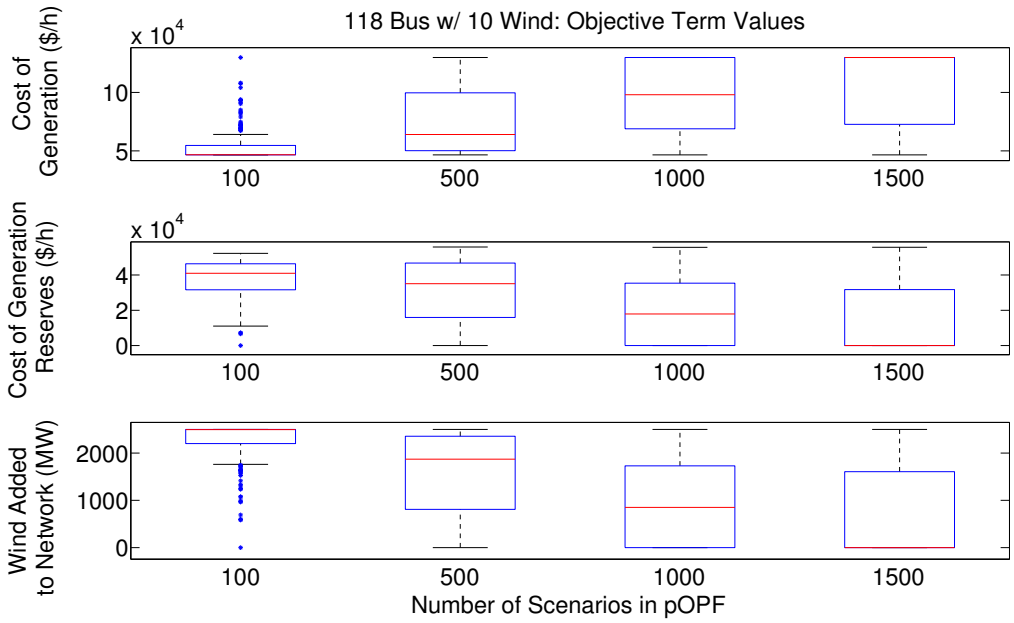

Figure 10.2: Test Case 1 AC-QP Objective Term Values

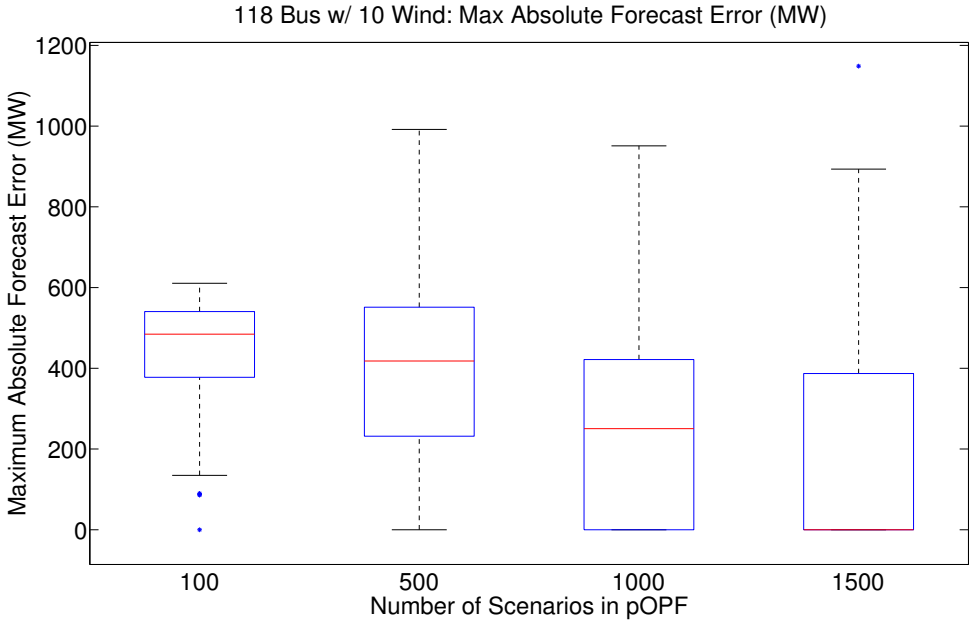

Figure 10.3: Test Case 1 AC-QP Maximum Total Forecast Error

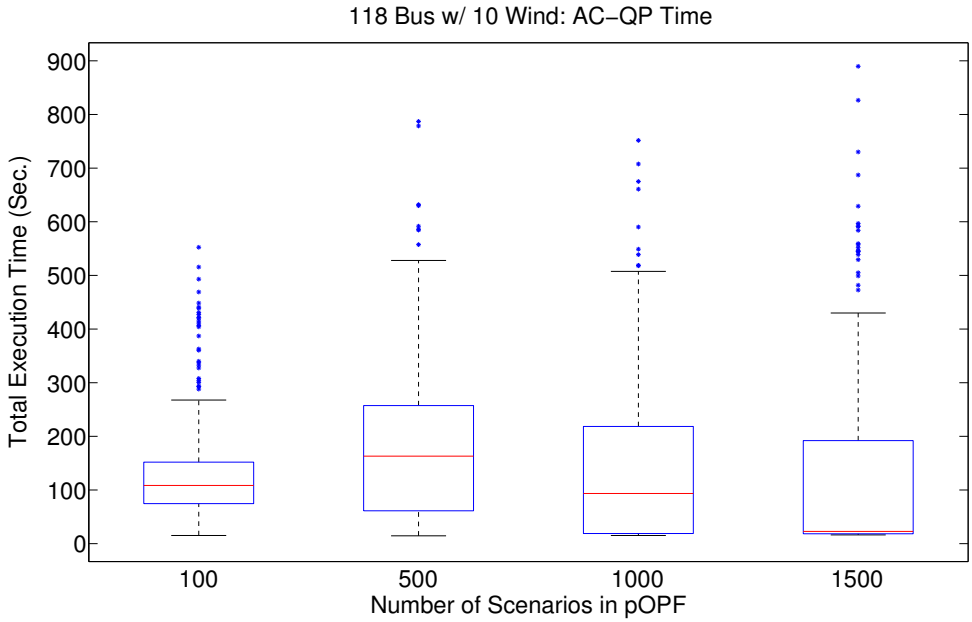

Figure 10.4: Test Case 1 AC-QP Execution Time

The scalability of the proposed method is highlighted by the results in Figure 10.4. In 99% of all trials, the AC-QP pOPF algorithm is solved within 10 minutes (600 seconds), which is an appropriate time frame for planning problems. In fact, in this case the execution time is significantly lower for cases considering larger sets of scenarios. This is due to the high cost on generator reserve capacity, which results in less wind being added to the network as more scenarios are considered. As shown in Figure 10.2, when 1500 scenarios are considered, the median value of wind added to the network is 0 MW. In such cases, the problem solved reverts to a standard AC OPF problem, and the solution to each scenario is identical to that of the base case. As this is a much less complex problem to solve, the computation time is greatly reduced. Moreover, due to the iterative manner in which scenarios are introduced into the problem, the median execution time is only slightly affected by increasing N in the pOPF problem. Thus, the method is scalable with respect to network size and to the number of scenarios for which the resulting solution must be feasible.

Figure 10.5 shows the cardinality of the set of support scenarios identified in each trial. This number is used to calculate the theoretical a-posteriori probability of violation for each trial (shown in Figure 10.6). The number of support scenarios remains a very small fraction of the large sets of N scenarios considered in the problem. As previously mentioned, less wind is added to the network as larger sets of scenarios are considered. As such, the number of support scenarios decreases. When 1500 scenarios are considered, the median number of support scenarios is only 2. This corresponds

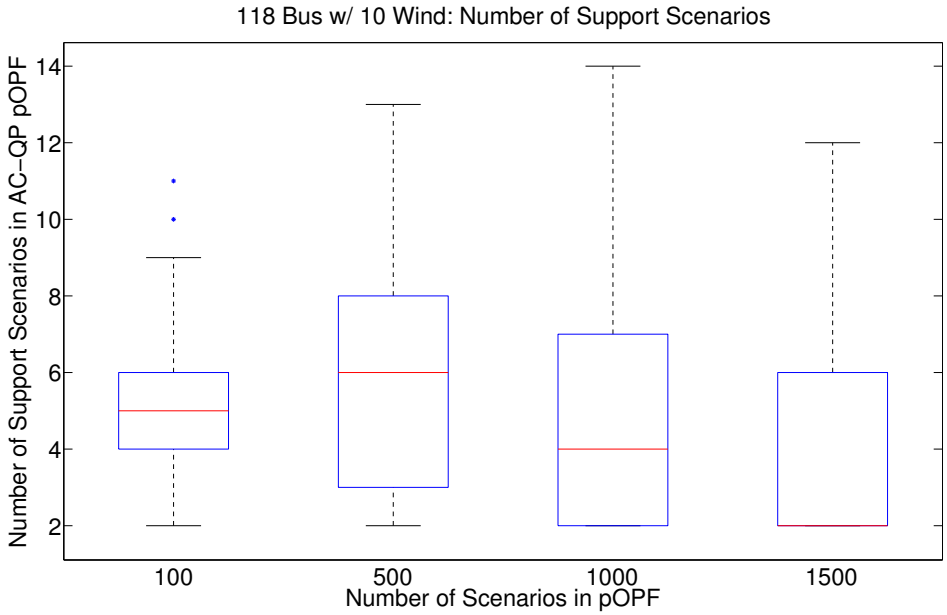

Figure 10.5: Test Case 1 AC-QP Support Scenarios

to the cases where it is already uneconomical to add wind to the network when only the first 2 scenarios are introduced into the problem. As the theoretical upper bounds on the probability of violation depend only on the cardinality of the set of support scenarios indentified, the results in Figure 10.5 translate into reasonably low theoretical guarantees. As Figure 10.6 shows, the support set results correspond to theoretical upper bounds ranging from 20-37% when only 100 scenarios are considered in the problem. However, after N is increased to 1000 scenarios, the theoretical probability of any constraint violation is below 10%.

The empirical quality of solution from the AC-QP pOPF algorithm is assessed via Monte Carlo simulations using 10,000 possible scenarios. For each scenario, an AC power flow is run and the violation of any constraint is checked. Out of those 10,000 scenarios, those that result in any constraint violations (including generator active and reactive power limits, voltage magnitude limits, and line flow limits) are recorded to provide an empirical probability of constraint violation. The results of these simulations are summarized in Figure 10.7. While the theoretical upper bound on the probability of violation is unacceptably high for the case of N = 100, the empirical results are more conservative. In this case, the empirical probability of violation is below 10% for all trials, and is less than 1% when N is increased to at least 1000 scenarios. Finally, Figure 10.8 shows the difference between the theoretical upper bound and empirical probability of violation found in each trial. As this difference is nonnegative in all trials, meaning that the empirical probability of

violation is lower than the calculated theoretical upper bound, this figure demonstrates that the empirical probability of violation results satisfy the theoretical upper bounds given in Figure 10.6.

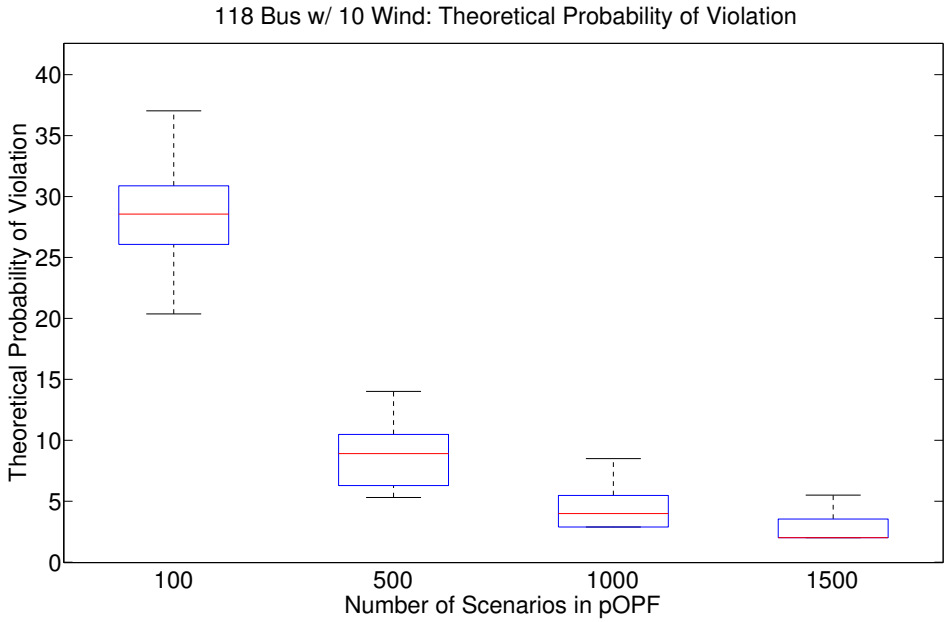

Figure 10.6: Test Case 1 AC-QP A-Posteriori Theoretical Probability of Violation

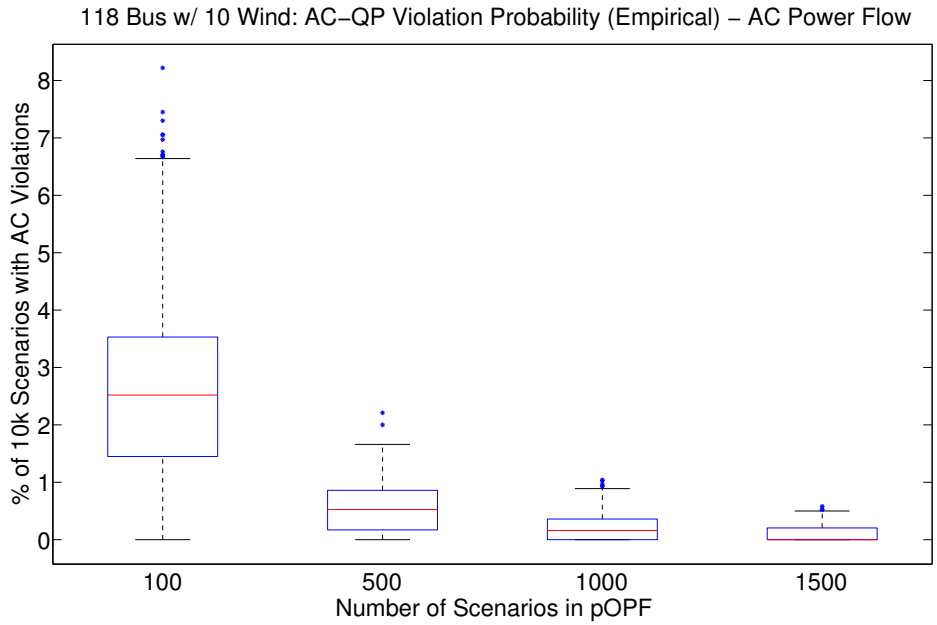

Figure 10.7: Test Case 1 AC-QP Empirical Probability of Violation

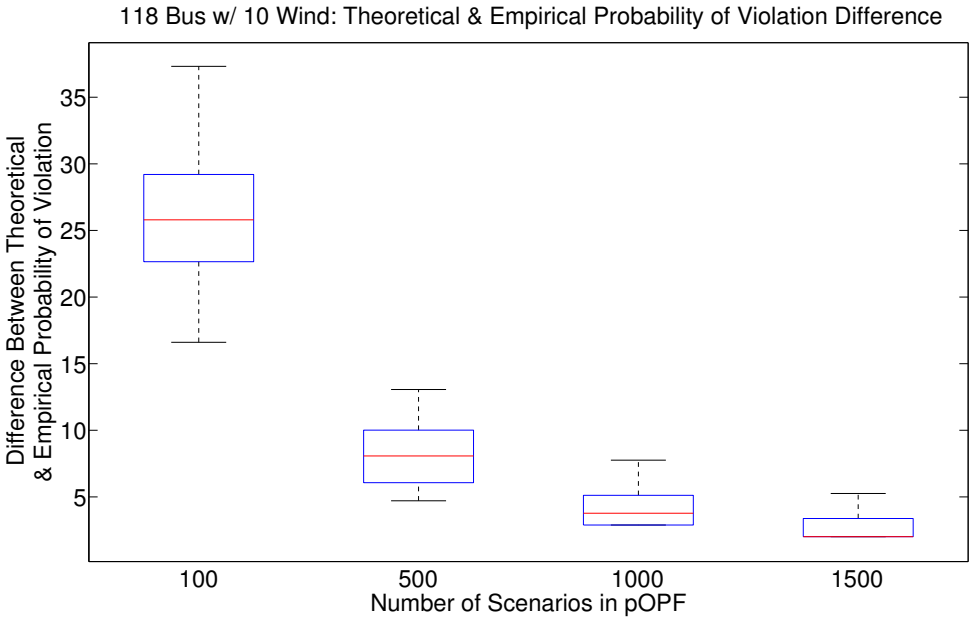

Figure 10.8: Test Case 1 AC-QP Difference Between Theoretical & Empirical Probability of Violation

10.3 Test Case 2: Assuming Generator Reserve Capacity is Twice as Expensive as Cost of Conventional Generation

The previous case study was revisited, assuming a lower cost of generator reserve capacity. In this case, reserves are assumed to be twice as expensive as conventional generation, rather than four times as in the previous case. In each trial, the pOPF problem was solved considering the same set of N scenarios as in the previous case. In other words, for a trial considering N=100 scenarios, the same set of E vectors was used in both cases. The results of this second test case for increasing numbers of scenarios included in the pOPF problem are given in Figures 10.9-10.15.

Figure 10.9 shows the value of each term in the objective function for various sets of N scenarios. As in the previous test case, less wind can be added in the network as the number of scenarios considered increases, as shown in the bottom subplot. This results in a higher cost of conventional generation as the number of scenarios considered increases, as shown in the top subplot. However, in this case, there is a significant amount of wind added in the network in every trial. Using a lower cost on generator reserve capacity, it is always economical to add wind into the network. As the number of scenarios considered in the problem increases, the solution is feasible for more extreme scenarios. A more "extreme" scenario is one with larger deviations from the base case wind

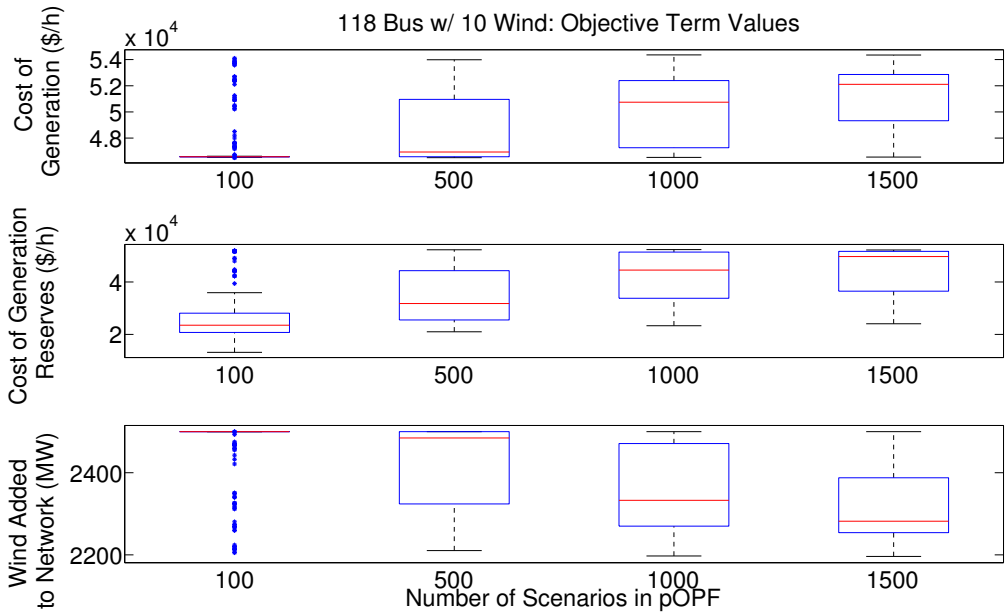

Figure 10.9: Test Case 2 AC-QP Objective Term Values

generation schedule (i.e. having entries of E^m significantly different from 1). This is demonstrated in Figure 10.10, which gives the maximum absolute forecast error, calculated as in the previous test case. Although the amount of wind added to the network decreases as larger sets of scenarios are considered, the magnitude of forecast error increases due to the presence of these extreme scenarios. This is opposite of the trend observed in the previous test case, where it is uneconomical to add wind when extreme scenarios are considered. This maximum absolute forecast error is directly related to the generator reserves required, so conventional generators must maintain larger reserve capacities to respond. The cost of generator reserves thus increases as the number of scenarios considered in the pOPF problem increases, as seen in the middle subplot.

Compared to the results of the previous test case, the cost of conventional generation is lower, as more wind is added in the network. There are also opposite trends observed regarding the cost of generator reserve capacity. With a higher cost of generator reserves assumed, the number of scenarios considered and reserve cost are inversely related. However, they are directly related when a lower cost is assumed. This is due to the fact that in this case, it is still economical to add wind in the network, even considering the additional cost of reserve capacity incurred.

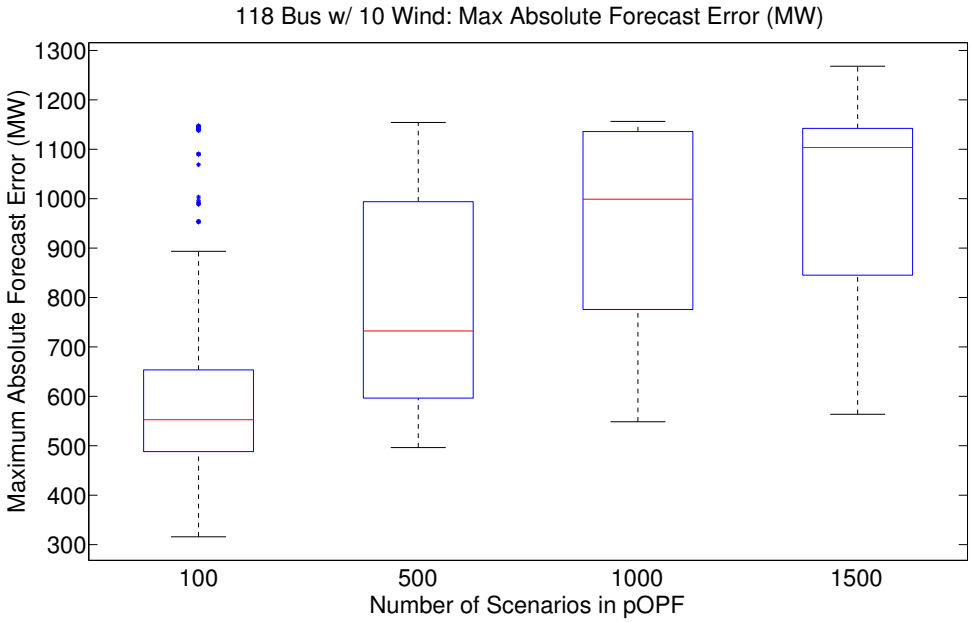

Figure 10.10: Test Case 2 AC-QP Maximum Total Forecast Error

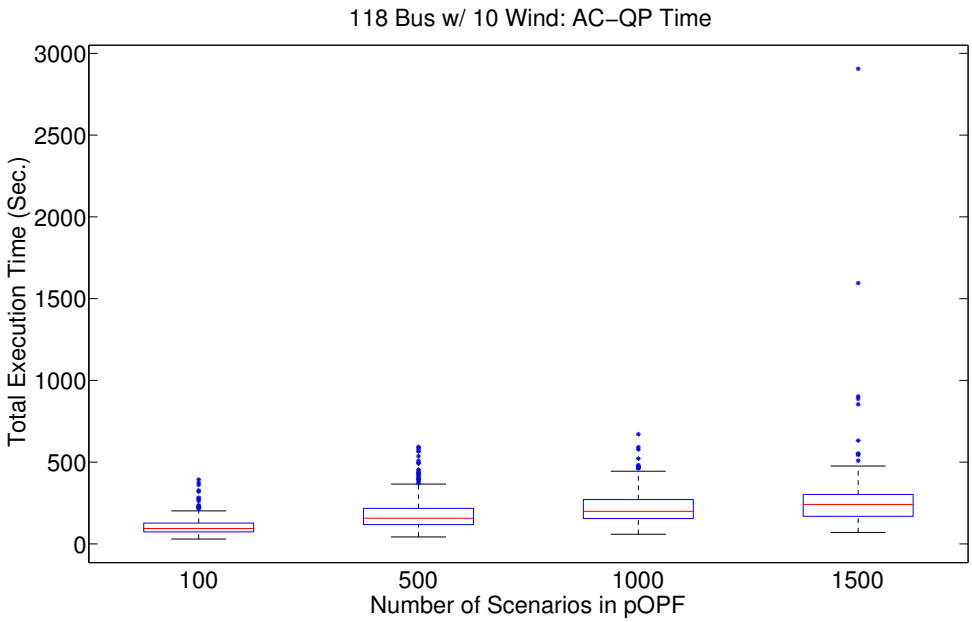

Figure 10.11: Test Case 2 AC-QP Execution Time

Figure 10.11 highlights the scalability of the proposed method for this case considering a lower cost of generator reserves. In 99% of all trials the AC-QP pOPF algorithm is solved within 10 minutes (600 seconds), and the median execution time is negligibly affected by increasing N in the

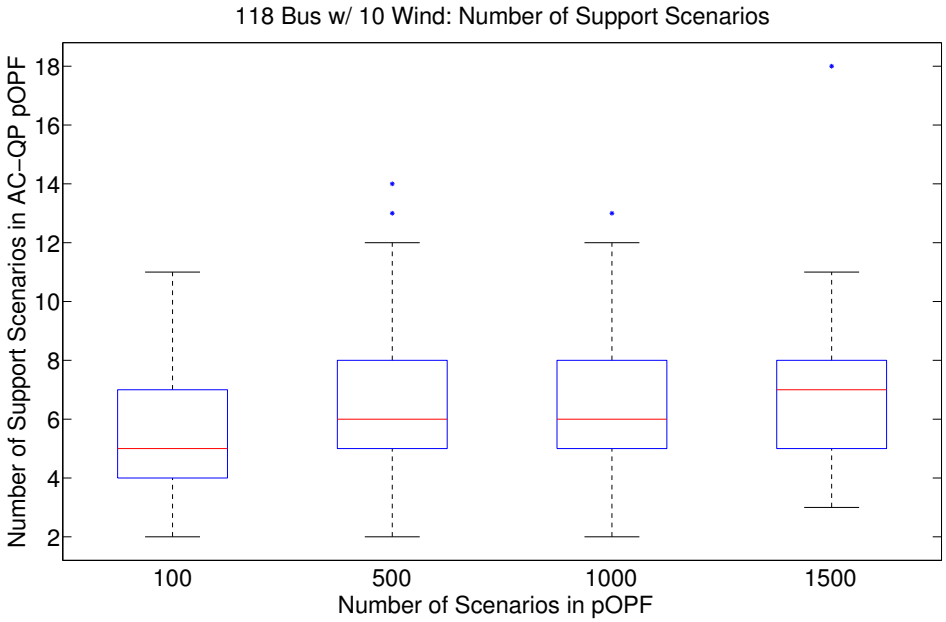

Figure 10.12: Test Case 2 AC-QP Support Scenarios

pOPF problem. Thus, as in the previous test case, the method is scalable with respect to network size and to the number of scenarios for which the resulting solution must be feasible. This is due to the fact that the cardinality of the support set is not significantly affected as the number of scenarios considered increases.

The cardinality of the set of support scenarios identified in each trial is given in Figure 10.12, and the corresponding theoretical upper bound on the probability of violation is shown in Figure 10.13. Compared to the previous test case, the number of support scenarios is greater, as a larger amount of wind has been added to the network. This translates to a higher theoretical probability of violation. However, similar to the results of the previous case, these theoretical bounds range from 20-41% when only 100 scenarios are considered in the problem. When N is sufficiently large (at least 1000 scenarios), the theoretical probability of any constraint violation is below 10%.

The empirical probability of violation results are summarized in Figure 10.14. As in the previous case, the empirical probability of violation is below 10% for all trials and less than 1% when N is increased to at least 1000 scenarios. The empirical results also satisfy the theoretical upper bounds, as demonstrated in Figure 10.15. Moreover, compared to the results in Figure 10.7, the empirical results are slightly lower when 100 scenarios are considered, and slightly higher when N = 1500.

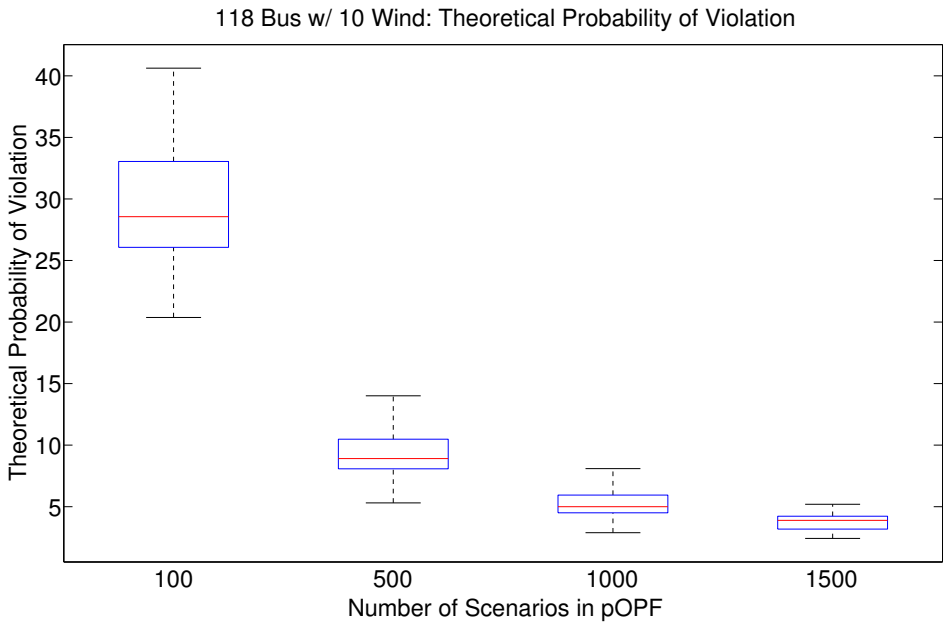

Figure 10.13: Test Case 2 AC-QP A-Posteriori Theoretical Probability of Violation

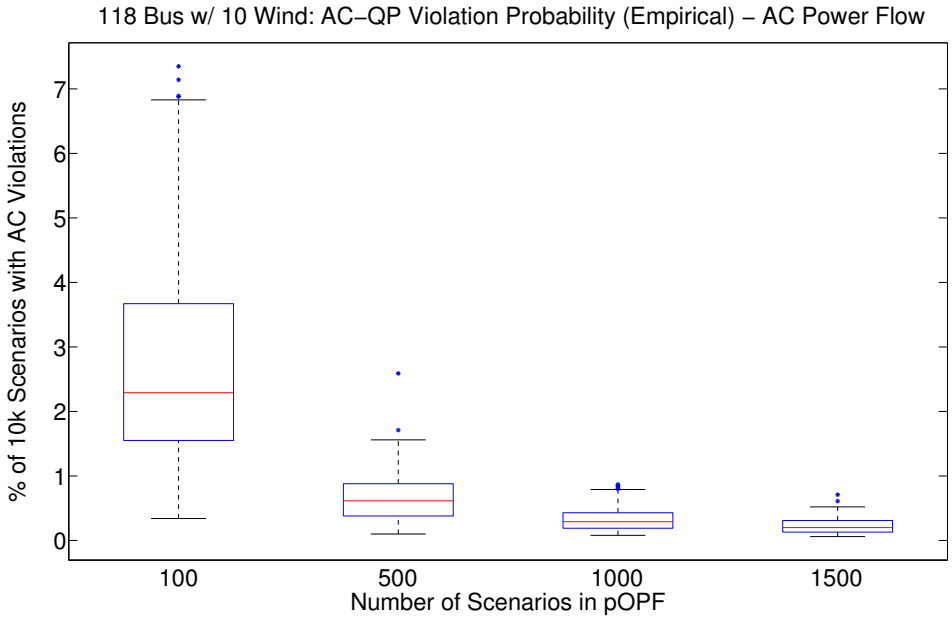

Figure 10.14: Test Case 2 AC-QP Empirical Probability of Violation

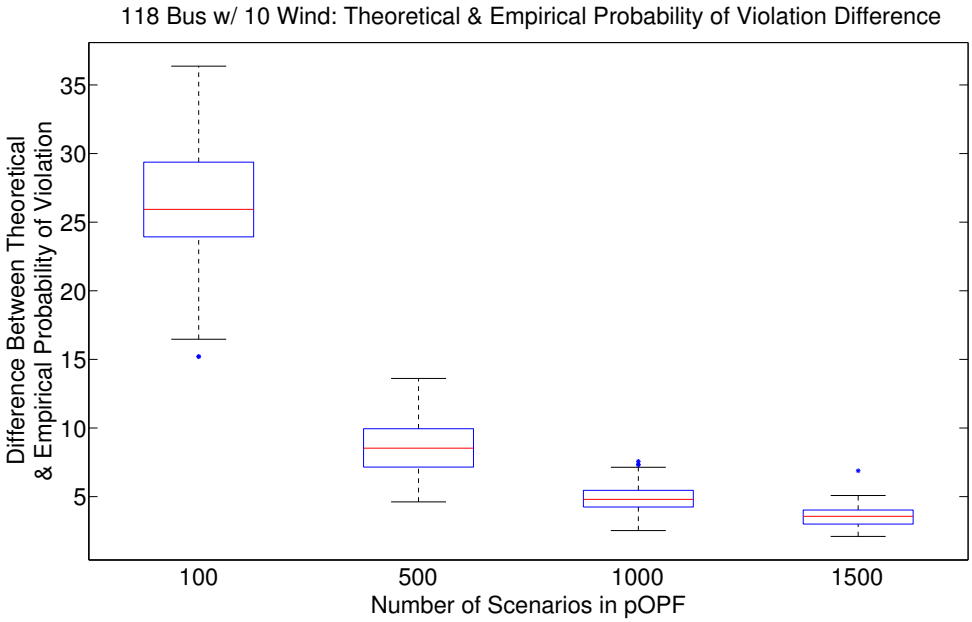

Figure 10.15: Test Case 2 AC-QP Difference Between Theoretical & Empirical Probability of Violation

10.4 Conclusions

The stochastic AC-QP pOPF algorithm from Chapter IX has been extended to consider the cost of conventional generation, as well as the cost of generator reserve capacity, in determining the maximum base case wind generation that can be added in a network. The scalability of this method with respect to large numbers of wind scenarios and moderate network size has been demonstrated. The final solution is accompanied with theoretical a-posteriori guarantees on the probability of violation. Moreover, the sensitivity study has demonstrated that the cost placed on generator reserve capacity significantly impacts the maximum wind penetration that can be reliably added in a network.

CHAPTER XI

Conclusions and Future Extensions

The AC OPF problem is of critical importance to ensure the economic operation of power systems. At the same time, the nonconvexity introduced by the nonlinear power balance and line flow constraints make it a particularly challenging optimization problem to solve. As such, there is a great need for developing accurate, reliable solution methods that can be solved in a reasonable amount of time for operational settings. The work presented is based on the AC-QP successive linearization algorithm. Compared to other techniques, this iterative method offers two advantages. First, it does not rely upon any model approximations or relaxations of the nonconvex constraints embedded in the AC OPF problem. It thus provides an AC-feasible solution. Second, each iteration of the method consists of solving a QP and running an AC power flow. Mature solvers exist for both steps, even for realistically large networks comprised of several thousand nodes. The method therefore offers promising scalability properties. This algorithm has been well established for traditional electricity networks. However, the work in this dissertation has focused on extending the AC-QP method to address two challenges facing future power systems, namely the integration of energy storage devices and of stochastic renewable generation sources.

Incorporating energy storage into the OPF problem introduces temporal coupling through the state-of-charge dynamic equations. This requires shifting the traditional, single-period OPF formulation to a multiperiod one. This can significantly impact the scalability benefits offered by the AC-QP method for realistically large networks when long horizons are considered. The algorithm has been expanded to a multiperiod formulation, including both renewable generation and energy storage devices. Recent advances from the field of convex optimization have then been applied to improve the performance and solution quality of this algorithm for solving multiperiod AC OPF problems in large-scale networks and moderate time horizons.

An improved initialization technique using an SOCP relaxation has been developed. This initialization offers several benefits compared to other approaches. The SOCP relaxation often provides an accurate prediction of the subset of line-flow constraints that require explicit representation in the QP. This reduces both the total number of iterations needed in the AC-QP algorithm as well as the number of inequality constraints in the QP. These factors improve the solution time of the AC-QP algorithm. The SOCP initialization reduces the likelihood of the AC-QP algorithm converging to a local optimum that is far from the global solution. Furthermore, the lower bound on the OPF objective given by the SOCP relaxation provides an indication of the quality of the AC-QP solution. A small "gap" between the SOCP lower bound and the AC-QP solution indicates that a nearly globally optimal outcome has been achieved. As the AC-QP method is a local solution method, assessing the quality of solution is of particular importance.

Renewable generation sources offer many economic and environmental benefits. As such, they must be included in OPF formulations to determine their optimal operation. However, such sources introduce uncertainty into power systems that present challenges from a reliability perspective. Stochastic OPF formulations are thus crucial for maintaining reliability standards in the presence of significant renewable penetration. The AC-QP OPF solution method has been extended to include wind power uncertainty, captured through the addition of a finite number of possible wind scenarios. The scalability of this algorithm with respect to large numbers of scenarios and moderate network size has been demonstrated, and the timing results support its utility for real-time applications. The algorithm fits in the framework of a randomized optimization technique that can characterize the solution with a-posteriori theoretical probabilistic guarantees. This modified AC-QP pOPF algorithm offers several advantages compared to other stochastic OPF techniques. It does not rely upon model approximations as in DC OPF formulations. It therefore produces an AC feasible solution where convex relaxations may not be tight. Moreover, it maintains scalability with respect to the number of scenarios to be optimized over, which is a limitation of convex relaxations. Finally, it provides a probabilistically robust solution with a-posteriori probabilistic violation guarantees.

Stochastic OPF formulations are also needed for planning decisions involving renewable generation. As such, the stochastic AC-QP OPF method has been adapted to solve two planning problems. The first is used to find the maximum wind penetration that can be added in a network, while maintaining reliability standards. Greater amounts of generator reserve capacity are needed when the amount of wind generation in a network increases. As this is a relatively expensive service to provide, it should be considered when determining the optimal amount of wind to install at a

particular location. The cost of conventional generation and of generator reserve capacity are included in the second reformulation, providing a tool to explore the tradeoff between the cost placed on generator reserves and the optimal wind penetration.

11.1 Future Extensions

The work presented in this dissertation motivates several extensions that will be topics of future research. In the multiperiod OPF context, further improving the initialization process of the AC-QP method could offer significant timing benefits for online applications. Future research will explore using recently developed linear and SOCP relaxations and approximations of the power flow equations, such as those in [19, 20, 55, 69, 70], to provide an initialization for the AC-QP method. The tradeoff between the computational speed, problem complexity, and accuracy of each will then be assessed.

There are also several open questions in the stochastic AC-QP context. The first involves the iterative process for introducing scenarios into the pOPF problem. This choice not only influences the execution time of the method, but also determines the size of the set of support scenarios identified. The latter has important implications for deriving a-posteriori probabilistic guarantees on the probability of violation to accompany the solution. In addition to the two approaches described in Chapters VII and IX, other methods (for example, a 2-norm ranking) will be explored to identify which scenarios should be introduced in the pOPF problem. Comparisons will then be drawn as to which ranking produces the minimal support set. Moreover, the dependence of this conclusion on the types of constraints that are violated most frequently will be investigated.

Another direction of future research is to apply various mathematical decomposition techniques to the pOPF problem. These could include the alternating direction method of multipliers (ADMM), dual decomposition methods, and other recently developed augmented Lagrangian methods offering improved convergence properties. These can be used to split the pOPF problem spatially, dividing the network into subnetworks. They could also be used to divide the problem with respect to the scenarios included in the problem. In such a formulation, each subproblem would be an AC OPF that assumes a particular wind generation pattern. The coupling constraints between the base case and each scenario are those maintaining consistent generator voltage magnitude setpoints and implementing the linear policy to adjust the base case generation to compensate for wind forecast errors. Comparisons of each decomposition approach, or possibly a combination of both, will be made to determine which offers the greatest computation time reduction.

The included stochastic pOPF work focused on one source of uncertainty in power systems, namely wind generation forecast error. However, the AC-QP pOPF method is directly applicable to other sources of uncertainty, such as transmission line outages. While the current operation of power systems relies upon maintaining the $(N-1)$ security criteria, such constraints could instead be enforced in a probabilistic sense using a scenario approach. The operating cost of the probabilistic $(N-1)$ solution should theoretically be lower than the solution that strictly enforces those criteria. However, there could be outage scenarios for which the probabilistic solution is infeasible. This tradeoff will be explored, and insights into which scenarios create particular vulnerabilities in a power system will be investigated.

One final possible extension of this work is to develop a multiperiod version of the AC-QP pOPF formulation. As such, energy storage devices can be incorporated into the problem, and the role of storage to mitigate wind forecast error will be explored. The presented case studies will be revisited, investigating how the optimality and reliability of the resulting solution is affected by the presence of energy storage. This will also provide insight into how the operation of storage differs when its purpose shifts from a purely economic role to one considering reliability as well.

BIBLIOGRAPHY

BIBLIOGRAPHY

[1] A. Wood, B. Wollenberg, and G. Sheble, *Power Generation, Operation and Control*, 3rd ed. John Wiley and Sons, Inc., 2013.

[2] M. Huneault and F. Galiana, "A Survey of the Optimal Power Flow Literature," *IEEE Trans. Power Syst.*, vol. 6, no. 2, pp. 762–770, May 1991.

[3] J. Momoh, R. Adapa, and M. El-Hawary, "A Review of Selected Optimal Power Flow Literature to 1993. Parts I & II," *IEEE Trans. Power Syst.*, vol. 14, no. 1, pp. 96–111, Feb. 1999.

[4] A. Castillo and R. O'Neill, "Survey of Approaches to Solving the ACOPF (OPF Paper 4)," US Federal Energy Regulatory Commission, Tech. Rep., Mar. 2013.

[5] A. Motto, F. Galiana, A. Conejo, and J. Arroyo, "Network-Constrained Multiperiod Auction for a Pool-Based Electricity Market," *IEEE Trans. Power Syst.*, vol. 17, no. 3, pp. 646–653, Aug. 2002.

[6] T. Overbye, X. Cheng, and Y. Sun, "A Comparison of the AC and DC Power Flow Model for LMP Calculations," in *37th Hawaii Int. Conf. Syst. Sci. (HICSS)*, Jan. 2006.

[7] M. Amini, R. Jaddivada, S. Mishra, and O. Karabasoglu, "Distributed Security Constrained Economic Dispatch," in *IEEE Innovative Smart Grid Technologies Conference (ISGT)*, Bangkok, Thailand, Nov. 2015.

[8] K. Purchala, L. Meeus, D. Van Dommelen, and R. Belmans, "Usefulness of DC Power Flow for Active Power Flow Analysis," *IEEE PES General Meeting*, pp. 454–459, June 2005.

[9] B. Stott, J. Jardim, and O. Alsac, "DC Power Flow Revisited," *IEEE Transactions on Power Systems*, vol. 24, no. 3, pp. 1290–1300, Aug. 2009.

[10] K. Dvijotham and D. Molzahn, "Error Bounds on Linear Power Flow Approximations: A Convex Relaxation Approach," in *IEEE 55th Annu. Conf. Decis. Control (CDC)*, Dec. 2016.

[11] X. Bai, H. Wei, K. Fujisawa, and Y. Wang, "Semidefinite Programming for Optimal Power Flow Problems," *Int. J. Electr. Power Energy Syst.*, vol. 30, no. 6, pp. 383–392, 2008.

[12] J. Lavaei and S. Low, "Zero Duality Gap in Optimal Power Flow Problem," *IEEE Transactions on Power Systems*, vol. 27, no. 1, pp. 92–107, Feb. 2012.

[13] S. Low, "Convex Relaxation of Optimal Power Flow–Part I: Formulations and Equivalence," *IEEE Transactions on Control of Network Systems*, vol. 1, no. 1, pp. 15–27, March 2014.

[14] D. Molzahn, J. Holzer, B. Lesieutre, and C. DeMarco, "Implementation of a Large-Scale Optimal Power Flow Solver Based on Semidefinite Programming," *IEEE Trans. Power Syst.*, vol. 28, no. 4, pp. 3987–3998, Nov. 2013.

[15] D. Molzahn and I. Hiskens, "Moment-Based Relaxation of the Optimal Power Flow Problem," *18th Power Syst. Comput. Conf. (PSCC)*, 18-22 Aug. 2014.

[16] B. Ghaddar, J. Marecek, and M. Mevissen, "Optimal Power Flow as a Polynomial Optimization Problem," *IEEE Trans. Power Syst.*, vol. 31, no. 1, pp. 539–546, Jan. 2016.

[17] C. Josz, J. Maeght, P. Panciatici, and J. Gilbert, "Application of the Moment-SOS Approach to Global Optimization of the OPF Problem," *IEEE Trans. Power Syst.*, vol. 30, no. 1, pp. 463–470, Jan. 2015.

[18] D. Molzahn and I. Hiskens, "Sparsity-Exploiting Moment-Based Relaxations of the Optimal Power Flow Problem," *IEEE Trans. Power Syst.*, vol. 30, no. 6, pp. 3168–3180, Nov. 2015.

[19] B. Kocuk, S. Dey, and A. Sun, "Strong SOCP Relaxations of the Optimal Power Flow Problem," To appear in *Oper. Res.*

[20] C. Coffrin, H. Hijazi, and P. Van Hentenryck, "The QC Relaxation: Theoretical and Computational Results on Optimal Power Flow," To appear in *IEEE Trans. Power Syst.*

[21] E. Dall'Anese, H. Zhu, and G. Giannakis, "Distributed Optimal Power Flow for Smart Microgrids," *IEEE Trans. Smart Grid*, vol. 4, no. 3, pp. 1464–1475, Sept. 2013.

[22] D. Molzahn and I. Hiskens, "Mixed SDP/SOCP Moment Relaxations of the Optimal Power Flow Problem," in *IEEE Eindhoven PowerTech*, June 2015.

[23] R. Madani, S. Sojoudi, and J. Lavaei, "Convex Relaxation for Optimal Power Flow Problem: Mesh Networks," *IEEE Trans. on Power Systems*, vol. 30, no. 1, pp. 199–211, Jan. 2015.

[24] B. Lesieutre, D. Molzahn, A. Borden, and C. DeMarco, "Examining the Limits of the Application of Semidefinite Programming to Power Flow Problems," in *49th Annu. Allerton Conf. Commun., Control, Comput.*, Sept. 2011, pp. 1492–1499.

[25] D. Molzahn, B. Lesieutre, and C. DeMarco, "Investigation of Non-Zero Duality Gap Solutions to a Semidefinite Relaxation of the Optimal Power Flow Problem," in *47th Hawaii Int. Conf. Syst. Sci. (HICSS)*, 6-9 Jan. 2014.

[26] D. Molzahn and I. Hiskens, "Convex Relaxations of Optimal Power Flow Problems: An Illustrative Example," *IEEE Trans. Circuits Syst. I: Reg. Papers*, vol. 63, no. 5, pp. 650–660, May 2016.

[27] K. Chandy, S. Low, U. Topcu, and H. Xu, "A Simple Optimal Power Flow Model with Energy Storage," in *IEEE 49th Ann. Conf. Decis. Contr. (CDC)*, Atlanta, GA, 2010, pp. 1051–1057.

[28] M. Almassalkhi and I. Hiskens, "Cascade Mitigation in Energy Hub Networks," in *IEEE 50th Ann. Conf. Decis. Contr. (CDC)*, Orlando, FL, 2011, pp. 2181–2188.

[29] N. Nguyen, D. Bovo, and A. Berizzi, "Optimal Power Flow with Energy Storage Systems: Single-Period Model vs. Multi-Period Model," in *IEEE Eindhoven PowerTech*, June 2015.

[30] R. Jabr, S. Karaki, and J. Korbane, "Robust Multi-Period OPF With Storage and Renewables," *IEEE Trans. Power Syst.*, vol. 30, no. 5, pp. 2790–2799, September 2015.

[31] F. Bouffard and F. F. Galiana, "Stochastic security for operations planning with signiffcant wind power generation," *IEEE Transactions on Power Systems*, vol. 23, no. 2, pp. 306–316, 2008.

[32] A. Papavasiliou, S. Oren, and R. ONeill, "Reserve requirements for wind power integration: A scenario-based stochastic programming framework," *IEEE Transactions on Power Systems*, vol. 26, no. 4, pp. 2197–2206, 2011.

[33] J. Morales, A. Conejo, and J. Perez-Ruiz, "Economic valuation of reserves in power systems with high penetration of wind power," *IEEE Transactions on Power Systems*, vol. 24, no. 2, pp. 900–910, 2009.

[34] M. Vrakopoulou, K. Margellos, J. Lygeros, and G. Andersson, "Probabilistic guarantees for the N-1 security of systems with wind power generation," in *Probabilistic Methods Applied to Power Systems Conference*, 2012.

[35] L. Roald, F. Oldewurtel, T. Krause, and G. Andersson, "Analytical Reformulation of Security Constrained Optimal Power Flow with Probabilistic Constraints," in *IEEE PowerTech Conference*, 2013.

[36] D. Bienstock, M. Chertkov, and S. Harnett, "Chance-constrained optimal power flow: Risk-aware network control under uncertainty," *SIAM Review*, vol. 56, no. 3, pp. 461–495, 2014.

[37] D. Bertsimas, E. Litvinov, X. Sun, J. Zhao, and T. Zheng, "Adaptive robust optimization for the security constrained unit commitment problem," *IEEE Transactions on Power Systems*, vol. 28, no. 1, pp. 52–62, 2013.

[38] G. Calafore and M. C. Campi, "The scenario approach to robust control design," *IEEE Transactions on Automatic Control*, vol. 51, no. 5, pp. 742–753, 2006.

[39] T. Alamo, R. Tempo, and A. Luque, "On the sample complexity of randomized approaches to the analysis and design under uncertainty," *Proceedings of the American Control Conference*, 2010.

[40] K. Margellos, P. Goulart, and J. Lygeros, "On the road between robust optimization and the scenario approach for chance constrained optimization problems," *IEEE Transactions on Automatic Control*, vol. 59, no. 8, pp. 2258–2263, 2014.

[41] M. Vrakopoulou, M. Katsampani, K. Margellos, J. Lygeros, and G. Andersson, "Probabilistic security-constrained AC optimal power flow," in *IEEE PowerTech Conference*, 2013.

[42] M. Campi, S. Garatti, and F. Ramponi, "Non-convex scenario optimization with application to system identification," in *54th IEEE Conference on Decision and Control*, 2015.

[43] M. Vrakopoulou, S. Chatzivasileiadis, E. Iggland, M. Imhof, T. Krause, O. Makela, J. L. Mathieu, L. Roald, R. Wiget, and G. Andersson, "A unified analysis of security-constrained

OPF formulations considering uncertainty, risk, and controllability in single and multi-area systems," in *IREP Symposium Bulk Power System Dynamics and Control - IX Optimization, Security and Control of the Emerging Power Grid*, 2013.

[44] A. M. Giacomoni and B. F. Wollenberg, "Linear Programming Optimal Power Flow Utilizing a Trust Region Method," in *North Amer. Power Symp.*, 2010.

[45] D. Molzahn, C. Josz, I. Hiskens, and P. Panciatici, "Solution of Optimal Power Flow Problems using Moment Relaxations Augmented with Objective Function Penalization," *IEEE 54th Ann. Conf. Decis. Control (CDC)*, Dec. 2015.

[46] Siemens PTI, "Volume II: Program Application Guide," *Power System Simulation for Engineering (PSS/E)*, vol. 31.0, Dec. 2007.

[47] X. Chen and J. Ye, "A class of quadratic programs with linear complementarity constraints," *Set-Valued and Variational Analysis*, vol. 17, no. 2, pp. 113–133, 2009.

[48] S. Braun and J. Mitchell, "A semidefinite programming heuristic for quadratic programming problems with complementarity constraints," *Computational Optimization and Applications*, vol. 31, no. 1, pp. 5–29, 2005.

[49] J. Jian, J. Li, and X. Mo, "A strongly and superlinearly convergent SQP algorithm for optimization problems with linear complementarity constraints," *Applied Mathematics and Optimization*, vol. 54, no. 1, pp. 17–46, 2006.

[50] L. Bai, J. Mitchell, and J. Pang, "On convex quadratic programs with linear complementarity constraints," *Computational Optimization and Applications*, vol. 54, no. 3, pp. 517–554, 2012.

[51] J. Felder and I. Hiskens, "Optimal Power Flow with Storage," in *18th Power Syst. Comput. Conf. (PSCC)*, Aug. 2014.

[52] C. Grigg, P. Wong, P. Albrecht, R. Allan, M. Bhavaraju, R. Billinton, Q. Chen, C. Fong, S. Haddad, S. Kuruganty, W. Li, R. Mukerji, D. Patton, N. Rau, D. Reppen, A. Schneider, M. Shahidehpour, and C. Singh, "The IEEE reliability test system - 1996," *IEEE Transactions on Power Systems*, vol. 14, no. 3, pp. 1010–1020, August 1999.

[53] M. Almassalkhi and I. Hiskens, "Model-Predictive Cascade Mitigation in Electric Power Systems With Storage and Renewables, Part I: Theory and Implementation," *IEEE Trans. Power Syst.*, to appear.

[54] S. Low, "Convex Relaxation of Optimal Power Flow: Parts I & II," *IEEE Trans. Control Network Syst.*, vol. 1, no. 1, pp. 15–27, Mar. 2014.

[55] L. Gan and S. Low, "Convex Relaxations and Linear Approximation for Optimal Power Flow in Multiphase Radial Networks," in *18th Power Syst. Comput. Conf. (PSCC)*, Aug. 2014.

[56] M. Baran and F. Wu, "Optimal Capacitor Placement on Radial Distribution Systems," *IEEE Trans. Power Del.*, vol. 4, no. 1, pp. 725–734, Jan. 1989.

[57] Z. Li, Q. Guo, H. Sun, and J. Wang, "Sufficient Conditions for Exact Relaxation of Complementarity Constraints for Storage-Concerned Economic Dispatch," *IEEE Trans. Power Syst.*, vol. 31, no. 2, pp. 1653–1654, Mar. 2016.

[58] Z. Li , Q. Guo, H. Sun, and J. Wang, "Further Discussions on Sufficient Conditions for Exact Relaxation of Complementarity Constraints for Storage-Concerned Economic Dispatch," June 2015, arXiv:1505.02493.

[59] R. Zimmerman, C. Murillo-Sánchez, and R. Thomas, "MATPOWER: Steady-State Operations, Planning, and Analysis Tools for Power Systems Research and Education," *IEEE Trans. Power Syst.*, no. 99, pp. 1–8, 2011.

[60] W. A. Bukhsh, A. Grothey, K. McKinnon, and P. Trodden, "Local Solutions of Optimal Power Flow Problem," *IEEE Trans. Power Syst.*, vol. 28, no. 4, pp. 4780–4788, Nov. 2013.

[61] S. Fliscounakis, P. Panciatici, F. Capitanescu, and L. Wehenkel, "Contingency Ranking with Respect to Overloads in Very Large Power Systems Taking into Account Uncertainty, Preventive and Corrective Actions," *IEEE Trans. Power Syst.*, vol. 28, no. 4, pp. 4909–4917, 2013.

[62] E. Camacho and C. Bordons, *Model Predictive Control*, 2nd ed. New York: Springer Verlag, 2004.

[63] N. Janssens and A. Kamagate, "Loop Flows in a Ring AC Power System," in *14th Power Syst. Comput. Conf. (PSCC)*, June 2002.

[64] K. Margellos, M. Prandini, and J. Lygeros, "On the connection between compression learning and scenario based single-stage and cascading optimization problems," *IEEE Transactions on Automatic Control*, vol. 60, no. 10, pp. 2716–2721, 2015.

[65] G. Papaefthymiou and B. Klöckl, "MCMC for wind power simulation," *IEEE Transactions on Energy Conversion*, vol. 23, no. 1, pp. 234–240, 2008.

[66] M. Vrakopoulou, K. Margellos, J. Lygeros, and G. Andersson, "A probabilistic framework for security constrained reserve scheduling of networks with wind power generation," in *2nd IEEE ENERGYCON Conference & Exhibition*, 2012.

[67] V. Rostampour, K. Margellos, M. Vrakopoulou, M. Prandini, G. Andersson, and J. Lygeros, "Reserve Requirements in AC Power Systems With Uncertain Generation," in *4th IEEE PES Innovative Smart Grid Technologies Europe (ISGT Europe) Conference*, 2013.

[68] J. F. Marley, D. K. Molzahn, and I. A. Hiskens, "An improved initialization for the AC-QP OPF method using an SOCP relaxation," *IEEE Transactions on Power Systems*, to appear.

[69] D. Bienstock and G. Munoz, "On Linear Relaxations of OPF Problems," 2015, Preprint: http://arxiv.org/abs/1411.1120.

[70] C. Coffrin and P. V. Hentenryck, "A Linear-Programming Approximation of AC Power Flows," *INFORMS J. Comput.*, vol. 26, no. 4, pp. 718–734, May 2014.